

Antimycobacterial activity of ascidian fungal symbionts

by

Kudzanai Ian Tapfuma



Dissertation presented for the degree of Doctor of Philosophy in Molecular Biology in the
Faculty of Medicine and Health Sciences at Stellenbosch University

Supervisor : Dr. Vuyo Mavumengwana
Co-supervisors: Dr. Rehana Malgas-Enus
Prof. Andre G. Loxton
Dr. Nasiema Allie

December 2022

Declaration

By submitting this thesis/dissertation, I declare that the entirety of the work contained therein is my own, original work, that I am the sole author thereof (save to the extent explicitly otherwise stated), that reproduction and publication thereof by Stellenbosch University will not infringe any third-party rights and that I have not previously in its entirety or in part submitted it for obtaining it for obtaining any qualification.

December 2022

Copyright © 2022 Stellenbosch University

All rights reserved

Abstract

Tuberculosis (TB) is an infectious disease which primarily affects the lungs. Treatment of TB is complicated because the causative agent, *Mycobacterium tuberculosis*, is an intracellular pathogen which infects and kills cells of the innate immune system, while exhibiting intrinsic and extrinsic resistance to many of the currently available antimicrobial agents. A sizeable percentage of TB patients in the world-population are infected by *M. tuberculosis* strains which are resistant to currently utilized first- and second-line anti-TB drugs. Drug-discovery studies bioprospecting for compounds with novel anti-TB activities are therefore essential in order to control the spread of TB and to prevent a catastrophic pandemic.

In this study, extracts from marine fungi were considered for antimycobacterial activity bioprospecting as they are largely underexplored. A total of 46 cultivable fungi were isolated from ascidians and 32 of these fungal isolates were sequenced and consequently identified. Among these fungi, the methanol crude extract from *Clonostachys rogersoniana* MGK33 was found to possess the highest antimycobacterial activity with minimum inhibitory concentrations of 0.125 and 0.200 $\mu\text{g/mL}$ against *Mycobacterium smegmatis* mc²155 and *M. tuberculosis* H37Rv, respectively. Untargeted metabolite profiling of the crude extract from *C. rogersoniana* MGK33 revealed the presence of bionectin F (among other compounds) which has previously been shown to possess antimicrobial activity in other studies. *In silico* molecular docking and simulation experiments in this study showed that bionectin F is a potential inhibitor of *M. tuberculosis* β -ketoacyl-ACP reductase (MabA).

An attempt was then made to generate novel agents that would be composed of nanoparticles surface functionalized with the bioactive fungal extract from *C. rogersoniana* MGK33. In particular, mono-metallic SPIONs were synthesized using the co-precipitation method and then surface modified to produce bi-metallic superparamagnetic iron oxide nanoparticles (SPIONs)

using nickel, zinc, gold, copper and silver, to produce Ni-SPIONs, Zn-SPIONs, Au-SPIONs, Cu-SPIONs and Ag-SPIONs. Functionalization was then performed using the MGK33 extract to produce Ni-SPIONs@MGK33, Zn-SPIONs@MGK33, Au-SPIONs@MGK33, Cu-SPIONs@MGK33 and Ag-SPIONs@MGK33. Among these agents, Cu-SPIONs and Ag-SPIONs were found to exhibit the strongest antimycobacterial activity, comparatively stronger than that of the counterparts, Cu-SPIONs@MGK33 and Ag-SPIONs@MGK33. In an experiment involving the treatment of RAW 264.7 macrophage cells infected with *M. smegmatis* mc²155, the MGK33 extract exhibited the highest early apoptosis activity (9.61%), followed by Cu-SPIONs@MGK33 (3.34%), both agents tested at 1.96 µg/mL for 24 hours. The MGK33 extract further showed strong antimycobacterial activity against intracellular *M. smegmatis* mc²155, compared with the nanoparticles synthesized in this study.

Results in this study led to the conclusion that the marine fungus, *C. rogersoniana* MGK33 is a prolific source of compounds with antimycobacterial and immunomodulatory activity, and that further studies should be done to develop Cu-SPIONs and Ag-SPIONs into lead agents for anti-TB drug development.

Opsomming

Tuberkulose (TB) is 'n aansteeklike siekte wat hoofsaaklik die longe affekteer. Behandeling van TB is ingewikkeld omdat die veroorsakende middel, *Mycobacterium tuberculosis* (*M. Tuberculosis*), 'n intrasellulêre patogeen is wat selle van die aangebore immuunstelsel infekteer en doodmaak, terwyl dit intrinsieke en ekstrasieke weerstand teen baie van die tans beskikbare antimikrobiese middels toon. 'n Aansienlike persentasie TB-pasiënte in die wêreldbevolking is besmet met *M. tuberculosis*-stamme wat weerstand bied teen tans gebruikte eerste- en tweedelyn-anti-TB-middels. Geneesmiddel-ontdekkingstudies bioprospektering vir verbindings met nuwe anti-TB-aktiwiteite is dus noodsaaklik om die verspreiding van TB te beheer en 'n katastrofiese pandemie te voorkom.

In hierdie studie is ekstrakte van mariene swamme met antimikobakteriële aktiwiteit oorweeg vir bioprospektering aangesien hulle grootliks onderontgin is. 'n Totaal van 46 kweekbare swamme is uit ascidians geïsoleer en 32 van hierdie swam-isolate is gevolglik geïdentifiseer. Onder hierdie swamme het die metanol ru-ekstrak van *Clonostachys rogersoniana* (*C. Rogersoniana*) MGK33 die hoogste antimikobakteriese aktiwiteit met minimum inhiberende konsentrasies van 0.125 en 0.200 $\mu\text{g/mL}$ teen *Mycobacterium smegmatis* mc²155 en *M. tuberculosis* H37Rv onderskeidelik getoon. Ongeteikende metabolietprofilering van die ru-ekstrak van *C. rogersoniana* MGK33 het die teenwoordigheid van bionektien F (onder ander verbindings) bevestig wat in vorige studies getoon het om antimikrobiese aktiwiteit te besit. In silico molekulêre dok- en simulatie-eksperimente in hierdie studie het getoon dat bionektien F 'n potensiële inhibeerder van *M. tuberculosis* β -ketoacyl-ACP reductase (MabA) is.

'n Poging is aangewend om nuwe middels te genereer wat bestaan uit nanopartikels wat met die bioaktiewe swamekstrak van *C. rogersoniana* MGK33 gefunksionaliseer is. 'n Mono-metaal SPIONs is gesintetiseer deur gebruik te maak van die mede-presipitasie metode. Die

oppervlak is gemodifiseer om bi-metaal SPIONs te produseer deur nikkel, sink, goud, koper en silwer te gebruik om Ni-SPIONs, Zn-SPIONs, Au-SPIONs, Cu-SPIONs en Ag-SPIONs te produseer. Funkstionalisering is dan uitgevoer met die MGK33-ekstrak om Ni-SPIONs@MGK33, Zn-SPIONs@MGK33, Au-SPIONs@MGK33, Cu-SPIONs@MGK33 en Ag-SPIONs@MGK33 te produseer. Onder hierdie middels is gevind dat Cu-SPIONs en Ag-SPIONs die sterkste antimikobakteriële aktiwiteit toon, betreklik sterker as dié van die eweknieë, Cu-SPIONs@MGK33 en Ag-SPIONs@MGK33. In 'n eksperiment waar *M. smegmatis* mc²155 geïnfecteerde RAW 264.7 makrofaagselle *M. smegmatis* mc²155 behandel was het die MGK33-ekstrak die hoogste vroeë apoptose-aktiwiteit (9.61%) getoon, gevolg deur Cu-SPIONs@MGK33 (3.34%), albei middels getoets teen 1.96 µg /mL vir 24 uur. Die MGK33-ekstrak het verder sterk antimikobakteriële aktiwiteit teen intrasellulêre *M. smegmatis* mc²155 getoon, in vergelyking met die nanopartikels wat in hierdie studie gesintetiseer is.

Resultate in hierdie studie het gelei tot die gevolgtrekking dat die mariene swam, *C. rogersoniana* MGK33 'n produktiewe bron van verbindings met antimikobakteriese en immunomodulerende aktiwiteit is, en dat verdere studies gedoen behoort te word om Cu-SPIONs en Ag-SPIONs te ontwikkel tot hoofmiddels vir anti-TB geneesmiddel ontwikkeling.

Acknowledgements

I would like to thank my Supervisors, Dr. Vuyo Mavumengwana, Dr. Rehana Malgas-Enus, Dr. Nasiema Allie and Prof. Andre Loxton for mentoring and supporting me throughout my PhD journey. Not only did you impart scientific knowledge, but also social values which molded my attitudes and character to become a better person.

Special thanks go to Dr. Liezel Smith, Dr. Lucinda Baatjies and Prof. Marshall Keyster for also playing a supportive role in soliciting funding, providing access to laboratory facilities and for providing valuable resources supporting the actual experiments in the project.

This study would not have been possible without the VuyoLab members who have been amazingly supportive in and out of the laboratory. Mr. Francis Adu-Amankwaah, Ms. Ricquelle Williams, Ms. Raesa Hussan, Ms. Vivette Soko, Mr. Kudakwashe Nyambo and Ms. Valerie Masiphephethu were all always dependable and ready to assist in their different ways throughout the study.

I would like to thank the members of the RME-Nano Research Group for helping with the synthesis and characterization of nanoparticles, especially Mrs. Annamé Lourens who assisted with the synthesis of nanoparticles and their characterization.

I am most grateful to Ingrid Herbst and Donnie Herbst for the love and kindness that you have shown me and my family. Thank you for supporting my studies financially and my making my dreams become a reality.

I will be forever grateful to my family, Ms. Cynthia Tapfuma, Mrs. Maureen Tapfuma, Mrs. Elina Buzuzi and Ms. Maureen Zungu, who all went beyond humanly imaginable capabilities to make this study a success. Above all, I thank God for all the lessons learnt and achievements made in this project.

Table of Contents

Declaration.....	i
Abstract.....	ii
Opsomming.....	iv
Acknowledgements.....	vi
Table of Contents.....	vii
List of Figures.....	xi
List of Tables.....	xv
List of Abbreviations.....	xvi
Chapter 1.....	1
General Introduction.....	1
1.1 The tuberculosis (TB) disease and the need for new drugs.....	1
1.2 Rationale and justification of the study.....	2
1.3 Study aims and objectives.....	3
1.4 Thesis outline.....	3
1.5 References.....	6
Chapter 2.....	8
Fungal-derived compounds and mycogenic nanoparticles with antimycobacterial activity – A review.....	8
2.0 Abstract.....	9
2.1 Tuberculosis.....	9
2.2 Fungal secondary metabolites with antimycobacterial activity.....	15
2.2.1 Compounds from endophytic fungi and plant-pathogenic fungi.....	16
2.2.2 Compounds from marine fungi.....	17
2.2.3 Compounds from entomopathogenic fungi.....	18
2.2.4 Compounds from lichenicolous fungi.....	19
2.2.5 Compounds from mushrooms (macrofungi), soil fungi and others.....	30
2.3 Chemically modified fungal compounds.....	32
2.4 Mycogenic nanoparticles.....	34
2.5 Conclusions.....	41
2.6 References.....	43

Chapter 3.....	57
Anti- <i>Mycobacterium tuberculosis</i> activity of marine derived <i>Clonostachys rogersoniana</i> methanol extract and virtual assessment of Bionectin F as a potential inhibitor of β -ketoacyl-ACP reductase (MabA).....	57
3.0 Abstract.....	58
3.1 Introduction	59
3.2 Methods and materials.....	61
3.2.1 Collection of ascidians and their identification	61
3.2.2 Isolation of fungi from ascidians, DNA sequencing and species identification.	61
3.2.3 Fungal DNA isolation, sequencing and phylogenetic analysis	62
3.2.4 Extraction of crude secondary metabolites from fungi	63
3.2.5 Antimycobacterial activity screening and minimum inhibitory concentrations (MICs) of fungal crude extracts.....	63
3.2.6 Metabolite profiling of fungal extracts	64
3.2.7 Molecular docking	65
3.2.8 Molecular dynamics	66
3.3 Results and Discussion	67
3.3.1 Culture-dependent isolation and identification of fungi associated with ascidians	67
3.3.2 Antimycobacterial activity of extracts from fungi associated with ascidians	69
3.3.3 Metabolite profiling of fungal isolates	74
3.3.4 Molecular docking and molecular dynamics simulation of fungal metabolites.	78
3.4 Conclusions	84
3.5 References	85
Chapter 4.....	94
Antimycobacterial activity of metal-coated iron oxide nanoparticles and their functionalization with an extract from <i>Clonostachys rogersoniana</i> MGK33.....	94
4.0 Abstract.....	94
4.1 Introduction	95
4.2 Methods and materials.....	97
4.2.1 Synthesis naked superparamagnetic iron oxide nanoparticles (SPIONs).....	97
4.2.2 Synthesis of nickel coated SPIONs (Ni-SPIONs)	97

4.2.3	Synthesis of zinc coated SPIONs (Zn-SPIONs).....	98
4.2.4	Synthesis of gold coated SPIONs (Au-SPIONs).....	99
4.2.5	Synthesis of copper coated SPIONs (Cu-SPIONs)	99
4.2.6	Synthesis of silver coated SPIONs (Ag-SPIONs)	99
4.2.7	Ultraviolet–visible (UV-Vis) spectroscopy	100
4.2.8	Fourier transform infrared (FTIR) spectroscopy	100
4.2.9	High resolution transmission electron microscopy (HRTEM).....	100
4.2.10	Functionalization of nanoparticles with a crude extract from <i>Clonostachys rogersoniana</i> MGK33 and liquid chromatography mass spectrometry	101
4.2.11	Antimycobacterial activity of nanoparticles.....	101
4.3	Results and discussion	102
4.3.1	Synthesis and characterization of SPIONs	102
4.3.2	Functionalization of mono- and bi-metallic SPIONs with the MGK33 fungal extract	105
4.3.3	Antimycobacterial activity of mono- and bi-metallic SPIONs	109
4.5	Conclusions	112
4.6	References	113
Chapter 5.....		118
Bioactivity of bi-metallic SPIONs and a <i>Clonostachys rogersoniana</i> MGK33 crude extract on RAW 264.7 macrophage cells infected with <i>Mycobacterium smegmatis</i> mc ² 155		118
5.0	Abstract.....	118
5.1.	Introduction	120
5.2	Methods and materials.....	123
5.2.1	Cytotoxic activity of bi-metallic SPIONs on RAW 264.7 macrophage cells ..	123
5.2.2	Infection of RAW 264.7 macrophage cells with <i>M. smegmatis</i> mc ² 155 and subsequent treatment with bi-metallic SPIONs.....	123
5.2.3	Flow cytometry Annexin V-FITC and PI stained cells	124
5.2.4	Enumeration of colony forming units.....	124
5.3	Results and discussion	125
5.3.1	Cytotoxic activity of Cu-SPIONs and Ag-SPIONs on RAW 264.7 macrophage cells.....	125
5.3.2	Apoptosis and necrosis of infected RAW 264.7 macrophage cells after treatment with bi-metallic SPIONs.....	127

5.3.3	Time-dependent survival of intracellular bacteria in RAW 264.7 macrophages ...	131
5.4	Conclusions	132
5.5	References	133
Chapter 6.....		138
General conclusions and future directions		138
6.1	Conclusions from this study	138
6.2	Limitations of this study	139
6.3	Future directions	141
Appendix A.....		144
Appendix B1		148
Appendix B2		149
Appendix B3		151
Appendix B4		152
Appendix C.....		156

List of Figures

Figure 2.1. Approved drugs (1-11) commonly used to treat TB.	14
Figure 2.1. (Continued). Approved drugs (12-17) commonly used to treat TB.	15
Figure 3.1. The evolutionary history was inferred by using the maximum likelihood method and Kimura 2-parameter model. The tree with the highest log likelihood (-6061.78) is shown. The percentage of trees in which the associated taxa clustered together is shown next to the branches, while GenBank accession numbers are also displayed next to the respective sequences. <i>Allomyces macrogynus</i> was used as an outgroup.	71
Figure 3.2. Three-dimensional representation of the binding pocket of 1UZN docked with bionectin F (A), and the two-dimensional representation of the molecular interactions observed between bionectin F and the binding site residues of 1UZN docked (B).	80
Figure 3.3. RMSD plots of the protein-ligand (1UZN and bionectin F) complex, ligand, and the protein back-bone for a 50 ns simulation.	Error! Bookmark not defined.
Figure 3.4. RMSD plots of the protein-ligand (1UZN and bionectin F) complex, ligand, and the protein back-bone for a 50 ns simulation.	Error! Bookmark not defined.
Figure 3.5. The binding interactions of bionectin F with 1UZN during the simulation.	Error! Bookmark not defined.
Figure 4.1. Figurative representation of the study design.	98
Figure 4.2. UV-Vis spectra of mono- and bi-metallic SPIONs synthesized in this study.	103

Figure 4.3. FTIR spectra of mono- and bi-metallic SPIONs synthesized in this study..... 104

Figure 4.4. HRTEM analysis of mono- and bi-metallic SPIONs synthesized in this study. In the figure, mono-metallic SPIONs are shown in **A**, Ni-SPIONs are shown in **B**, Zn-SPIONs are shown in **C**, Au-SPIONs are shown in **D**, Cu-SPIONs are shown in **E**, and Ag SPIONs are shown in **F**. Within each sample, the area of 150-200 individual nanoparticles was measured and the calculated average diameter was then assigned to each respective sample in nanometers (nm).**Error! Bookmark not defined.**

Figure 4.5. Base peak chromatograms obtained after performing untargeted LC-QTOF-MS/MS. In the figure, A shows the base peak chromatogram of the MGK33 extract, while B shows chromatograms from the “*spent*” extracts of mono-metallic SPIONs (SPIONs@MGK33) and bi-metallic SPIONs (Ni-SPIONs@MGK33, Zn-SPIONs@MGK33, Au-SPIONs@MGK33, Cu-SPIONs@MGK33 and Ag-SPIONs@MGK33). Aligned spectral data is available in Appendix B1 (<https://www.scidb.cn/s/ni6Jby>)..... 107

Figure 4.6. Bionectin F extraction efficiency by nanoparticles. The original MGK33 extract was used as a standard (0%), while extraction by the mono- and bi-metallic SPIONs was as follows: Zn-SPIONs@MGK33 = 0%, Ag-SPIONs@MGK33 = 12.32%, Cu-SPIONs@MGK33 = 16.15%, SPIONs@MGK33 = 18.34%, Au-SPIONs@MGK33 = 20.58% and Ni-SPIONs@MGK33 = 22.94%. Base peak intensities of bionectin F were used in the calculations..... 107

Figure 4.7. Length and width of bionectin F measured in angstroms (Å). 108

Figure 4.8. Percentage cell viability of cultures after treatment with mono-metallic, bi-metallic and functionalized nanoparticles. INH (isoniazid) was used as a positive control while untreated cells were used as a negative control. Treatment with nanoparticles was done at a concentration of 62.5 $\mu\text{g/mL}$ for 72 hours. Cell viability was determined from optical density measurements at 600 nm..... 110

Figure 4.9. Growth curves of *M. smegmatis* mc²155 after treatment with Cu-SPIONs (**A**), Cu-SPIONs@MGK33 (**A1**), Ag-SPIONs (**B**) and Ag-SPIONs@MGK33 (**B1**) for 72 hours. Cell growth was determined by measuring optical density at 600 nm (OD600 nm) while untreated cells were used a negative control. 111

Figure 5.1. Cell viability percentages of RAW 264.7 macrophage cells obtained after treatment with various agents for 48 hours. In the figure, Cu-SPIONs and Ag-SPIONs are represented by **A** and **B** respectively, while **C** represents isoniazid which was used as a control. Error bars represents standard deviation where $n = 3$. Cell viability is expressed as a percentage of untreated cells..... 125

Figure 5.2. Flow cytometry dot-plots obtained after 24 hours of treatment of RAW 264.7 macrophage cells. In the figure, samples are presented as follows: Uninfected cells (**A**), infected cells (**B**), isoniazid (**C**), MGK33 (**D**), Cu-SPIONs (**E**), Cu-SPIONs@MGK33 (**F**), Ag-SPIONs (**G**) and Ag SPIONs@MGK33 (**H**). Isoniazid was used as a control for antimycobacterial activity while $n = 2$. Appendix C shows the Annexin V-FITC and PI gates for each sample displayed in this figure. 128

Figure 5.3. Percentage number of viable, early apoptotic, late apoptotic and necrotic cells after 24 hours of treatment with Cu-SPIONs, Cu-SPIONs@MGK33, Ag-SPIONs, Ag-SPIONs@MGK33 and MGK33. Isoniazid was used as a control for antimycobacterial activity. In the figure, $n = 2$ 130

List of Tables

Table 2.1. First-, second- and third-line drugs commonly used for the treatment of TB	13
Table 2.2. Fungal compounds with antimycobacterial activity.	20
Table 2.3. Fungal compounds tested against Mycobacterial enzymes.	35
Table 2.4. Fungal compounds modified using chemical (semi-) synthesis and their antimycobacterial activity.	37
Table 3.1. List of sampled ascidians, their identities and number of fungi isolated.	68
Table 3.2. Percentage sequence similarity of fungal isolates and their closest relatives in the GenBank database.	70
Table 3.3. Minimum inhibitory concentration (MIC) values of fungal extracts tested against <i>M. smegmatis</i> mc ² 155 and <i>M. tuberculosis</i> H37Rv.	72
Table 3.4. Unique metabolites identified from extracts of six selected fungi and their docking scores.	75
Table 3.5. Metabolites common to fungal isolates and their molecular docking scores.	78
Table 4.1. Average sizes of SPIONs.	104
Table 5.1. Survival of intracellular <i>M. smegmatis</i> determined by counting of colony forming units (CFUs) after plating out at 4 different time-points ($n = 3$, mean \pm standard deviation).	131

List of Abbreviations

Abbreviation	Description
Ag-SPIONs	Silver modified superparamagnetic iron oxide nanoparticles
Ag-SPIONs@MGK33	Silver modified superparamagnetic iron oxide nanoparticles functionalized with MGK33
AgNO ₃	Silver nitrate
Annexin V-FTIC	Fluorescein isothiocyanate conjugated Annexin V
Au-SPIONs	Gold modified superparamagnetic iron oxide nanoparticles
Au-SPIONs@MGK33	Gold modified superparamagnetic iron oxide nanoparticles functionalized with MGK33
BGC	Biosynthetic gene clusters
Blac	β-lactamase
BLASTN	Basic Local Alignment Search Tool (nucleotides)
CFU	Colony forming units
CHPC	Center for High Performance Computing
Cu-SPIONs	Copper modified superparamagnetic iron oxide nanoparticles
Cu-SPIONs@GK33	Copper modified superparamagnetic iron oxide nanoparticles functionalized with MGK33
CuNO ₃	Copper(I) nitrate

DMSO	Dimethyl sulfoxide
ESI+	Electro spray ionization (positive mode)
FeCl ₃ ·6H ₂ O	Ferric chloride
FeSO ₄ ·7H ₂ O	Ferrous sulphate
fHMAD	F420-dependent hydroxymycolic acids dehydrogenase
FTIR spectroscopy	Fourier-transform infrared spectroscopy
HAuCl ₄	Chloroauric(III) acid
HPLC	High-performance liquid chromatography
HRTEM	High resolution transmission electron microscopy
KasA	β-ketoacyl-acyl carrier protein synthase
LCMS	Liquid chromatography mass spectrometry
LC-QTOF-MS/MS	Tandem liquid chromatography quadrupole time of flight mass spectrometry
MabA	β-ketoacyl-acyl carrier protein reductase A
MDR-TB	Multi-drug resistant tuberculosis
MGK33	Fungal extract from <i>Clonostachys rogersoniana</i> (isolate MGK33)
MIC	Minimum inhibitory concentration
MS/MS	Tandem mass spectrometry
NaBH ₄	Sodium borohydride

NADH	Reduced nicotinamide adenine dinucleotide
NADPH	Reduced nicotinamide adenine dinucleotide phosphate
Ni(NO ₃) ₂ .6H ₂ O	Nickel (II) nitrate hexahydrate
Ni-SPIONs	Nickel modified superparamagnetic iron oxide nanoparticles
Ni-SPIONs@MGK33	Nickel modified superparamagnetic iron oxide nanoparticles functionalized with MGK33
OADC	Oleic acid, albumin, dextrose, catalase
OD600nm	Optical density measured at 600 nm
OPLS	Optimized potentials for liquid simulations
PDA	Potato dextrose agar
PDB ID	Protein Data Bank identification
PI	Propidium iodine
RMSF	Root mean square fluctuation
ROS	Reactive oxygen species
SER140	Serine 140
SPIONs	Superparamagnetic iron oxide nanoparticles
TB	Tuberculosis
UPLC	Ultra-performance liquid chromatography
UV-Vis spectroscopy	Ultraviolet-visible spectroscopy

WHO	World Health Organization
XDR-TB	Extensively drug-resistant tuberculosis
Zn-SPIONs	Zinc modified superparamagnetic iron oxide nanoparticles
Zn-SPIONs@MGK33	Zinc modified superparamagnetic iron oxide nanoparticles functionalized with MGK33

Chapter 1

General Introduction

1.1 The tuberculosis (TB) disease and the need for new drugs

South Africa is listed among the 30 highest tuberculosis (TB) burden countries, collectively contributing 87 % of the world's new TB cases [1]. In 2020, about 5.8 million new TB cases and 1.5 million TB-related deaths were reported worldwide [1]. Even though the statistical trends show that the incidence of new TB cases in South Africa and across the globe is decreasing, that there is an imminent crisis of rifampicin resistant (RR-TB)/multi-drug resistant (MDR-TB) and extensively drug resistant TB (XDR-TB) whose treatment success rate is only 54% and 58% respectively [2].

In order to stop the spread and eradicate TB, the World Health Organization has devised the 'End TB Strategy' which is a world program aiming to reduce TB mortality and incidence by 95% and 90% respectively, between 2015-2035 [3]. Current global reports show that incidence is falling at a rate of 2% per year and should be accelerated to 5% in order to reach the 2020 milestone of the aforementioned program [3]. Reasons for the slow decline in incidence rate are mostly associated with the current TB treatment in use, including: (i) Non-adherence of patients to anti-TB drugs due to missing appointment dates, lack of social support and poor communication between patients and health care workers [4]. This leads to suboptimal response, development of drug resistance and continued spread of the disease [5]. (ii) The side effects caused by the anti-TB regimen which include gastrointestinal disturbance, ototoxicity, psychiatric disorders, arthritis, hyperthyroidism and even death also results in non-adherence [6]. (iii) The rising incidence of MDR-TB and XDR-TB which are expensive to diagnose and treat with second line drugs, often with these drugs unavailable in developing countries [5].

There is therefore an increasing need to improve the TB treatment process by introducing new diagnostic tool, drugs and fast-tracking the eradication of tuberculosis. . In particular, new and effective anti-TB drugs should overcome the limitations of the present and consequently be able to control latent-, active-, MDR- and XDR-TB, simplify and reduce treatment duration and cost, useful in HIV infected patients and have an acceptable to no toxicity profile [5,7].

1.2 Rationale and justification of the study

Over dependence on first-line TB drugs is a major risk factor in the fight against the spread of TB due to the development of resistance by the pathogen. Drug resistant strains threaten to undo progress achieved by clinicians, scientists, and Non-Governmental Organizations over the past decades in reducing the incidence rates. There is an imminent need for the development of safer and more effective anti-TB drugs to add to the arsenal in current use.

An interesting source of bioactive compounds for potential exploration in TB drug-discovery studies is marine fungi. This group of fungi is adapted to living in and/or on other organisms such as algae, ascidians, sponges, marine plants, and inanimate such as rocks and sediments. Metabolites from marine fungi and their synthetic derivatives have been shown to exhibit antiviral, antibacterial and anticancer activities [8], yet a small percentage of these has successfully reached the market. Optimization of marine products from marine fungi may result in the discovery of novel anti-TB compounds.

Using superparamagnetic iron oxide nanoparticles (SPIONs) together with marine derived fungal compounds to form ‘nano-drugs’ is one interesting way of generating organic nanoparticles (NPs) as a production platform for producing novel bioactive agents that will be less prone to resistance by *M. tuberculosis*. The use of SPIONs in biomedical research is well documented [9]. Modification of SPION surfaces with different metals such as gold, copper and silver confers specific chemical properties subject to the metal used, for instance gold

coated SPIONs will particularly conjugate with thiol compounds [10], silver with phosphates [11] and copper with oxides [12]. Coating SPIONs with active fungal metabolites may potentially result in new agents with enhanced antimycobacterial activity.

1.3 Study aims and objectives

In this study, the aim was to investigate the antimycobacterial and immunomodulatory activity of marine fungal crude secondary metabolites and the resulting functionalized SPIONs.

To achieve the above aims, the following objectives were formulated:

- i. Sample ascidians from Saldanha Bay and False Bay, isolate and identify their fungal associates and then perform phylogenetic analysis.
- ii. Extract crude secondary metabolites from fungal cultures and perform antimycobacterial activity assays against *Mycobacterium smegmatis* mc²155 and *M. tuberculosis* H37Rv.
- iii. Perform untargeted mass spectrometry-based metabolite profiling of crude extracts and *in silico* molecular docking against essential targets in *M. tuberculosis* H37Rv.
- iv. Synthesize SPIONs and modify them using gold, silver, nickel, copper and zinc to make bi-metallic SPIONs, functionalize the resulting bi-metallic SPIONs using crude fungal extracts with antimycobacterial activity and then assess their bioactivity.
- v. Infect RAW 264.7 macrophage cells with *M. smegmatis* mc²155 and then treat them with SPIONs and fungal extracts with antimycobacterial activity determined in (ii) and (iv) respectively, and then perform flow cytometry to measure apoptosis and necrosis of the treated RAW 264.7 macrophage cells.

1.4 Thesis outline

This thesis has been divided into six chapters, of which four of them were written as manuscripts ready for submission. Descriptions of the chapters are as follows:

CHAPTER 1 – General Introduction

This chapter introduces the readers to the problem statement, rationale, justifications, aims and objectives of the study.

CHAPTER 2 – Fungal-Derived Compounds and Mycogenic Nanoparticles with Antimycobacterial Activity – A Review

This chapter is a literature review that appraises reports on antimycobacterial activity of fungal derived compounds and mycogenic nanoparticles. This work was accepted for publication in SN Applied Sciences, a peer reviewed Springer Nature journal (<https://doi.org/10.1007/s42452-022-05010-2>).

CHAPTER 3 – Anti-*Mycobacterium tuberculosis* activity of marine derived *Clonostachys rogersoniana* methanol extract and virtual assessment of Bionectin F as a potential inhibitor of β -ketoacyl-ACP reductase (MabA)

This is a research chapter which reports the isolation of fungi from ascidians, antimycobacterial activity of the fungal extracts, their immunomodulatory properties and mass-spectrometry based metabolite profiling. A manuscript resulting from this chapter is under review in a peer reviewed journal, Heliyon (manuscript no. HELIYON-D-22-05818).

CHAPTER 4 – Antimycobacterial Activity of Metal-Coated Iron Oxide Nanoparticles and their Functionalization with Metabolites from *Clonostachys rogersoniana* MGK33

This is a research chapter which reports the synthesis, characterization, functionalization and antimycobacterial activity of SPIONs. The manuscript from this chapter is ready for submission.

CHAPTER 5 – Bioactivity of bi-metallic SPIONs and a *Clonostachys rogersoniana* MGK33 crude extract on RAW 264.7 macrophage cells infected with *Mycobacterium smegmatis* mc²155

This is a research chapter which reports the infection of RAW 264.7 macrophage cells with *M. smegmatis* mc²155, followed by treatment with bi-metallic SPIONs and a *Clonostachys rogersoniana* MGK33. The manuscript from this chapter is ready for submission.

CHAPTER 6 – General conclusions and future directions

This chapter presents the conclusions, limitations and recommendations for future studies.

1.5 References

1. WHO *Global Tuberculosis Report 2021*; World Health Organization: Geneva, 2021.
2. WHO *Global Tuberculosis Report 2019*; World Health Organization: Geneva, 2019.
3. WHO *Global Strategy and Targets for Tuberculosis Prevention, Care and Control after 2015*; Geneva, 2014.
4. Mekonnen, H.S.; Azagew, A.W. Non-Adherence to Anti-Tuberculosis Treatment, Reasons and Associated Factors among TB Patients Attending at Gondar Town Health Centers , Northwest Ethiopia. *BMC Res. Notes* **2018**, *11*, 1–8, doi:10.1186/s13104-018-3789-4.
5. Boogaard, J. Van Den; Kibiki, G.S.; Kisanga, E.R.; Boeree, M.J.; Aarnoutse, R.E. New Drugs against Tuberculosis: Problems, Progress, and Evaluation of Agents in Clinical Development. *Antimicrob. Agents Chemother.* **2009**, *53*, 849–862, doi:10.1128/AAC.00749-08.
6. Yang, T.W.; Park, H.O.; Jang, H.N.; Yang, J.H.; Kim, S.H.; Moon, S.H.; Byun, J.H.; Lee, C.E.; Kim, J.W.; Kang, D.H. Side Effects Associated with the Treatment of Multidrug-Resistant Tuberculosis at a Tuberculosis Referral Hospital in South Korea. *Medicine (Baltimore)* **2017**, *96*, 1–5, doi:10.1097/MD.00000000000007482.
7. Quan, D.; Nagalingam, G.; Payne, R.; Triccas, J.A. New Tuberculosis Drug Leads from Naturally Occurring Compounds. *Int. J. Infect. Dis.* **2017**, *56*, 212–220, doi:10.1016/j.ijid.2016.12.024.
8. Deshmukh, S.K.; Prakash, V.; Ranjan, N. Marine Fungi: A Source of Potential Anticancer Compounds. *Front. Microbiol.* **2018**, *8*, 1–24, doi:10.3389/fmicb.2017.02536.

9. Dulińska-Litewka, J.; Łazarczyk, A.; Hałubiec, P.; Szafranski, O.; Karnas, K.; Karewicz, A. Superparamagnetic Iron Oxide Nanoparticles—Current and Prospective Medical Applications. *Materials* **2019**, *12*, 1–26, doi:10.3390/ma12040617.
10. Xue, Y.; Li, X.; Li, H.; Zhang, W. Quantifying Thiol-Gold Interactions towards the Efficient Strength Control. *Nat. Commun.* **2014**, *5*, 1–9, doi:10.1038/ncomms5348.
11. Norman, B.C.; Xenopoulos, M.A.; Braun, D.; Frost, P.C. Phosphorus Availability Alters the Effects of Silver Nanoparticles on Periphyton Growth and Stoichiometry. *PLoS ONE* **2015**, *10*, 1–13, doi:10.1371/journal.pone.0129328.
12. Korzhavyi, P.A.; Soroka, I.L.; Isaev, E.I.; Lilja, C.; Johansson, B. Exploring Monovalent Copper Compounds with Oxygen and Hydrogen. *Proc. Natl. Acad. Sci. U. S. A.* **2012**, *109*, 686–689, doi:10.1073/pnas.1115834109.

Chapter 2

Fungal-derived compounds and mycogenic nanoparticles with antimycobacterial activity – A review

**Kudzanai Ian Tapfuma¹, Kudakwashe Nyambo¹, Lucinda Baatjies¹, Marshal Keyster²,
Lukhanyo Mekuto³, Liezel Smith¹, Nasiema Allie¹, Andre Gareth Loxton¹, Rehana Malgas-
Enus⁴, Vuyo Mavumengwana^{1,*}**

¹ DST-NRF Centre of Excellence for Biomedical Tuberculosis Research; South African Medical Research Council Centre for Tuberculosis Research; Division of Molecular Biology and Human Genetics, Faculty of Medicine and Health Sciences, Stellenbosch University, Cape Town, South Africa.

² Department of Biotechnology, Faculty of Natural Sciences, University of the Western Cape, Cape Town, South Africa.

³ Department of Chemical Engineering, Faculty of Engineering and the Built Environment, University of Johannesburg, Johannesburg, South Africa.

⁴ Department of Chemistry and Polymer Science, Faculty of Science, Stellenbosch University, Cape Town, South Africa.

*** Correspondence:**

Email address: vuyom@sun.ac.za; Tel.: +27 21 938 9952.

Published in SN Applied Sciences (<https://doi.org/10.1007/s42452-022-05010-2>).

2.0 Abstract

Tuberculosis (TB) is a persistent lung infection caused by *Mycobacterium tuberculosis*. The disease is characterized by high mortality rates of over 1 million per year. Unfortunately, the potency and effectiveness of currently in use anti-TB drugs is gradually decreasing due to the constant development of persistence and resistance by *M. tuberculosis*. The adverse side effects associated with current anti-TB drugs, along with anti-TB drug resistance, present an opportunity to bio-prospect novel potent anti-TB drugs from unique sources. Fundamentally, fungi are a rich source of bioactive secondary metabolites with valuable therapeutic potential. Enhancing the potency and effectiveness of fungal-based anti-TB drug leads by chemical synthesis and/or modification with nanomaterials may result in the discovery of novel anti-TB drugs. In this review, studies that focus on antimycobacterial activity of fungal-derived compounds and mycogenic nanoparticles are summarized. Numerous fungal-derived compounds and some mycogenic nanoparticles that exhibited strong antimycobacterial activities comparable to that of approved drugs were found. If fully explored, fungi hold promise to become key drivers in the generation of lead compounds in TB-drug discovery programs.

Keywords: *Mycobacterium tuberculosis*, fungi, secondary metabolites, bioprospecting, drug discovery, mycogenic nanoparticles.

2.1 Tuberculosis

Mycobacterium tuberculosis is the causative agent of tuberculosis (TB). TB results in high yearly mortalities and negatively impacts economies of the most affected countries each year [1]. The World Health Organization (WHO) estimates that one-third of the global population is infected with the latent form of TB [2]. In 2020, an estimated 5.8 million new TB cases and 1.5 million TB-related deaths were reported worldwide [3].

The recommended treatment for drug susceptible TB involves the use of four first-line drugs which include isoniazid (1), rifampicin (2), pyrazinamide (3) and ethambutol (4), which are administered for six months (Table 2.1 and Figure 2.1) [4,5]. The principle of using multidrug therapy for TB

treatment is founded upon the fact that these drugs have different mechanisms of action. When used together, they reduce selective pressure that may lead to mutant strains surviving because of using a single antibiotic. Isoniazid (1) is a prodrug activated by KatG (a catalase-peroxidase enzyme in Mycobacteria), which blocks the synthesis of the cell wall by inhibiting the enoyl-acyl carrier protein reductase, InhA, which forms part of the class II fatty acid synthase multi-enzyme (FAS-II) system. Perturbations of the InhA consequently tempers with the production of the vital components of the mycobacterial cell wall, the mycolic acids [6]. Resistance to isoniazid (1) by *M. tuberculosis* commonly results from mutations in the *katG*, *kasA* and *inhA* genes. Rifampicin (2) is known to bind to the RNA polymerase β subunit which results in the inhibition of DNA-dependent RNA synthesis, resistance is commonly caused by mutations in the *rpoB* gene [7].

Pyrazinamide's (3) mechanism of action is poorly understood, the current hypothesis is that the drug is activated by pyrazinamidase in *M. tuberculosis* to form pyrazinoic acid, which then binds to aspartate decarboxylase PanD and causes its degradation [8]. This action leads to a halt in the synthesis of pantothenate and co-enzyme A downstream. Mutations in *rpsA*, *pncA* and *panD* genes have been implicated in pyrazinamide (3) resistance [9]. Ethambutol (4) targets three arabinosyltransferases, namely EmbA, EmbB and EmbC [10]. Both EmbA and EmbB are involved in arabinogalactan synthesis, while EmbC is involved in lipoarabinomannan synthesis, both metabolites being essential components of the cell wall. Mutations in the *embA*, *embB* and *embC* genes commonly result in resistance.

Multi-drug resistant (MDR) and extensively-drug resistant (XDR) *M. tuberculosis* simply refers to strains which no longer respond to first-line drugs. The occurrence of these strains is prevalent and necessitates the use of second-line anti-TB drugs which commonly include bedaquiline (5), pretomanid (6), linezolid (7), streptomycin (8) and amikacin (9), kanamycin (10), capreomycin (11), delamanid (12), clofazimine (13), moxifloxacin (14), levofloxacin (15), ofloxacin (16) and ciprofloxacin (17) [4,5]. Second-line TB drugs have been reported to be more toxic and are administered for nine to 24 months with only about half the number of patients being cured [3].

Bedaquiline (**5**) inhibits the synthesis of ATP by inhibiting the F₁F₀ ATP synthase (proton pump), and mutations in *atpE* and *rv0678* genes are known to confer resistance [11,12].

In hypoxic conditions where *M. tuberculosis* is non-replicating, lethality of the nitroimidazole, pretomanid (**6**), is due to its prior activation by a deazaflavin dependent nitroreductase (Ddn), which produces *des*-nitro metabolites that interfere with cytochrome oxidases and ATP homeostasis consequently [13]. In replicating *M. tuberculosis*, pretomanid (**6**) inhibits F₄₂₀-dependent hydroxy mycolic acid dehydrogenase (fHMAD) which produces ketomycolic acids and thus interferes with synthesis of mycolic acids [14]. Resistance to pretomanid (**6**) is conferred by mutations in *fbiA*, *fbiB*, *fbiC*, *fbiD* and *ddn* genes which are involved in the F₄₂₀ system.

Linezolid (**7**) inhibits protein synthesis by binding to the 23S ribosomal RNA of the 50S subunit, thus preventing its complexation with the 30S subunit, mRNA and other components required for the assembly of a functional protein synthesis complex [15]. Mutations in the *rrl* gene encoding 23S rRNA, and the *rplC* gene encoding the L3 ribosomal protein, are both responsible for resistance to linezolid (**7**) [16]. The primary mechanism of action for aminoglycosides (streptomycin (**8**), amikacin (**9**), kanamycin (**10**) and capreomycin (**11**)) is very similar, they inhibit protein synthesis by irreversibly binding to RNA-binding S12 protein and 16S rRNA, which form part of the 30S ribosomal subunit and are encoded by the *rpsL* and *rrs* genes and [17,18]. This alters the ribosome's shape which leads to failure in the formation of the protein synthesis complex. Mutations in the *rpsL*, *rrs* and *tlyA* genes have been observed to confer resistance to aminoglycosides.

Delamanid (**12**) is recognized as an inhibitor of mycolic acid synthesis [19]. Since delamanid (**12**) drug it is thought to undergo the same activation process and exhibit the same mechanism of action as pretomanid (**6**).

Clofazimine (**13**) has a poorly understood mechanism of action in *M. tuberculosis*. One hypothesis is that it binds to guanine residues in *M. tuberculosis* DNA and thus blocks DNA replication. Since clofazimine (**13**) appears to compete with menaquinone (type II NADH:quinone oxidoreductase

substrate) for electrons, it is thought to undergo spontaneous oxidation which results in the generation of free oxygen species (ROS) which are antimicrobial. In addition, clofazimine (**13**) is a cationic amphiphile which is thought to inhibit ion transporting ATPases and thus interfering with ion uptake [20]. Mutations in the *rv1979c*, *rv2535c* and *pepQ* genes have been linked with clofazimine (**13**) resistance [21].

Moxifloxacin (**14**), levofloxacin (**15**), ofloxacin (**16**) and ciprofloxacin (**17**) are fluoroquinolones which also have a similar mechanism of action. These drugs inhibit the DNA ligase action of type II topoisomerases (DNA gyrase and topoisomerase IV) while allowing for the nuclease action to continue, this results in the release of DNA with single and double stranded breaks by the enzyme which consequently leads to cell death [22]. Mutations in the *gyrA* and *gyrB* genes confers resistance to fluoroquinolones.

It is evident that the discovery of new anti-TB drugs needs to be continued as resistance has been reported for drugs **1-17**. A very interesting natural source of chemically diverse and biologically active compounds is fungi. Over the years, numerous fungal compounds with excellent antimycobacterial activity have been reported, yet no reports on the exploration of these compounds in clinical trials are available. It is the view of the authors that fungal compounds have the potential of becoming key drivers in contributing lead compounds for TB-drug development studies. Enhancing these compounds using a variety of semi-synthetic approaches and nanotechnology can potentially impart novel properties that reduce cytotoxicity to normal cells while maintaining excellent bioactive profiles to both resistant and susceptible *M. tuberculosis* strains.

In this review, fungal-derived compounds with antimycobacterial activity and those that have been subjected to chemical synthetic modifications are presented. Since mycogenic nanoparticles (nanoparticles incorporating fungal secondary metabolites) are stabilized by fungal compounds during synthesis, it may be viewed as a unique mechanism of modifying fungal compounds, thus mycogenic nanoparticles were included in this review.

Table 2.1. First-, second- and third-line drugs commonly used for the treatment of TB ¹.

No.	Compound name	Compound type	Year	Inhibited activity	Target protein	Resistance mutations	MIC range	
							µg/mL	µM
1	Isoniazid	Synthetic	1952	Mycolic acid synthesis	InhA	<i>katG, kasA, inhA</i>	0.02-0.2	0.15-1.46
2	Rifampicin	Semi-synthetic	1963	Nucleic acid synthesis	DNA-dependent RNA polymerase	<i>rpoB</i>	0.05-1	0.06-1.22
3	Pyrazinamide	Synthetic	1954	Pantothenate, co-enzyme A synthesis	PanD	<i>rpsA, pncA, panD</i>	16-100	129.97-812.28
4	Ethambutol	Synthetic	1961	Arabinogalactan, lipoarabinomannan synthesis	EmbA, EmbB, EmbC	<i>embA, embB, embC</i>	1-5	4.89-24.47
5	Bedaquiline	Synthetic	2005	ATP synthesis	F ₁ F ₀ ATP synthase	<i>atpE, rv0678</i>	0.06-1	0.11-1.80
6	Pretomanid	Synthetic	2000	ATP synthesis, mycolic acids synthesis	Cytochrome oxidase, fHMAD	<i>fbiA, fbiB, fbiC, fbiD, ddn</i>	0.15-0.25	0.42-0.70
7	Linezolid	Synthetic	1996	Protein synthesis	50 ribosomal subunit	<i>rplC, rrl</i>	0.25-0.5	0.74-1.48
8	Streptomycin	Natural	1944	Protein synthesis	30S ribosomal subunit	<i>rpsL, rrs</i>	2-8	3.44-13.76
9	Amikacin	Semi-synthetic	1976	Protein synthesis	30S ribosomal subunit	<i>rrs, tlyA</i>	2-4	2.56-5.12
10	Kanamycin	Natural	1957	Protein synthesis	30S ribosomal subunit	<i>rrs, tlyA</i>	2-4	4.13-8.26
11	Capreomycin	Natural	1963	Protein synthesis	30S and 50S ribosomal subunit	<i>rrs, tlyA</i>	2-4	1.51-3.03
12	Delamanid	Synthetic	2006	Mycolic acid synthesis	fHMAD	<i>fbiA, fbiB, fbiC, fbiD, ddn</i>	0.006-0.24	0.01-0.45
13	Clofazimine	Semi-synthetic	1954	Poorly understood	Poorly understood	<i>rv1979c, rv2535c, pepQ</i>	0.1-1.2	0.21-2.53
14	Moxifloxacin	Synthetic	1996	Nucleic acid synthesis	Inhibits DNA synthesis	<i>gyrA, gyrB</i>	0.5-2.5	1.14-5.41
15	Levofloxacin	Synthetic	1987	Nucleic acid synthesis	Inhibits DNA synthesis	<i>gyrA, gyrB</i>	0.5-2.5	1.38-6.92
16	Ofloxacin	Synthetic	1982	Nucleic acid synthesis	Inhibits DNA synthesis	<i>gyrA, gyrB</i>	0.5-2.5	1.38-6.92
17	Ciprofloxacin	Synthetic	1980	Nucleic acid synthesis	Inhibits DNA synthesis	<i>gyrA, gyrB</i>	0.5-2.5	1.51-7.55

¹ Table 2.1 was prepared using information from previously published literature [6–22].

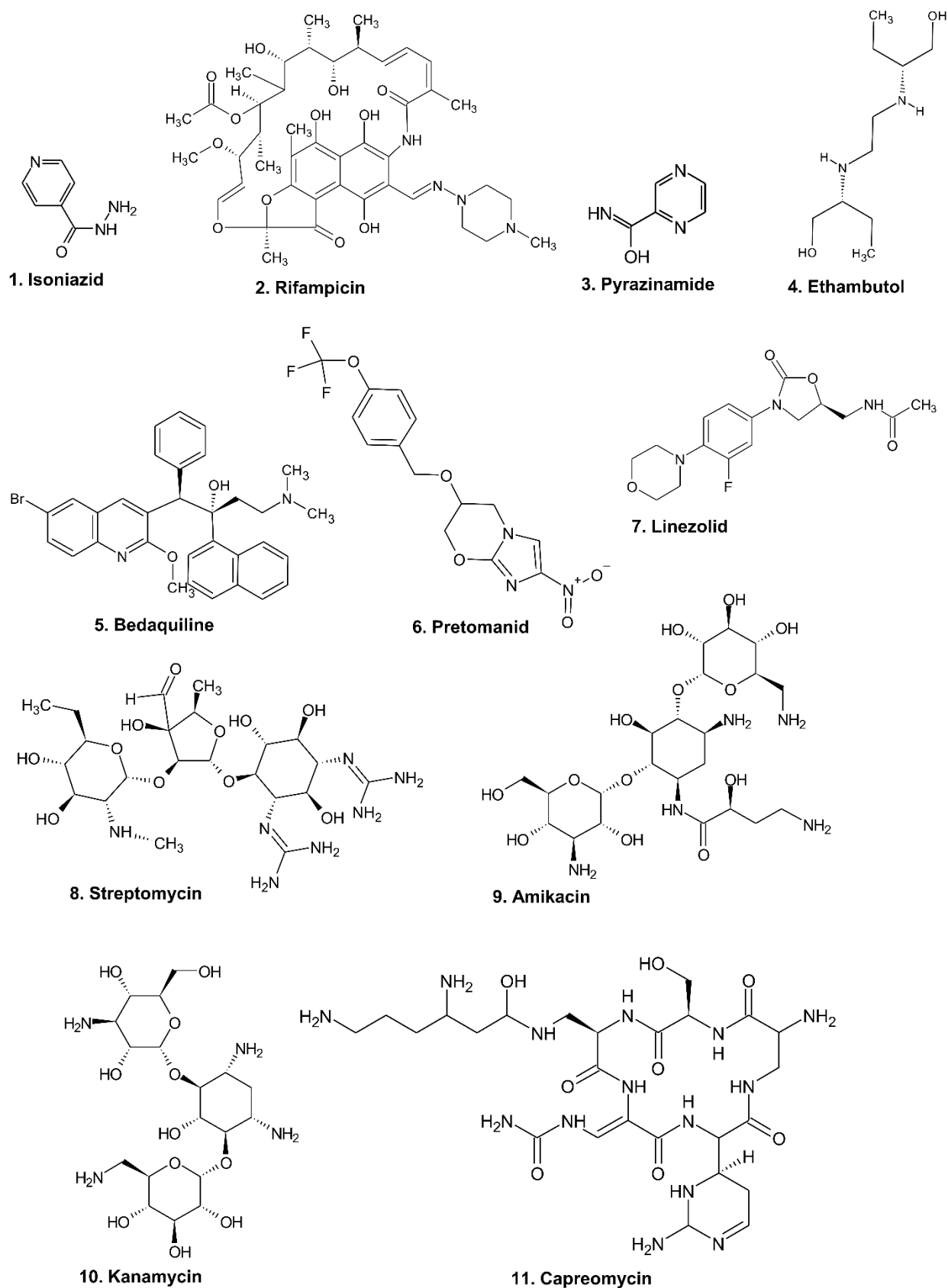


Figure 2.1. Approved drugs (1-11) commonly used to treat TB.

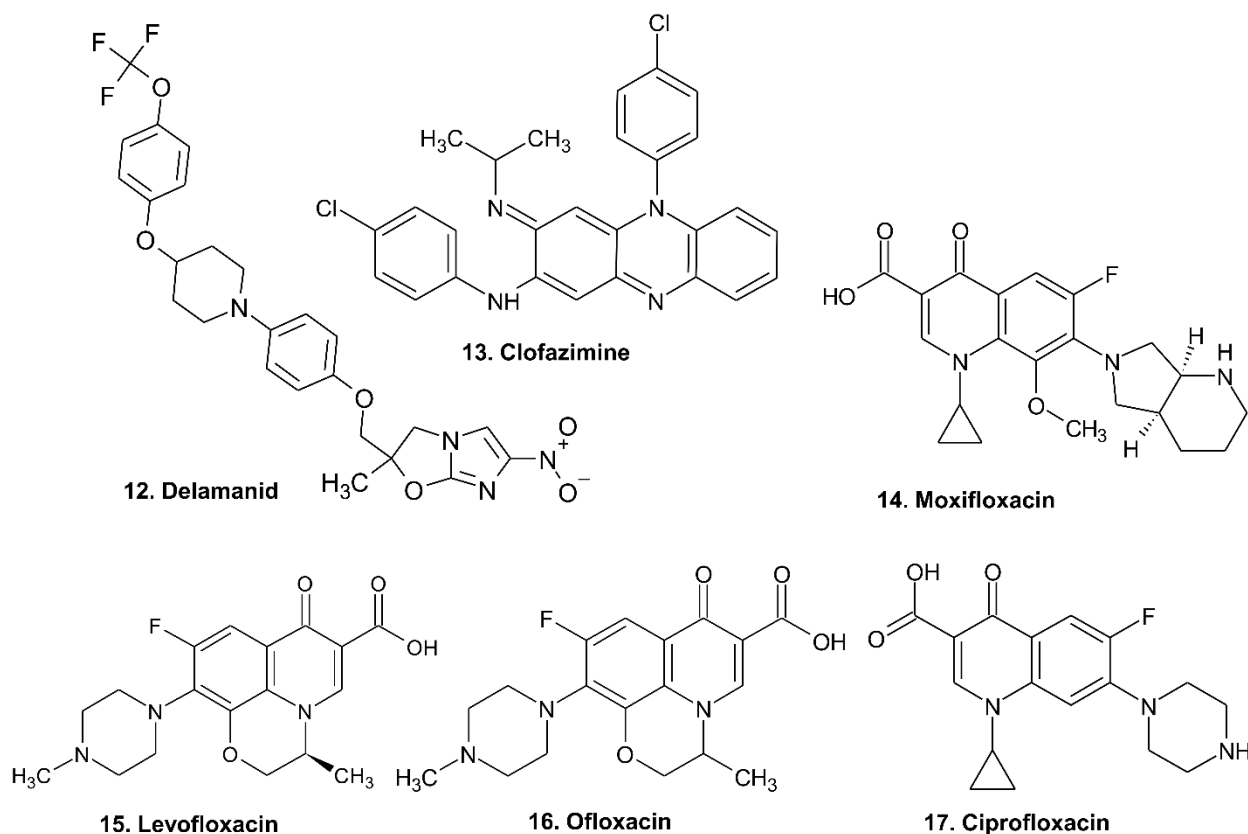


Figure 2.2. (Continued). Approved drugs (12-17) commonly used to treat TB.

The list of compounds and nanoparticles was obtained by searching for articles in PubMed and by free-text searching using the following key words and their combinations: Fungi, TB, anti-TB, antimycobacterial, minimum inhibitory concentration (MIC), *M. tuberculosis*, nanoparticles, mycogenic nanoparticles, modification, synthesis, semi-synthesis. Only compounds which had an MIC of less than 100 $\mu\text{g/mL}$ were considered for inclusion. Concentrations given in micromole (μM) in the original studies were converted to micrograms per milliliter ($\mu\text{g/mL}$) to maintain consistency.

2.2 Fungal secondary metabolites with antimycobacterial activity

Fungal secondary metabolites are produced in metabolic pathways encoded by biosynthetic gene clusters (BGCs) [23]. Numerous bioactive fungal secondary metabolites have been reported and include several antibiotics such as the penicillins, ergot alkaloids and cephalosporins, all commonly used in the treatment of microbial infections [24]. Even though there are no approved anti-TB drugs of fungal origin to date, there are numerous fungal-derived compounds which have been previously

shown to possess strong natural antimycobacterial activity which is comparable to that of anti-TB drugs currently in use. A summary of fungal compounds with antimycobacterial activity is given in Table 2.2.

2.2.1 *Compounds from endophytic fungi and plant-pathogenic fungi*

Endophytes are a ubiquitous class of endosymbiotic microorganisms (most common are bacteria and fungi) that spend part/all of their life cycle in plant tissues without causing them harm or disease [25]. They can be isolated from any part of the plant, including roots, flowers, fruits, stems, leaves and buds. Endophytes often benefit the plants by producing phytohormones and metabolites that enhance plant growth and tolerance to abiotic and biotic stresses [25]. In the plant microbiome, fungal pathogens may also exist and have a rather negative effect to the plant's growth and health as compared to endophytes.

Fungal endophyte PSU-N24 was isolated from the branch of *Garcinia nigrolineata* collected in Thailand and was fermented to produce 9 α -hydroxyhalorosellinia A (**18**), which was found to have an MIC of 13.3 $\mu\text{g/mL}$ after testing against *M. tuberculosis* H37Ra [26]. Desoxybostrycin (**19**) and 9 β -hydroxydihydrodesoxybostrycin (**20**) produced by the same fungus were found to be less active against *M. tuberculosis* H37Ra, having an MIC of 50 and 25 $\mu\text{g/mL}$, respectively [26].

Diaporthe sp. P133 was isolated as an endophyte from *Pandanus amaryllifolius* leaves and was fermented in potato dextrose broth for three weeks to produce diaportheone B (**21**), a benzopyranone [27]. The MIC value of diaportheone B (**21**) against *M. tuberculosis* H37Rv was found to be 0.77 $\mu\text{g/mL}$. *Phomopsis* sp. BCC 1323, and endophyte isolated from a teak leaf (*Tectona grandis* L.), produced two novel xanthone dimers, phomoxanthenes A and B (**22** and **23**), which had MIC values of 0.5 and 6.25 $\mu\text{g/mL}$ respectively against *M. tuberculosis* H37Ra [28]. Three alkaloids designated phomapyrrolidones A–C (**24–26**) were purified from extracts of the endophytic fungus, *Phoma* sp. NRRL 46751, isolated from the lower crown of *Saurauia scaberrinae* collected in Papua New Guinea [29]. The phomapyrrolidones A–C (**24–26**) had MIC values of 20.1, 5.9 and 5.2 $\mu\text{g/mL}$, respectively against *M. tuberculosis* H37Rv. *Chaetomium*

globosum IFB-E036 was isolated as a root endophyte of *Cynodon dactylon* in China and was fermented over a solid substrate to produce chaetoglocins A and B (**27** and **28**), which both had MIC values of 16 µg/mL against *M. smegmatis* CGMCC1.562 [30].

Fusarium avenaceum DAOM 196490 was isolated as a pathogen from needles of the balsam fir tree (*Abies balsamea*) infested with spruce budworm (*Choristoneura funiferana* Clem.) [31]. *F. avenaceum* DAOM 196490 was found to produce several enniatins, among them was enniatin A1 (**29**) which was tested in another study against *M. tuberculosis* H37Rv, *M. tuberculosis* H37Ra, *M. bovis*, *M. bovis* BCG and *M. smegmatis* mc²155 [32]. Enniatin A1 (**29**) was found to be slightly more active against virulent *M. tuberculosis* H37Rv (MIC = 1 µg/mL), compared to the avirulent *M. tuberculosis* H37Ra (MIC = 2 µg/mL). Against *M. bovis* and *M. bovis* BCG, enniatin A1 (**29**) had an MIC of 2 µg/mL for both strains. *M. smegmatis* mc²155 was the least susceptible with an MIC of 8 µg/mL.

2.2.2 Compounds from marine fungi

Marine fungi are described as those fungi that are able to colonize and adapt to the conditions in marine environments [33]. They are ubiquitous in the ocean and can be found decomposing organic matter, in sediments or as associates of other organisms. In one study, a water hyacinth pathogen, *Alternaria eichhorniae*, produced the anthraquinone, 4-deoxybostrycin (**30**), whose MIC values on *M. tuberculosis* H37Rv and clinical MDR *M. tuberculosis* K2903531 were 15 µg/mL and <5 µg/mL respectively [34]. Transcriptomics of *M. tuberculosis* H37Rv exposed to 4-deoxybostrycin (**30**) showed that the compound significantly altered the expression of 119 genes, 46 of these genes (24 upregulated genes and 22 down-regulated) are known to be functional genes involved in DNA replication and translation, carbohydrate metabolism, signal transduction and lipid metabolism [34]. Sclerotiotides M and N (**31** and **32**) were isolated from the fungus *Aspergillus insulicola* HDN151418, a symbiont of a marine sponge collected 410 m deep from Prydz Bay, Antarctica [35]. Sclerotiotides M and N (**31** and **32**) were found to be active against *Mycobacterium phlei* with a MIC of 1.37 and 5.63 µg/mL [35].

Trichoderins A, A1 and B (**33-35**) were isolated from the culture of *Trichoderma* sp., from an unidentified marine sponge, were tested for antimycobacterial activity against *M. tuberculosis* H37Rv, *M. bovis* BCG and *M. smegmatis* [36]. The MIC values of the trichoderins (**33-35**) were in the range of 0.02-2.0 µg/mL, the virulent *M. tuberculosis* H37Rv being more susceptible to trichoderin A (**33**) (MIC = 0.12 µg/mL). *Fusarium* spp. PSU-F14 was isolated from a sea fan (*Annella* sp.) and was found to produce nigrosporin B (**36**) and anhydrofusarubin (**37**), which had an MIC of 12.5 and 25.1 µg/mL respectively against *M. tuberculosis* H37Ra [37].

2.2.3 Compounds from entomopathogenic fungi

Entomopathogenic fungi can best be described as fungi that are capable of infecting and killing insects. They are popular in agriculture where they are explored as natural biological control agents against insect pests that attack crops [38]. Fungi from the *Hirsutella* genus are among the most abundant and important entomopathogens and are popularly known for their antimicrobial proteins. The entomopathogenic fungus, *Hirsutella kobayasii* BCC 1660, was collected from the Kaeng Krachan National Park in Thailand and fermented in potato dextrose broth to produce hirsutellide A (**38**), a cyclohexadepsipeptide [39]. The MIC of hirsutellide A (**38**) against *M. tuberculosis* H37Ra ranged between 6-12 µg/mL, while showing no cytotoxicity on Vero cells at 50 µg/mL. Cyclohexadepsipeptides hirsutatins A and B (**39** and **40**) were isolated from *Hirsutella nivea* BCC 2594 and were found to possess antimycobacterial activity [40]. Hirsutatins A and B (**39** and **40**) both had an MIC of 50 µg/mL against *M. tuberculosis* H37Ra. The fungus, *Paecilomyces tenuipes* BCC 1614 was collected from Khlong Naka Wildlife Sanctuary in Thailand, and was shown to produce the two bioactive cyclodepsipeptides, beauvericin (**41**) and beauvericin A (**42**) [41]. The MIC of beauvericin (**41**) and beauvericin A (**42**) against *M. tuberculosis* H37Ra was found to be 12.5 and 25 µg/mL, respectively. *Torrubiella tenuis* BCC 12732 is an entomopathogenic fungus which was isolated from a Homoptera scale insect, also collected in Thailand [42]. *T. tenuis* BCC 12732 produced 6,8-dihydroxy-3-hydroxymethylisocoumarin (**43**) which had an MIC of 25 µg/mL against *M. tuberculosis* H37Ra.

Seven enniatins, namely, enniatins B, B4, C, G, H, I and MK1688 (**44-50**) were isolated from *Verticillium hemipterigenum* BCC 1449, a fungus isolated from an adult leaf hopper of the Homoptera suborder, collected in Thailand [43]. After testing against *M. tuberculosis* H37Ra, both enniatins B and B4 (**44** and **45**) were found to have an MIC of 2.12 µg/mL, while enniatins C, G, H and I (**46-48**) had an MIC 6.25 µg/mL. MK1688 (**50**) was the most active of the seven enniatins, exhibiting an MIC of 1.56 µg/mL. In another study also involving enniatins, a spore of an unidentified fungus BCC 2629, was collected from the synemma of *Hirsutella fornicarum*, attached to an unnamed ant [44]. Solvent extraction and purification of metabolites from the fermentation broth of the BCC 2629 yielded enniatin L (**51**), a 1:1 mixture of enniatins M₁ and M₂ (**52**), and enniatin N (**53**). These enniatins were found to be active against *M. tuberculosis* H37Ra, whereby enniatin L (**51**) exhibited an MIC of 12.5 µg/mL, while the 1:1 mixture of enniatins M₁ and M₂ (**52**) and enniatin N (**53**) both exhibited an MIC of 6.25 µg/mL.

2.2.4 Compounds from lichenicolous fungi

Lichens are macroscopic structures which are a composite of heterotrophic filamentous fungi and autotrophic photosynthetic algae/cyanobacteria, which associate in a mutualistic relationship [45]. The type of fungi that can colonize lichens are called lichenicolous fungi and may sometimes be lichen specific. The crude extract of *Microsphaeropsis* sp. BCC 3050 was tested for antimycobacterial activity against *M. tuberculosis* H37Ra and was found to be active [46].

Following bioassay guided fractionation, preussomerins E-I (**54-58**), 3'-O-demethylpreussomerin I (**59**), deoxypreussomerin A (**60**) and bipendinsin (61) were isolated and their MICs were 25, 3.12, 3.12-6.25, 6.25, 12.5, 25, 1.56-3.12 and 50 µg/mL, respectively. The same preussomerins E-I (**54-58**) and 3'-O-demethylpreussomerin I (**59**) were also found to be significantly cytotoxic to KB and BC-1 cancer cell lines, and Vero cells which are a model of normal mammalian cells.

Table 2.2. Fungal compounds with antimycobacterial activity.

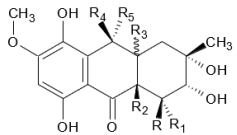
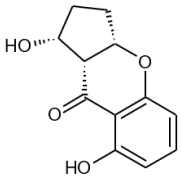
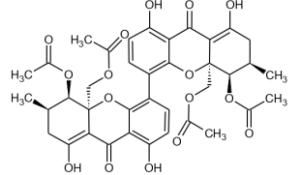
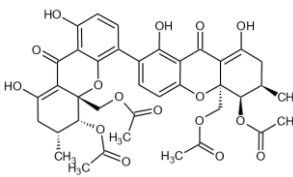
Type of fungi	Fungal species	No.	Compound name	Compound structure	Inhibited pathogen	MIC		Year	Ref.
						$\mu\text{g/mL}$	μM		
Endophytic and plant-pathogenic fungi	Endophytic fungus PSU-N24	18	9 α -Hydroxyhalorosellinia A	 <p>18. R = OH, R₁ = R₂ = R₄ = H, R₃ = α-H, R₅ = OH 19. R = R₁ = R₂ = R₄ = H, R₃ = β-H, R₅ = OH 20. R = R₁ = H, R₂ = R₃ = double bond, R₄ + R₅ = O</p>	<i>M. tuberculosis</i> H37Ra	12.5	36.7	2008	[26]
		19	Desoxybostrycin		<i>M. tuberculosis</i> H37Ra	50	154.2		
		20	9 β -Hydroxy-dihydrodesoxybostrycin		<i>M. tuberculosis</i> H37Ra	50	146.9		
	<i>Diaporthe</i> sp. P133	21	Diaportheone B		<i>M. tuberculosis</i> H37Rv	0.77	3.5	2011	[27]
	<i>Phomopsis</i> sp. BCC 1323	22	Phomoxanthone A		<i>M. tuberculosis</i> H37Ra	0.5	0.67	2001	[28]
<i>Phomopsis</i> sp. BCC 1323	23	Phomoxanthone B		<i>M. tuberculosis</i> H37Ra	6.25	8.33	2001	[28]	

Table 2.2 (Continued). Fungal compounds with antimycobacterial activity.

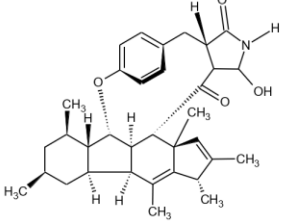
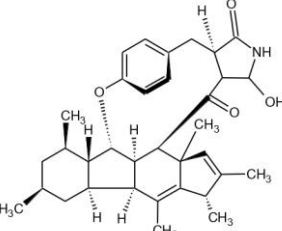
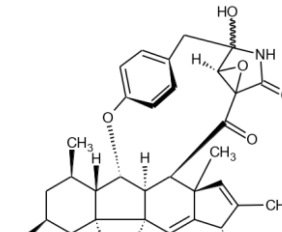
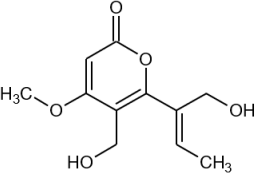
Type of fungi	Fungal species	No.	Compound name	Compound structure	Inhibited pathogen	MIC		Year	Ref.
						$\mu\text{g/mL}$	μM		
Endophytic and plant-pathogenic fungi	<i>Phoma</i> sp. NRRL 46751	24	Phomapyrrolidone A		<i>M. tuberculosis</i> H37Rv	20.1	38.1	2013	[29]
	<i>Phoma</i> sp. NRRL 46751	25	Phomapyrrolidone B		<i>M. tuberculosis</i> H37Rv	5.9	11.2	2013	[29]
	<i>Phoma</i> sp. NRRL 46751	26	Phomapyrrolidone C		<i>M. tuberculosis</i> H37Rv	5.2	9.56	2013	[29]
	<i>C. globosum</i> IFB-E036	27	Chaetoglocin A		<i>M. smegmatis</i> CGMCC1.562	16	70.7	2011	[30]

Table 2.2 (Continued). Fungal compounds with antimycobacterial activity.

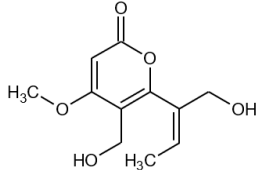
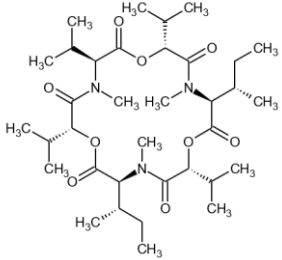
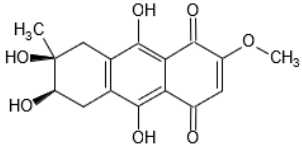
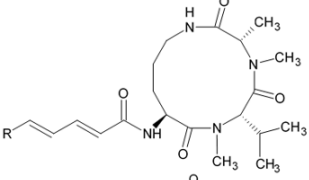
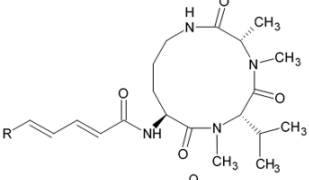
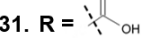
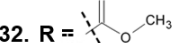
Type of fungi	Fungal species	No.	Compound name	Compound structure	Inhibited pathogen	MIC		Year	Ref.
						$\mu\text{g/mL}$	μM		
Endophytic and plant-pathogenic fungi	<i>C. globosum</i> IFB-E036	28	Chaetoglocin B		<i>M. smegmatis</i> CGMCC1.562	16	70.7	2011	[30]
	<i>F. avenaceum</i> DAOM 196490	29	Enniatin A1		<i>M. tuberculosis</i> H37Rv	1	1.50	2002, 2020	[31,32]
					<i>M. tuberculosis</i> H37Ra	2	2.99		
					<i>M. bovis</i>	2	2.99		
					<i>M. bovis</i> BCG	2	2.99		
				<i>M. smegmatis</i> mc ² 155	8	12.0			
Marine fungi	<i>A. eichhorniae</i>	30	4-Deoxybostrycin		<i>M. tuberculosis</i> H37Rv	15	46.8	2013	[34]
	<i>A. insulicola</i> HDN151418	31	Sclerotiotide M		MDR <i>M. tuberculosis</i> K2903531	< 5	< 15.6		
					<i>M. phlei</i>	1.37	3.13	2020	[35]
		32	Sclerotiotide N		<i>M. phlei</i>	5.63	12.5		
				31. R = 					
				32. R = 					

Table 2.2 (Continued). Fungal compounds with antimycobacterial activity.

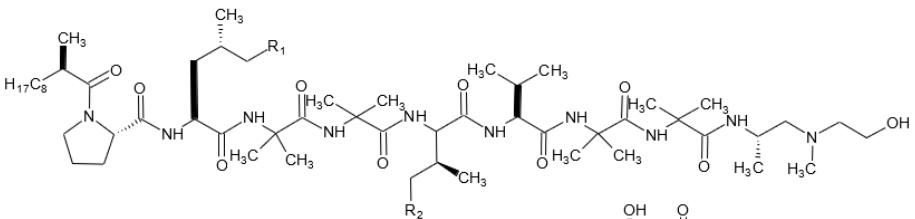
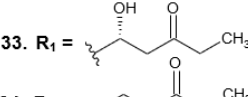
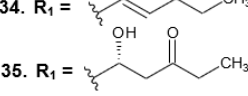
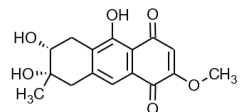
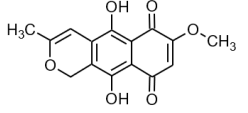
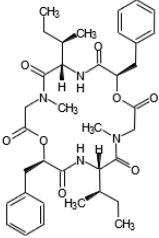
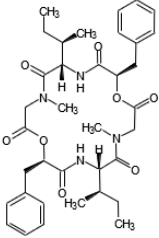
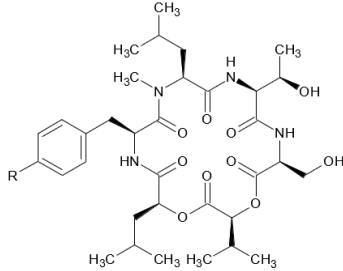
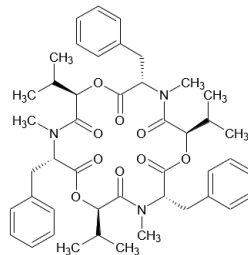
Type of fungi	Fungal species	No.	Compound name	Compound structure	Inhibited pathogen	MIC		Year	Ref.
						µg/mL	µM		
Marine fungi	<i>Trichoderma</i> sp. 05FI48	33	Trichoderin A		<i>M. bovis</i> BCG	0.02	0.02	2010	[36]
		34	Trichoderin A1	34. R ₁ =  R ₂ = CH ₃	<i>M. tuberculosis</i> H37Rv	2.0	1.72		
		35	Trichoderin B	35. R ₁ =  R ₂ = H	<i>M. smegmatis</i>	1.56	1.36		
	<i>Fusarium</i> spp. PSU-F14	36	Nigrosporin B		<i>M. tuberculosis</i> H37Ra	12.5	41	2010	[37]
		37	Anhydrofusarubin		<i>M. tuberculosis</i> H37Ra	25.1	87		
		38	Hirsutellide A		<i>M. tuberculosis</i> H37Ra	6-12	9-18		
Entomopathogenic fungi	<i>H. kobayashii</i> BCC 1660	38	Hirsutellide A		<i>M. tuberculosis</i> H37Ra	6-12	9-18	2002	[39]

Table 2.2 (Continued). Fungal compounds with antimycobacterial activity.

Type of fungi	Fungal species	No.	Compound name	Compound structure	Inhibited pathogen	MIC		Year	Ref.
						$\mu\text{g/mL}$	μM		
Entomopathogenic fungi	<i>H. nivea</i> BCC 2594	39	Hirsutatin A		<i>M. tuberculosis</i> H37Ra	50	73.9	2005	[40]
		40	Hirsutatin B		<i>M. tuberculosis</i> H37Ra	50	70.7		
	<i>P. tenuipes</i> BCC 1614	41	Beauvericin		<i>M. tuberculosis</i> H37Ra	12.5	16.0	2000	[41]

39. R = H
40. R = OCH₃

Table 2.2 (Continued). Fungal compounds with antimycobacterial activity.

Type of fungi	Fungal species	No.	Compound name	Compound structure	Inhibited pathogen	MIC		Year	Ref.	
						$\mu\text{g/mL}$	μM			
Entomopathogenic fungi	<i>T. tenuis</i> BCC 12732	43	6,8-Dihydroxy-3-hydroxymethylisocoumarin		<i>M. tuberculosis</i> H37Ra	25	120.1	2009	[42]	
	<i>V. hemipterigenum</i> BCC 1449	44	Enniatin B		<i>M. tuberculosis</i> H37Ra	3.12	4.88	2003	[43]	
		45	Enniatin B4		<i>M. tuberculosis</i> H37Ra	3.12	4.77			
		46	Enniatin C		<i>M. tuberculosis</i> H37Ra	6.25	9.17			
		47	Enniatin G		<i>M. tuberculosis</i> H37Ra	6.25	9.36			
		48	Enniatin H		<i>M. tuberculosis</i> H37Ra	6.25	9.56			
		49	Enniatin I		<i>M. tuberculosis</i> H37Ra	6.25	9.36			
		50	MK1688	<i>M. tuberculosis</i> H37Ra	1.56	2.29				
		Unidentified fungus BCC 2629	51	Enniatin L		<i>M. tuberculosis</i> H37Ra	12.5	18.7	2004	[44]
			52 (a/b)	Enniatin M ₁ /Enniatin M ₂ (1:1 mixture)		<i>M. tuberculosis</i> H37Ra	6.25	9.14		
			53	Enniatin N		<i>M. tuberculosis</i> H37Ra	6.25	8.96		

51. R₁ = R₂ = H
 52a. R₁ = CH₃, R₂ = H
 52b. R₁ = H, R₂ = CH₃
 53. R₁ = R₂ = CH₃

Table 2.2 (Continued). Fungal compounds with antimycobacterial activity.

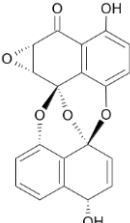
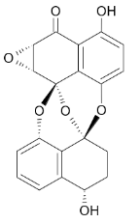
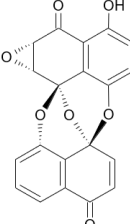
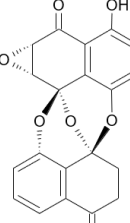
Type of fungi	Fungal species	No.	Compound name	Compound structure	Inhibited pathogen	MIC		Year	Ref.
						$\mu\text{g/mL}$	μM		
Lichenicolous fungi	<i>Microsphaeropsis</i> sp. BCC 3050	54	Preussomerin E		<i>M. tuberculosis</i> H37Ra	25	68.6	2002	[46]
	<i>Microsphaeropsis</i> sp. BCC 3050	55	Preussomerin F		<i>M. tuberculosis</i> H37Ra	3.12	8.52	2002	[46]
	<i>Microsphaeropsis</i> sp. BCC 3050	56	Preussomerin G		<i>M. tuberculosis</i> H37Ra	3.12-6.25	8.61-17.25	2002	[46]
	<i>Microsphaeropsis</i> sp. BCC 3050	57	Preussomerin H		<i>M. tuberculosis</i> H37Ra	6.25	17.2	2002	[46]

Table 2.2 (Continued). Fungal compounds with antimycobacterial activity.

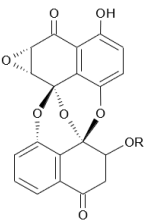
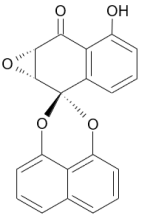
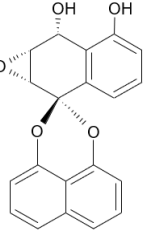
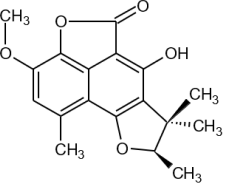
Type of fungi	Fungal species	No.	Compound name	Compound structure	Inhibited pathogen	MIC		Year	Ref.
						$\mu\text{g/mL}$	μM		
Lichenicolous fungi	<i>Microsphaeropsis</i> sp. BCC 3050	58	Preussomerin I	 <p>58. R = Me 59. R = H</p>	<i>M. tuberculosis</i> H37Ra	12.5	31.7	2002	[46]
		59	3'- <i>O</i> -demethylpreussomerin I		<i>M. tuberculosis</i> H37Ra	25	63.4		
	<i>Microsphaeropsis</i> sp. BCC 3050	60	Deoxypreussomerin A		<i>M. tuberculosis</i> H37Ra	1.56-3.12	4.69-9.39	2002	[46]
	<i>Microsphaeropsis</i> sp. BCC 3050	61	Bipendinsin (palmarumycin C ₁₁)		<i>M. tuberculosis</i> H37Ra	50	149.6	2002	[46]
	<i>T. eluteriae</i> Spreng.	62	Lactone		<i>M. tuberculosis</i> H37Rv	50	219.1	2020	[47]

Table 2.2 (Continued). Fungal compounds with antimycobacterial activity.

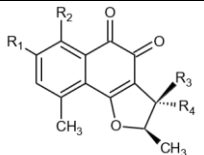
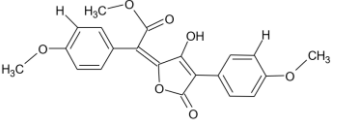
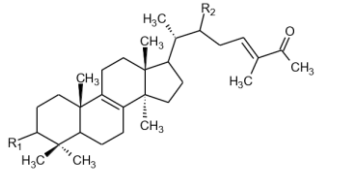
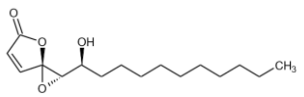
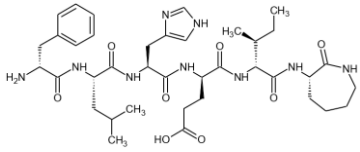
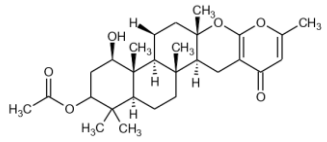
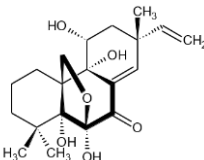
Type of fungi	Fungal species	No.	Compound name	Compound structure	Inhibited pathogen	MIC		Year	Ref.
						$\mu\text{g/mL}$	μM		
Lichenicolous fungi	<i>T. eluteriae</i> Spreng.	63	Trypethelone	 <p>63. $R_1 = \text{OH}$, $R_2 = \text{H}$, $R_3 = R_4 = \text{CH}_3$ 64. $R_1 = R_2 = \text{OCH}_3$, $R_3 = \text{CH}_2\text{OH}$, $R_4 = \text{CH}_3$</p>	<i>M. tuberculosis</i> H37Rv	12.5	45.9	2020	[47]
		64	4'-Hydroxy-8-methoxytrypethelone methyl ether		<i>M. tuberculosis</i> H37Rv	50	150.4		
Mushrooms and soil fungi	<i>S. citrinum</i> KMILT-SCL01	65	4,4'-dimethoxyvulpinic acid		<i>M. tuberculosis</i> H37Ra	25	65.4	2003	[51]
	<i>A. odoratus</i>	66	Astraodoric acid A	 <p>66. $R_1 = \text{O}$, $R_2 = \alpha\text{-OAc}$ 67. $R_1 = \text{H}$, $R_2 = \alpha\text{-OH}$</p>	<i>M. tuberculosis</i> H37Ra	50	97.5	2012	[52]
		67	Astraodoric acid B		<i>M. tuberculosis</i> H37Ra	25	53.1	2012	[52]
	<i>R. cystidiophora</i>	68	Ramariolide A		<i>M. smegmatis</i>	8	28.3	2012	[53]
					<i>M. tuberculosis</i>	64-128	226-453	2012	[53]
	<i>M. alpina</i> FKI-4905	69	Calpinactam		<i>M. tuberculosis</i>	12.5	16.3	2010	[54]
<i>M. smegmatis</i>					0.78	1.02	2010	[54]	
<i>N. spinosa</i> KKU-1NK1	70	1-Hydroxychevalone C		<i>M. tuberculosis</i> H37Ra	12.5	26.5	2016	[55]	

Table 2.2 (Continued). Fungal compounds with antimycobacterial activity.

Type of fungi	Fungal species	No.	Compound name	Compound structure	Inhibited pathogen	MIC		Year	Ref.
						$\mu\text{g/mL}$	μM		
Mushrooms and soil fungi	<i>Diaporthe</i> sp. BCC6140	71	Diaporthein B		<i>M. tuberculosis</i> H37Ra	3.1	8.51	2003	[56]

The lichenized fungus, *Trypethelium eluteriae* Spreng., was fermented for 240 days in malt-yeast extract to produce lactone (**62**), trypethelone (**63**) and 4'-hydroxy-8-methoxytrypethelone methyl ether (**64**), which had MIC values of 50, 12.5 and 50, respectively against *M. tuberculosis* H37Rv [47]. Lichenicolous fungi are still underexplored as sources of antimycobacterial agents, and thus studies in this area are very few.

2.2.5 Compounds from mushrooms (macrofungi), soil fungi and others

Mushrooms, also known as macrofungi, are distinct from their microfungi counterparts in that they produce visible sporocarps (fruiting bodies) which typically appear above the ground (epigeous), or below the ground (hypogeous). Several medicinal mushrooms and the pharmacological activities of their compounds have been widely reported [48,49]. Mushrooms belong to the phylum Basidiomycota and are predominantly found in soils of grasslands and forests as decomposers of organic matter. In agricultural soils, fungi from the phylum Ascomycota has been found to be predominant [50]. Fresh fruiting bodies of the macro-fungus *Scleroderma citrinum* KMILT-SCL01, were extracted with methanol and later fractionated to obtain 4,4'-dimethoxyvulpinic acid (**65**) which had an MIC of 25 µg/mL against *M. tuberculosis* H37Ra [51].

Two lanostane triterpenes, astradoric acids A and B (**66** and **67**), isolated from an edible mushroom, *Astraeus odoratus* collected in Thailand, were found to have MIC values of 50 and 25 µg/mL, respectively against *M. tuberculosis* H37Rv [52]. The fruiting body of the mushroom, *Ramaria cythiophora*, was subjected to a series of extraction and purification steps to yield ramariolide A (**68**) [53]. The MIC values of ramariolide A (**68**) were found to be 8 and 64-128 µg/mL against *M. smegmatis* and *M. tuberculosis*, respectively.

Mortierella alpina FKI-4905 was isolated from soil collected from the Bonin Islands in Japan, and was found to produce the peptide, calpinactam (**69**) [54]. The compound was tested against *M. smegmatis* and *M. tuberculosis* and the MIC values were found to be 0.78 and 12.5 µg/mL, respectively. A new meroterpenoid, 1-hydroxychevalone C (**70**), was isolated from a forest-soil fungus, *Neosartorya spinosa* KKKU-1NK1 [55].

Neosartorya species are the teleomorphic (sexual) state of the *Aspergillus* species and thus have been both found to have metabolites in common. 1-hydroxychevalone C (**70**) from *N. spinosa* KKU-1NK1 was found to have an MIC value of 12.5 µg/mL against *M. tuberculosis* H37Ra [55]. The fungus *Diaporthe* sp. BCC 6140 was isolated from an unidentified wood in Thailand and was found to produce a pimarane diterpene designated diaporthein B (**71**), which had an MIC value of 3.1 µg/mL against *M. tuberculosis* H37Ra [56].

2.2.6 Fungal compounds active against Mycobacterial enzymes

About half of the marketed drugs are profiled as enzyme inhibitors or inactivators [57]. This is clear evidence that mechanistic enzyme studies in drug discovery are increasingly being used for hit-identification and validation of enzyme-targeted drugs. [58]. Existence of substrate binding pockets and the inherent nature of enzymes to catalyze reactions, both make enzymes druggable targets. Furthermore, some enzymes are uniquely expressed by *M. tuberculosis* and thus allow for selectivity. The data generated from enzyme assays can be used to guide lead optimization [57].

Mycobacterial protein tyrosine phosphatase A and B (MtpA and MtpB) are two interesting enzymes which selectively dephosphorylate human host signalling proteins, and thus have been identified as attractive targets in TB-drug discovery [59]. They are secreted by *M. tuberculosis* in phagosomes and are translocated to the cytosol of macrophages, where MtpA binds to the H subunit of V-ATPase to selectively restrict to catalytic substrate (VPS33B) which is found on the phagosome-lysosome fusion region [59]. The dephosphorylation of VPS33B is accompanied by a failure of the macrophage in forming the phagolysosome. At the same time, MtpB's activity in the cytosol leads to increased phosphorylation of Akt and decreased phosphorylation of p38, thus leading to reduced apoptosis and increased necrosis [59].

Several fungal compounds have been reported to exhibit activity against MtpA and MtpB. *Fusarium graminearum* SYSU-MS5127, a fungus isolated from an anemone and cultivated in rice medium produced fusarielin M (**72**) which was tested against MtpB [60]. Both the inhibition constant (K_i) and half-maximal inhibitory concentration (IC_{50}) were found to be 0.4 µg/mL (See

Table 2.2). Fusarielin M (**72**) proved efficacious against intracellular *M. bovis* BCG in infected J774A.1 macrophage cells, where treatment with the compound resulted in a 62% decrease of bacterial load burden without significant macrophage cytotoxicity [60]. An MIC value of 12.3 µg/mL was reported after testing against *M. tuberculosis* H37Ra [60].

Asperlones A and B (**73** and **74**) and mitorubrin (**75**) were isolated from mangrove endophytic fungus *Aspergillus* sp. 16-5C and exhibited strong inhibitory activity against MptpB, with IC₅₀ values between 1.5-1.6 µg/mL for the three metabolites [61]. Peniphenones B and C (**76** and **77**) were isolated from *Penicillium dipodomyicola*, an endophyte of mangrove *Acanthus ilicifolius*, collected from the South China Sea [62]. The two compounds (**76** and **77**) were found to have strong inhibitory activity against MptpB with IC₅₀ values of 6.37 and 0.45 µg/mL respectively.

Chemical analysis of a marine-sponge derived fungus from the East China sea, *Aspergillus sydowii* MF357, resulted in the identification of sydowiols A and C (**78** and **79**) with weak bioactivity against *M. bovis* BCG and *M. tuberculosis* H37Rv, both compounds recording an MIC value of > 50 µg/mL on both cell lines [63]. However, sydowiols A and C (**78** and **79**) were more effective in inhibiting *M. tuberculosis* protein tyrosine phosphatase A (MptpA), with IC₅₀ values of 14 and 24 µg/mL respectively for the two metabolites [63].

Mycobacterial proteasome is a protease which degrades intracellular proteins and has been validated as therapeutic target. Mycobacterial proteasome has been reported to offer protection from nitric oxide effects to the microbe [64,65]. In one study, fellutamide B (**80**) (originally isolated from *Penicillium fellutanum*) was found to effectively inhibit the Mycobacterial proteasome by binding to the active site in a time dependent and single step mechanism, with the *K_i* found to be 0.004 µg/mL [66].

2.3 Chemically modified fungal compounds

Synthetic chemical modification of natural products in drug discovery allows for tailor-made modifications of compound structures that could lead to successful medicinal drugs. Regrettably,

isolation and bioactivity studies of secondary metabolites are seldom conducted together with synthetic modifications even though all three stages are mutually beneficial. Combining these three stages undoubtedly accelerates discovery of compounds with novel antimycobacterial activity [67].

Pleuromutilin (**81**) was first reported in 1951 from extracts of Basidiomycetes *Pleurotus mutilus* and *Pleurotus passeckerianus* (now *Clitopilus passeckerianus*) and was shown to possess a significant antibiotic effect against *M. smegmatis* with a MIC of 32 µg/mL [68]. In a more recent study, four pleuromutilin D-leucine derivatives, UT-800, UT-810, UT-815 and UT-820 (**82-85**), which differed in the oxidation states of their C₃-carbonyl and C₁₂-vinyl groups exhibited MIC values ranging between 0.78–3.06 µg/mL against *M. tuberculosis* H37Rv, with UT-815 (**84**) showing the greatest MIC of 0.78 µg/mL [69]. Valnemulin (**86**), also a synthetic derivative of pleuromutilin (**81**) which is currently approved for treatment of a broad range of bacterial infections in animals exhibited antimycobacterial activity with a MIC value of 3.13 µg/mL in the same study [69]. Lefamulin (**87**) is another derivative of pleuromutilin (**81**) which is currently approved for treatment of community acquired pneumonia. In antimycobacterial studies involving clinical strains of rapid growing Mycobacteria, lefamulin (**87**) was found to have an MIC value of 16 µg/mL against 11 out of 30 *Mycobacterium abscessus* subsp. *abscessus* strains, an MIC value of 32 µg/mL against 15 out of 30 *M. abscessus* subsp. *massiliense* strains, and an MIC value of 16 µg/mL against all three *M. abscessus* subsp. *bolletii* strains used in the study (see Table 2.3) [70].

Methyl 4,4'-dimethoxyvulpinate (**88**) and 4,4'-dimethoxyvulpinic acid (**89**) were obtained from *S. citrinum* KMILT-SCL01 and subjected to synthetic modifications by bromination, methylation and acetylation to yield methyl 3,3'-dibromo-4,4'-dimethoxyvulpinate (**90**), 3,3'-dibromo-4,4'-dimethoxyvulpinic acid (**91**) and acetyl 4,4'-dimethoxyvulpinate (**92**) [51]. 3,3'-dibromo-4,4'-dimethoxyvulpinate (**90**) (derivative of **88**) was found to be inactive against *M. tuberculosis* H37Ra at 200 µg/mL, while **91** and **92** (derivatives of **91**) exhibited weak activity with a MIC of 100 µg/mL [51].

Ganoderma australe BCC 22314 naturally produces a wide variety of lanostane triterpenoids, one of these being a (24*E*)-3 β -acetoxy-15 α -hydroxy lanosta-7,9(11),24-trien-26-oic acid (also known as ganodermic acid T-O) (**93**) which was modified by an acylation reaction with propionyl chloride to produce (24*E*)-3 β -acetoxy-15 α -propionyloxy lanosta-7,9(11),24-trien-26-oic acid (also referred to as GA003) (**94**) [71]. GA003 (**94**) was tested against *M. tuberculosis* H37Ra and the MIC value was found to be 0.098 μ g/mL [71]. An oversight in this study is that naturally occurring ganodermic acid T-O (**93**) was not tested for antimycobacterial activity.

Aspergillus versicolor CHNSCLM-0063 was isolated from the coral *Rumphella aggregata* and fermented on rice solid medium to produce asperversiamide A (**95**) which exhibited an MIC of 10.5 μ g/mL against *M. marinum* [72,73]. Synthetic modifications involving the reacting asperversiamide A (**95**) with cinnamic acid derivatives in the presence of 4-(dimethylamino)pyridine (DAMP) and ethylene diamine hydrochloride (EDA-HCL) in dichloromethane were performed [73]. Eighteen new derivatives were synthesized and tested for antimycobacterial activity against *M. tuberculosis* H37Ra, four unnamed derivatives (**96-99**) displayed activity with MIC values of 13.9 and 56.2 μ g/mL for derivatives **96** and **97**, and 13.3 μ g/mL for derivatives **98** and **99** [73].

2.4 Mycogenic nanoparticles

Nanoparticles are particles with two or more dimensions with a size range of 1 nm to 100 nm [74]. Research and application of nanomaterials has gained prominence due to their tunable chemical, physical and biological properties which enhances their performance with respect to their bulk analogues [75–77]. As such, nanomaterials have found several biomedical applications which include drug delivery and targeting, *in vivo* and *in vitro* diagnostics, gene manipulations and immunomodulation [78].

Table 2.3. Fungal compounds tested against Mycobacterial enzymes.

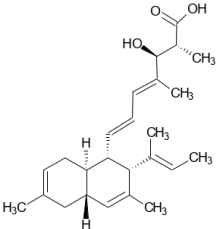
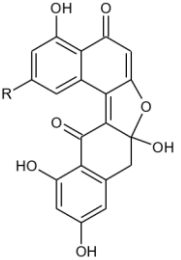
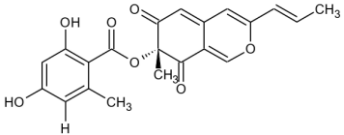
Fungal species	No.	Compound name	Compound structure	Enzyme	IC ₅₀		K _i		Year	Ref.
					µg/mL	µM	µg/mL	µM		
<i>F. graminearum</i> SYSU-MS5127	72	Fusarielin M		MptpB	0.40	1.05	0.40	1.03	2021	[60]
	73	Asperlone A		MptpB	1.54	4.24	No data		2015	[61]
	74	Asperlone B		MptpB	1.64	4.32	No data		2015	[61]
<i>Aspergillus</i> sp. 16-5C			73. R = H 74. R = OH							
	75	Mitorubrin		MptpB	1.53	3.99	No data		2015	[61]

Table 2.3 (Continued). Fungal compounds tested against Mycobacteria enzymes.

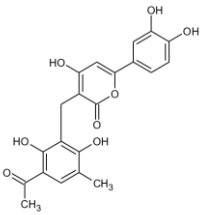
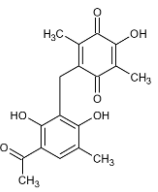
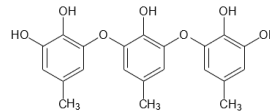
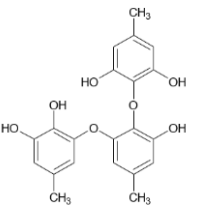
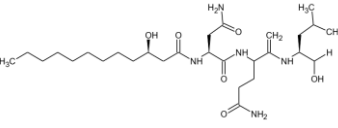
Fungal species	No.	Compound name	Compound structure	Enzyme	IC ₅₀		K _i		Year	Ref.
					μg/mL	μM	μg/mL	μM		
	76	Peniphenone B		MptpB	6.37	16	No data		2014	[62]
<i>P. dipodomyicola</i>	77	Peniphenone C		MptpB	0.45	1.37	No data		2014	[62]
	78	Sydowiol A		MptpA	14	36.4	No data		2013	[63]
<i>A. sydowii</i> MF357	79	Sydowiol C		MptpA	24	62.4	No data		2013	[63]
<i>P. fellutanum</i>	80	Fellutamide B		Proteasome	No data		0.004	0.0068	2010	[66]

Table 2.4. Fungal compounds modified using chemical (semi-) synthesis and their antimycobacterial activity.

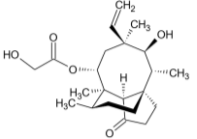
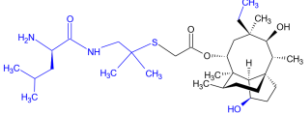
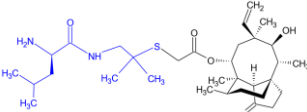
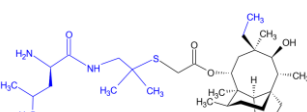
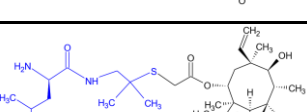
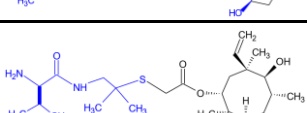
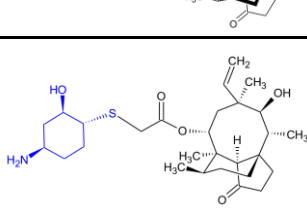
Fungal species	No.	Compound name	Compound type	Compound structure	Inhibited pathogen	MIC		Year	Ref.
						$\mu\text{g/mL}$	μM		
	81	Pleuromutilin	Natural		<i>M. smegmatis</i>	32	84.5	1951	[68]
	82	UT-800	Derivative of 81		<i>M. tuberculosis</i> H37Rv	0.83	1.55	2018	[69]
	83	UT-810	Derivative of 81		<i>M. tuberculosis</i> H37Rv	1.56	2.94	2018	[69]
<i>P. mutilus</i> ; <i>C. passeckerianus</i>	84	UT-815	Derivative of 81		<i>M. tuberculosis</i> H37Rv	0.78	1.46	2018	[69]
	85	UT-820	Derivative of 81		<i>M. tuberculosis</i> H37Rv	3.06	5.74	2018	[69]
	86	Valnemulin	Derivative of 81		<i>M. tuberculosis</i> H37Rv	3.13	5.54	2018	[69]
	87	Lefamulin	Derivative of 81		<i>M. abscessus</i> subsp. <i>abscessus</i> <i>M. abscessus</i> subsp. <i>massiliense</i> <i>M. abscessus</i> subsp. <i>bolletii</i>	≈ 16 ≈ 32 16	≈ 31.5 ≈ 63.0 31.5	2021	[70]

Table 2.4 (Continued). Fungal compounds modified using chemical (semi-) synthesis and their antimycobacterial activity.

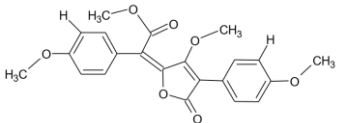
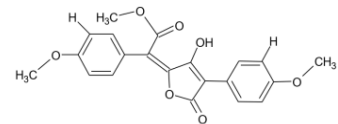
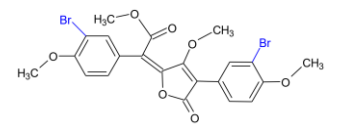
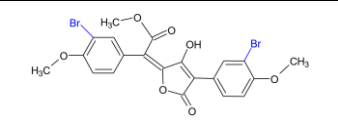
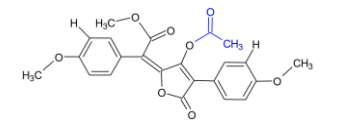
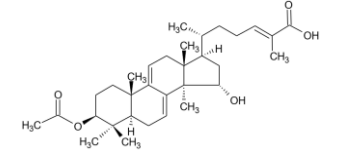
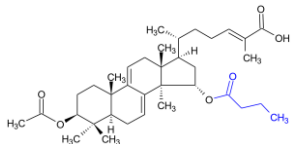
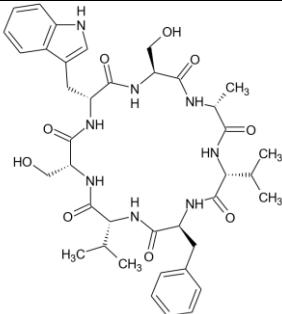
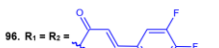
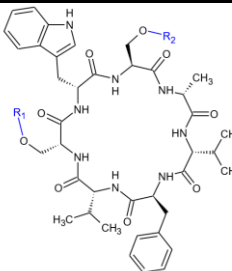

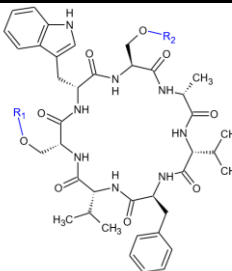

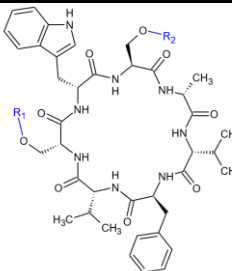
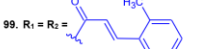
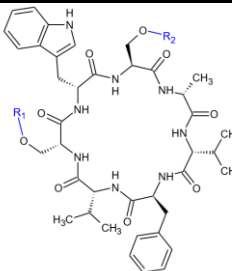
Fungal species	No.	Compound name	Compound type	Compound structure	Inhibited pathogen	MIC		Year	Ref.
						$\mu\text{g/mL}$	μM		
<i>S. citrinum</i> KMILT-SCL01	88	Methyl 4,4'-dimethoxyvulpinate	Natural		<i>M. tuberculosis</i> H37Ra	> 200	> 504	2003	[51]
	89	4,4'-dimethoxyvulpinic acid	Natural		<i>M. tuberculosis</i> H37Ra	25	65.4	2003	[51]
	90	Methyl 3,3'-dibromo-4,4'-dimethoxyvulpinate	Derivative of 88		<i>M. tuberculosis</i> H37Ra	> 200	> 361	2003	[51]
	91	3,3'-dibromo-4,4'-dimethoxyvulpinic acid	Derivative of 89		<i>M. tuberculosis</i> H37Ra	100	185	2003	[51]
	92	Acetyl 4,4'-dimethoxyvulpinate	Derivative of 89		<i>M. tuberculosis</i> H37Ra	100	235	2003	[51]
<i>G. australe</i> BCC 22314	93	Ganodermic acid T-O	Natural		No data provided			2021	[71]

Table 2.4 (Continued). Fungal compounds modified using chemical (semi-) synthesis and their antimycobacterial activity.

Fungal species	No.	Compound name	Compound type	Compound structure	Inhibited pathogen	MIC		Year	Ref.
						$\mu\text{g/mL}$	μM		
<i>G. australe</i> BCC 22314	94	GA003	Derivative of 93		<i>M. tuberculosis</i> H37Ra	0.39	0.69	2021	[71]
<i>A. versicolor</i> CHNSCLM-0063	95	Asperversiamide A	Natural		<i>M. tuberculosis</i> H37Ra <i>M. marinum</i>	> 77.7 18.6	> 100 24	2021 2019	[73] [72]
	96	Derivative 9			<i>M. tuberculosis</i> H37Ra	13.9	12.5	2021	[73]
	97	Derivative 12			<i>M. tuberculosis</i> H37Ra	56.2	50	2021	[73]
	98	Derivative 23			<i>M. tuberculosis</i> H37Ra	13.3	12.5	2021	[73]
	99	Derivative 24			<i>M. tuberculosis</i> H37Ra	13.3	12.5	2021	[73]

Metallic nanoparticles, as their name suggests, contain an inorganic metal at their core. They are commonly explored for their antimicrobial properties which include the ability to trigger the production of ROS, interact and destabilize the membrane potential and interact with biomolecules such as DNA, ribosomes, proton efflux pumps, enzymes which regulate processes such as ATP synthesis and proteins involved in the electron transport chain [79]. Popular metallic nanoparticles used as antimicrobial agents include gold (Au), silver (Ag), copper (Cu), zinc oxide (ZnO) and iron oxide (Fe_2O_3 and Fe_3O_4) and bimetallic magnesium aluminum oxide (MgAl_2O_4) [80].

The use of fungi to synthesize nanoparticles is a “green synthesis” approach which is gaining momentum and is being used to overcome the limitations of chemical synthesis which requires the use of highly toxic reducing and stabilizing agents, sometimes generating nanoparticles which are also highly toxic and prone to aggregation [81]. Mycogenic synthesis of metal nanoparticles is usually performed by exposing the fungal extracts/secondary metabolites to a metal salt under specified conditions. Intracellular (within the microbial cells) or extracellular synthesis (in growth media outside the cells) of nanoparticles can be achieved, the latter is preferred as harvesting the nanoparticles is easier. The use of culture filtrate which is mixed with a metal salt is also common, this reduces complications in harvesting intracellular nanoparticles. The exact mechanism is often unclear, however reducing enzymes such as NADH- and NADPH-dependent reductases, nitrate and nitrite reductases, and non-enzyme proteins and peptides with metallo-interaction activities are thought to participate in the reduction of M^{n+} to M^0 , thus resulting in nanoparticles [82]. Stabilization of the newly formed nanoparticles is then achieved by fungal secondary metabolites and proteins.

A few specific examples of mycosynthesis of metallic nanoparticles for antimycobacterial applications exist in literature. In one study, silver nitrate (AgNO_3) was reduced using the crude enzymes in the broth filtrate from cultures of the *Rhizopus stolonifera* to produce stable and

predominantly spherical Ag nanoparticles (**100**) with a size range between 3-20 nm [83]. These Ag nanoparticles (**100**) were tested against *M. tuberculosis* (clinical strain), an MIC value of 12.5 µg/mL was reported. In another study, extracts from commercial yeast (*Saccharomyces cerevisiae*) were used to synthesize spherical silver chloride (AgCl) nanoparticles (**101**) which were found to be approximately 17 nm in size [84]. The AgCl nanoparticles (**101**) had an MIC value of 37 µg/mL against *M. smegmatis* mc²155 and *M. tuberculosis* H37Rv.

Instead of using fungi to synthesize and stabilize nanoparticles, there have been times when fungal derived compounds and their derivatives have been used in modifying, capping or stabilizing chemically synthesized nanoparticles. An interesting case is that of the antibiotic ampicillin, a β-lactam derivative of a *Penicillium* sp. metabolite (benzylpenicillin) which has been modified by the addition of an amino group, was conjugated on gold nanoparticles (AuNPs) nucleated on self-assembled PEGylated rosette nanotubes (Amp-AuNPs-RNT) and utilized in antimicrobial studies [85].

Significant work has been done in the synthesis of nanoparticles using fungi for medical and industrial applications [86], however their application as antimicrobial agents against *M. tuberculosis* has been limited. Mycogenic metallic nanoparticles present opportunities that may potentially lead to the development of anti-TB nanodrugs.

2.5 Conclusions

Robust anti-TB drug discovery studies are crucial for the discovery of new compounds with antimycobacterial activity. Previous studies have shown that fungi are a reservoir of structurally diverse and biologically active secondary metabolites which may be explored to discover novel anti-TB drugs. A total of 82 fungal derived compounds and their semi-synthetic derivatives were presented in this review. A total of six fungal compounds were reported to have MIC values of ≤ 2 µg/mL against *M. tuberculosis*, namely diaporthone B (**21**),

phomoxanthone A (**22**), enniatin A1 (**29**), trichoderin A (**33**), trichoderin B (**35**) and MK1688 (**50**). Derivatives UT-800 (**82**), UT-815 (**83**), UT-815 (**84**) and GA003 (**94**) were also found to exhibit excellent antimycobacterial activity with MIC values of ≤ 2 $\mu\text{g/mL}$. Even though mycogenic synthesis of metallic nanoparticles has had application in both industrial and biomedical research, there is still a gap in exploring mycogenic synthesis for antimycobacterial studies. After careful consideration of the studies presented in this review, the authors concluded that the fungal kingdom is truly a reservoir of bioactive compounds which have the potential to become drivers of TB-drug discovery. Furthermore, mycogenic synthesis presents opportunities for the development of truly novel and efficacious TB-drugs of the future.

2.6 References

1. Barberis, I.; Bragazzi, N.L.; Galluzzo, L.; Martini, M. The History of Tuberculosis: From the First Historical Records to the Isolation of Koch's Bacillus. *J. Prev. Med. Hyg.* **2017**, *58*, E9–E12.
2. WHO Tuberculosis 18 January 2018 | Q&A Available online: <https://www.who.int/news-room/q-a-detail/tuberculosis> (accessed on 17 December 2020).
3. WHO *Global Tuberculosis Report 2021*; World Health Organization: Geneva, 2021.
4. WHO *Guidelines for Treatment of Tuberculosis*; 4th ed.; World Health Organization: Geneva, 2010; ISBN 978-92-4-154783-3.
5. Sotgiu, G.; Centis, R.; D'ambrosio, L.; Migliori, G.B. Tuberculosis Treatment and Drug Regimens. *Cold Spring Harb. Perspect. Med.* **2015**, *5*, 1–13, doi:10.1101/cshperspect.a017822.
6. Miesel, L.; Rozwarski, D.A.; Sacchettini, J.C.; Jacobs Jr, W.R. Mechanisms for Isoniazid Action and Resistance. In *Genetics and Tuberculosis*; John Wiley & Sons, Ltd, 1998; pp. 209–221, ISBN 978-0-470-84652-0.
7. Sinha, P.; Srivastava, G.N.; Tripathi, R.; Mishra, M.N.; Anupurba, S. Detection of Mutations in the RpoB Gene of Rifampicin-Resistant *Mycobacterium tuberculosis* Strains Inhibiting Wild Type Probe Hybridization in the MTBDR plus Assay by DNA Sequencing Directly from Clinical Specimens. *BMC Microbiol.* **2020**, *20*, 1–8, doi:10.1186/s12866-020-01967-5.
8. Gopal, P.; Sarathy, J.P.; Yee, M.; Ragunathan, P.; Shin, J.; Bhushan, S.; Zhu, J.; Akopian, T.; Kandrор, O.; Lim, T.K.; et al. Pyrazinamide Triggers Degradation of Its Target

- Aspartate Decarboxylase. *Nat. Commun.* **2020**, *11*, 1–10, doi:10.1038/s41467-020-15516-1.
9. Ramirez-Busby, S.M.; Rodwell, T.C.; Fink, L.; Catanzaro, D.; Jackson, R.L.; Pettigrove, M.; Catanzaro, A.; Valafar, F. A Multinational Analysis of Mutations and Heterogeneity in PZase, RpsA, and PanD Associated with Pyrazinamide Resistance in M/XDR *Mycobacterium tuberculosis*. *Sci. Rep.* **2017**, *7*, 1–9, doi:10.1038/s41598-017-03452-y.
 10. Goude, R.; Amin, A.G.; Chatterjee, D.; Parish, T. The Arabinosyltransferase EmbC is Inhibited by Ethambutol in *Mycobacterium tuberculosis*. *Antimicrob. Agents Chemother.* **2009**, *53*, 4138–4146, doi:10.1128/AAC.00162-09.
 11. Hards, K.; Robson, J.R.; Berney, M.; Shaw, L.; Bald, D.; Koul, A.; Andries, K.; Cook, G.M. Bactericidal Mode of Action of Bedaquiline. *J. Antimicrob. Chemother.* **2015**, *70*, 2028–2037, doi:10.1093/jac/dkv054.
 12. Degiacomi, G.; Sammartino, J.C.; Sinigiani, V.; Marra, P.; Urbani, A.; Pasca, M.R. *In vitro* Study of Bedaquiline Resistance in *Mycobacterium tuberculosis* Multi-Drug Resistant Clinical Isolates. *Front. Microbiol.* **2020**, *11*, 1–8, doi:10.3389/fmicb.2020.559469.
 13. Purwantini, E.; Mukhopadhyay, B. *Rv0132c* of *Mycobacterium tuberculosis* Encodes a Coenzyme F420-Dependent Hydroxymycolic Acid Dehydrogenase. *PLOS ONE* **2013**, *8*, 1–9, doi:10.1371/journal.pone.0081985.
 14. Singh, R.; Manjunatha, U.; Boshoff, H.I.M.; Ha, Y.H.; Niyomrattanakit, P.; Ledwidge, R.; Dowd, C.S.; Lee, I.Y.; Kim, P.; Zhang, L.; et al. PA-824 Kills Nonreplicating *Mycobacterium tuberculosis* by Intracellular NO Release. *Science* **2008**, *322*, 1392–1395, doi:10.1126/science.1164571.

15. Zahedi Bialvaei, A.; Rahbar, M.; Yousefi, M.; Asgharzadeh, M.; Samadi Kafil, H. Linezolid: A Promising Option in the Treatment of Gram-Positives. *J. Antimicrob. Chemother.* **2017**, *72*, 354–364, doi:10.1093/jac/dkw450.
16. Wasserman, S.; Louw, G.; Ramangoela, L.; Barber, G.; Hayes, C.; Omar, S.V.; Maartens, G.; Barry, C., III; Song, T.; Meintjes, G. Linezolid Resistance in Patients with Drug-Resistant TB and Treatment Failure in South Africa. *J. Antimicrob. Chemother.* **2019**, *74*, 2377–2384, doi:10.1093/jac/dkz206.
17. Ruiz, P.; Rodríguez-Cano, F.; Zerolo, F.J.; Casal, M. Investigation of the in Vitro Activity of Streptomycin against *Mycobacterium tuberculosis*. *Microb. Drug Resist. Larchmt. N* **2002**, *8*, 147–149, doi:10.1089/107662902760190707.
18. Jugheli, L.; Bzekalava, N.; Rijk, P. de; Fissette, K.; Portaels, F.; Rigouts, L. High Level of Cross-Resistance between Kanamycin, Amikacin, and Capreomycin among *Mycobacterium tuberculosis* Isolates from Georgia and a Close Relation with Mutations in the *Rrs* Gene. *Antimicrob. Agents Chemother.* **2009**, *53*, 5064-5068, doi:10.1128/AAC.00851-09.
19. Khoshnood, S.; Taki, E.; Sadeghifard, N.; Kaviar, V.H.; Haddadi, M.H.; Farshadzadeh, Z.; Kouhsari, E.; Goudarzi, M.; Heidary, M. Mechanism of Action, Resistance, Synergism, and Clinical Implications of Delamanid Against Multidrug-Resistant *Mycobacterium tuberculosis*. *Front. Microbiol.* **2021**, *12*, 1–13, doi:10.3389/fmicb.2021.717045.
20. Cholo, M.C.; Mothiba, M.T.; Fourie, B.; Anderson, R. Mechanisms of Action and Therapeutic Efficacies of the Lipophilic Antimycobacterial Agents Clofazimine and Bedaquiline. *J. Antimicrob. Chemother.* **2017**, *72*, 338–353, doi:10.1093/jac/dkw426.

21. Nimmo, C.; Millard, J.; Dorp, L. van; Brien, K.; Moodley, S.; Wolf, A.; Grant, A.D.; Padayatchi, N.; Pym, A.S.; Balloux, F.; et al. Population-Level Emergence of Bedaquiline and Clofazimine Resistance-Associated Variants among Patients with Drug-Resistant Tuberculosis in Southern Africa: A Phenotypic and Phylogenetic Analysis. *Lancet Microbe* **2020**, *1*, e165–e174, doi:10.1016/S2666-5247(20)30031-8.
22. Aldred, K.J.; Blower, T.R.; Kerns, R.J.; Berger, J.M.; Osheroff, N. Fluoroquinolone Interactions with *Mycobacterium tuberculosis* Gyrase: Enhancing Drug Activity against Wild-Type and Resistant Gyrase. *Proc. Natl. Acad. Sci. U.S.A.* **2016**, *113*, E839-E846, doi:10.1073/pnas.1525055113.
23. Rokas, A.; Wisecaver, J.H.; Lind, A.L. The Birth, Evolution and Death of Metabolic Gene Clusters in Fungi. *Nat. Rev. Microbiol.* **2018**, *16*, 731–744, doi:10.1038/s41579-018-0075-3.
24. Jakubczyk, D.; Dussart, F. Selected Fungal Natural Products with Antimicrobial Properties. *Molecules* **2020**, *25*, 1–18, doi:10.3390/molecules25040911.
25. Gouda, S.; Das, G.; Sen, S.K.; Shin, H.-S.; Patra, J.K. Endophytes: A Treasure House of Bioactive Compounds of Medicinal Importance. *Front. Microbiol.* **2016**, *7*, 1–8, doi:10.3389/fmicb.2016.01538.
26. Sommart, U.; Rukachaisirikul, V.; Sukpondma, Y.; Phongpaichit, S.; Sakayaroj, J.; Kirtikara, K. Hydronaphthalenones and a Dihydroramulosin from the Endophytic Fungus PSU-N24. *Chem. Pharm. Bull. (Tokyo)* **2008**, *56*, 1687–1690, doi:10.1248/cpb.56.1687.
27. Bungihan, M.E.; Tan, M.A.; Kitajima, M.; Kogure, N.; Franzblau, S.G.; dela Cruz, T.E.E.; Takayama, H.; Nonato, M.G. Bioactive Metabolites of *Diaporthe* sp. P133, an

- Endophytic Fungus Isolated from *Pandanus Amaryllifolius*. *J. Nat. Med.* **2011**, *65*, 606–609, doi:10.1007/s11418-011-0518-x.
28. Isaka, M.; Jaturapat, A.; Rukseree, K.; Danwisetkanjana, K.; Tanticharoen, M.; Thebtaranonth, Y. Phomoxanthonones A and B, Novel Xanthone Dimers from the Endophytic Fungus *Phomopsis* Species. *J. Nat. Prod.* **2001**, *64*, 1015–1018, doi:10.1021/np010006h.
29. Wijeratne, E.M.K.; He, H.; Franzblau, S.G.; Hoffman, A.M.; Gunatilaka, A.A.L. Phomapyrrolidones A–C, Antitubercular Alkaloids from the Endophytic Fungus *Phoma* sp. NRRL 46751. *J. Nat. Prod.* **2013**, *76*, 1860–1865, doi:10.1021/np400391p.
30. Ge, H.M.; Zhang, Q.; Xu, S.H.; Guo, Z.K.; Song, Y.C.; Huang, W.Y.; Tan, R.X. Chaetoglocins A–D, Four New Metabolites from the Endophytic Fungus *Chaetomium globosum*. *Planta Med.* **2011**, *77*, 277–280, doi:10.1055/s-0030-1250292.
31. Blais, L.A.; ApSimon, J.W.; Blackwell, B.A.; Greenhalgh, R.; Miller, J.D. Isolation and Characterization of Enniatins from *Fusarium avenaceum* DAOM 196490. *Can. J. Chem.* **1992**, *70*, 1281–1287, doi:10.1139/v92-165.
32. Wang, G.; Dong, W.; Lu, H.; Lu, W.; Feng, J.; Wang, X.; Chen, H.; Liu, M.; Tan, C. Enniatin A1, A Natural Compound with Bactericidal Activity against *Mycobacterium tuberculosis* *In vitro*. *Molecules* **2020**, *25*, 1–12, doi:10.3390/molecules25010038.
33. Kumar, V.; Sarma, V.V.; Thambugala, K.M.; Huang, J.-J.; Li, X.-Y.; Hao, G.-F. Ecology and Evolution of Marine Fungi With Their Adaptation to Climate Change. *Front. Microbiol.* **2021**, *12*, 1–12, 10.3389/fmicb.2021.719000.

34. Wang, C.; Wang, J.; Huang, Y.; Chen, H.; Li, Y.; Zhong, L.; Chen, Y.; Chen, S.; Wang, J.; Kang, J.; et al. Anti-Mycobacterial Activity of Marine Fungus-Derived 4-Deoxybostrycin and Nigrosporin. *Molecules* **2013**, *18*, 1728–1740, doi:10.3390/molecules18021728.
35. Sun, C.; Zhang, Z.; Ren, Z.; Yu, L.; Zhou, H.; Han, Y.; Shah, M.; Che, Q.; Zhang, G.; Li, D.; et al. Antibacterial Cyclic Tripeptides from Antarctica-Sponge-Derived Fungus *Aspergillus insulicola* HDN151418. *Mar. Drugs* **2020**, *18*, 532, doi:10.3390/md18110532.
36. Pruksakorn, P.; Arai, M.; Kotoku, N.; Vilchèze, C.; Baughn, A.D.; Moodley, P.; Jacobs, W.R.; Kobayashi, M. Trichoderins, Novel Aminolipopeptides from a Marine Sponge-Derived *Trichoderma* sp., are Active against Dormant Mycobacteria. *Bioorg. Med. Chem. Lett.* **2010**, *20*, 3658–3663, doi:10.1016/j.bmcl.2010.04.100.
37. Trisuwan, K.; Khamthong, N.; Rukachaisirikul, V.; Phongpaichit, S.; Preedanon, S.; Sakayaroj, J. Anthraquinone, Cyclopentanone, and Naphthoquinone Derivatives from the Sea Fan-Derived Fungi *Fusarium* spp. PSU-F14 and PSU-F135. *J. Nat. Prod.* **2010**, *73*, 1507–1511, doi:10.1021/np100282k.
38. Bamisile, B.S.; Akutse, K.S.; Siddiqui, J.A.; Xu, Y. Model Application of Entomopathogenic Fungi as Alternatives to Chemical Pesticides: Prospects, Challenges, and Insights for Next-Generation Sustainable Agriculture. *Front. Plant Sci.* **2021**, *12*, 1–21, doi: 10.3389/fpls.2021.741804.
39. Vongvanich, N.; Kittakoop, P.; Isaka, M.; Trakulnaleamsai, S.; Vimuttipong, S.; Tanticharoen, M.; Thebtaranonth, Y. Hirsutellide A, a New Antimycobacterial

- Cyclohexadepsipeptide from the Entomopathogenic Fungus *Hirsutella kobayasii*. *J. Nat. Prod.* **2002**, *65*, 1346–1348, doi:10.1021/np020055+.
40. Isaka, M.; Palasarn, S.; Sriklung, K.; Kocharin, K. Cyclohexadepsipeptides from the Insect Pathogenic Fungus *Hirsutella nivea* BCC 2594. *J. Nat. Prod.* **2005**, *68*, 1680–1682, doi:10.1021/np050246n.
41. Nilanonta, C.; Isaka, M.; Kittakoop, P.; Palittapongarnpim, P.; Kamchonwongpaisan, S.; Pittayakhajonwut, D.; Tanticharoen, M.; Thebtaranonth, Y. Antimycobacterial and Antiplasmodial Cyclodepsipeptides from the Insect Pathogenic Fungus *Paecilomyces tenuipes* BCC 1614. *Planta Med.* **2000**, *66*, 756–758, doi:10.1055/s-2000-9776.
42. Kornsakulkarn, J.; Thongpanchang, C.; Lapanun, S.; Srichomthong, K. Isocoumarin Glucosides from the Scale Insect Fungus *Torrubiella tenuis* BCC 12732. *J. Nat. Prod.* **2009**, *72*, 1341–1343, doi:10.1021/np900082h.
43. Nilanonta, C.; Isaka, M.; Chanphen, R.; Thong-orn, N.; Tanticharoen, M.; Thebtaranonth, Y. Unusual Enniatins Produced by the Insect Pathogenic Fungus *Verticillium hemipterigenum*: Isolation and Studies on Precursor-Directed Biosynthesis. *Tetrahedron* **2003**, *59*, 1015–1020, doi:10.1016/S0040-4020(02)01631-9.
44. Vongvilai, P.; Isaka, M.; Kittakoop, P.; Srikitikulchai, P.; Kongsaree, P.; Prabpai, S.; Thebtaranonth, Y. Isolation and Structure Elucidation of Enniatins L, M1, M2, and N: Novel Hydroxy Analogs. *Helv. Chim. Acta* **2004**, *87*, 2066–2073, doi:10.1002/hlca.200490185.
45. Eymann, C.; Lassek, C.; Wegner, U.; Bernhardt, J.; Fritsch, O.A.; Fuchs, S.; Otto, A.; Albrecht, D.; Schiefelbein, U.; Cernava, T.; et al. Symbiotic Interplay of Fungi, Algae, and Bacteria within the Lung Lichen *Lobaria pulmonaria* L. Hoffm. as Assessed by State-

- of-the-Art Metaproteomics. *J. Proteome Res.* **2017**, *16*, 2160–2173, doi:10.1021/acs.jproteome.6b00974.
46. Seephonkai, P.; Isaka, M.; Kittakoop, P.; Palittapongarnpim, P.; Kamchonwongpaisan, S.; Tanticharoen, M.; Thebtaranonth, Y. Evaluation of Antimycobacterial, Antiplasmodial and Cytotoxic Activities of Preussomerins Isolated from the Lichenicolous Fungus *Microsphaeropsis* sp. BCC 3050. *Planta Med.* **2002**, *68*, 45–48, doi:10.1055/s-2002-20055.
47. Srinivasan, M.; Shanmugam, K.; Kedike, B.; Narayanan, S.; Shanmugam, S.; Gopalsamudram, N.H. Trypethelone and Phenalenone Derivatives Isolated from the Mycobiont Culture of *Trypethelium eluteriae* Spreng. and Their Anti-Mycobacterial Properties. *Nat. Prod. Res.* **2020**, *34*, 3320–3327, doi:10.1080/14786419.2019.1566823.
48. Beelman, R.B.; Kalaras, M.D.; Richie, J.P.J. Micronutrients and Bioactive Compounds in Mushrooms: A Recipe for Healthy Aging? *Nutr. Today* **2019**, *54*, 16–22, doi:10.1097/NT.0000000000000315.
49. Venturella, G.; Ferraro, V.; Cirlincione, F.; Gargano, M.L. Medicinal Mushrooms: Bioactive Compounds, Use, and Clinical Trials. *Int. J. Mol. Sci.* **2021**, *22*, 1–30, doi:10.3390/ijms22020634.
50. Frąc, M.; Hannula, S.E.; Bełka, M.; Jędryczka, M. Fungal Biodiversity and Their Role in Soil Health. *Front. Microbiol.* **2018**, *9*, 1–9, doi:10.3389/fmicb.2018.00707.
51. Kanokmedhakul, S.; Kanokmedhakul, K.; Prajuabsuk, T.; Soyong, K.; Kongsaree, P.; Suksamrarn, A. A Bioactive Triterpenoid and Vulpinic Acid Derivatives from the Mushroom *Scleroderma citrinum*. *Planta Med.* **2003**, *69*, 568–571, doi:10.1055/s-2003-40639.

52. Arpha, K.; Phosri, C.; Suwannasai, N.; Mongkolthanaruk, W.; Sodngam, S. Astraodoric Acids A–D: New Lanostane Triterpenes from Edible Mushroom *Astraeus odoratus* and Their Anti-*Mycobacterium tuberculosis* H37Ra and Cytotoxic Activity. *J. Agric. Food Chem.* **2012**, *60*, 9834–9841, doi:10.1021/jf302433r.
53. Centko, R.M.; Ramón-García, S.; Taylor, T.; Patrick, B.O.; Thompson, C.J.; Miao, V.P.; Andersen, R.J. Ramariolides A–D, Antimycobacterial Butenolides Isolated from the Mushroom *Ramaria cystidiophora*. *J. Nat. Prod.* **2012**, *75*, 2178–2182, doi:10.1021/np3006277.
54. Koyama, N.; Kojima, S.; Fukuda, T.; Nagamitsu, T.; Yasuhara, T.; Ōmura, S.; Tomoda, H. Structure and Total Synthesis of Fungal Calpinactam, A New Antimycobacterial Agent. *Org. Lett.* **2010**, *12*, 432–435, doi:10.1021/ol902553z.
55. Rajachan, O.; Kanokmedhakul, K.; Sanmanoch, W.; Boonlue, S.; Hannongbua, S.; Saparpakorn, P.; Kanokmedhakul, S. Chevalone C Analogues and Globoscinic Acid Derivatives from the Fungus *Neosartorya spinosa* KKU-1NK1. *Phytochemistry* **2016**, *132*, 68–75, doi:10.1016/j.phytochem.2016.09.008.
56. Dettrakul, S.; Kittakoop, P.; Isaka, M.; Nopichai, S.; Suyarnsestakorn, C.; Tanticharoen, M.; Thebtaranonth, Y. Antimycobacterial Pimarane Diterpenes from the Fungus *Diaporthe* sp. *Bioorg. Med. Chem. Lett.* **2003**, *13*, 1253–1255, doi:10.1016/S0960-894X(03)00111-2.
57. Holdgate, G.A.; Meek, T.D.; Grimley, R.L. Mechanistic Enzymology in Drug Discovery: A Fresh Perspective. *Nat. Rev. Drug Discov.* **2018**, *17*, 115–132, doi:10.1038/nrd.2017.219.

58. Robertson, J.G. Mechanistic Basis of Enzyme-Targeted Drugs. *Biochemistry* **2005**, *44*, 5561–5571, doi:10.1021/bi050247e.
59. Ruddraraju, K.V.; Aggarwal, D.; Zhang, Z.-Y. Therapeutic Targeting of Protein Tyrosine Phosphatases from *Mycobacterium tuberculosis*. *Microorganisms* **2021**, *9*, 1–13, doi:10.3390/microorganisms9010014.
60. Chen, D.; Liu, L.; Lu, Y.; Chen, S. Identification of Fusarielin M as a Novel Inhibitor of *Mycobacterium tuberculosis* Protein Tyrosine Phosphatase B (MtpB). *Bioorganic Chem.* **2021**, *106*, 1–9, doi:10.1016/j.bioorg.2020.104495.
61. Xiao, Z.; Lin, S.; Tan, C.; Lu, Y.; He, L.; Huang, X.; She, Z. Asperlones A and B, Dinaphthalenone Derivatives from a Mangrove Endophytic Fungus *Aspergillus* sp. 16-5C. *Mar. Drugs* **2015**, *13*, 366–378, doi:10.3390/md13010366.
62. Li, H.; Jiang, J.; Liu, Z.; Lin, S.; Xia, G.; Xia, X.; Ding, B.; He, L.; Lu, Y.; She, Z. Peniphenones A–D from the Mangrove Fungus *Penicillium dipodomyicola* HN4-3A as Inhibitors of *Mycobacterium tuberculosis* Phosphatase MtpB. *J. Nat. Prod.* **2014**, *77*, 800–806, doi:10.1021/np400880w.
63. Liu, X.; Song, F.; Ma, L.; Chen, C.; Xiao, X.; Ren, B.; Liu, X.; Dai, H.; Piggott, A.M.; Av-Gay, Y.; et al. Sydowiols A–C: *Mycobacterium tuberculosis* Protein Tyrosine Phosphatase Inhibitors from an East China Sea Marine-Derived Fungus, *Aspergillus sydowii*. *Tetrahedron Lett.* **2013**, *54*, 6081–6083, doi:10.1016/j.tetlet.2013.08.137.
64. Jamaati, H.; Mortaz, E.; Pajouhi, Z.; Folkerts, G.; Movassaghi, M.; Moloudizargari, M.; Adcock, I.M.; Garssen, J. Nitric Oxide in the Pathogenesis and Treatment of Tuberculosis. *Front. Microbiol.* **2017**, *8*, 1–11, doi:10.3389/fmicb.2017.02008.

65. Darwin, K.H.; Ehrt, S.; Gutierrez-Ramos, J.-C.; Weich, N.; Nathan, C.F. The Proteasome of *Mycobacterium tuberculosis* Is Required for Resistance to Nitric Oxide. *Science* **2003**, *302*, 1963–1966, doi:10.1126/science.1091176.
66. Lin, G.; Li, D.; Chidawanyika, T.; Nathan, C.; Li, H. Fellutamide B Is a Potent Inhibitor of the *Mycobacterium tuberculosis* Proteasome. *Arch. Biochem. Biophys.* **2010**, *501*, 214–220, doi:10.1016/j.abb.2010.06.009.
67. Kuroda, Y.; Nicacio, K.J.; da Silva-Jr, I.A.; Leger, P.R.; Chang, S.; Gubiani, J.R.; Deflon, V.M.; Nagashima, N.; Rode, A.; Blackford, K.; et al. Isolation, Synthesis and Bioactivity Studies of Phomactin Terpenoids. *Nat. Chem.* **2018**, *10*, 938–945, doi:10.1038/s41557-018-0084-x.
68. Kavanagh, F.; Hervey, A.; Robbins, W.J. Antibiotic Substances From Basidiomycetes: VIII. *Pleurotus Multilus* (Fr.) Sacc. and *Pleurotus Passeckerianus* Pilat. *Proc. Natl. Acad. Sci.* **1951**, *37*, 570–574, doi:10.1073/pnas.37.9.570.
69. Lemieux, M.R.; Siricilla, S.; Mitachi, K.; Eslamimehr, S.; Wang, Y.; Yang, D.; Pressly, J.D.; Kong, Y.; Park, F.; Franzblau, S.G.; et al. An Antimycobacterial Pleuromutilin Analogue Effective against Dormant Bacilli. *Bioorg. Med. Chem.* **2018**, *26*, 4787–4796, doi:10.1016/j.bmc.2018.07.034.
70. Chew, K.L.; Octavia, S.; Yeoh, S.F.; Teo, J.W.P. MIC Values of Iclaprim and Lefamulin against *Mycobacterium abscessus* Complex. *Antimicrob. Agents Chemother.* **2021**, *65*, e0061921, doi:10.1128/AAC.00619-21.
71. Chinthanom, P.; Vichai, V.; Dokladda, K.; Sappan, M.; Thongpanchang, C.; Isaka, M. Semisynthetic Modifications of Antitubercular Lanostane Triterpenoids from *Ganoderma*. *J. Antibiot. (Tokyo)* **2021**, *74*, 435–442, doi:10.1038/s41429-021-00422-5.

72. Hou, X.-M.; Liang, T.-M.; Guo, Z.-Y.; Wang, C.-Y.; Shao, C.-L. Discovery, Absolute Assignments, and Total Synthesis of Asperversiamides A–C and Their Potent Activity against *Mycobacterium marinum*. *Chem. Commun.* **2019**, *55*, 1104–1107, doi:10.1039/C8CC09347D.
73. Chao, R.; Hou, X.-M.; Xu, W.-F.; Hai, Y.; Wei, M.-Y.; Wang, C.-Y.; Gu, Y.-C.; Shao, C.-L. Targeted Isolation of Asperheptatides from a Coral-Derived Fungus Using LC-MS/MS-Based Molecular Networking and Antitubercular Activities of Modified Cinnamate Derivatives. *J. Nat. Prod.* **2021**, *84*, 11–19, doi:10.1021/acs.jnatprod.0c00804.
74. Auffan, M.; Rose, J.; Bottero, J.-Y.; Lowry, G.V.; Jolivet, J.-P.; Wiesner, M.R. Towards a Definition of Inorganic Nanoparticles from an Environmental, Health and Safety Perspective. *Nat. Nanotechnol.* **2009**, *4*, 634–641, doi:10.1038/nnano.2009.242.
75. Salata, O.V. Applications of Nanoparticles in Biology and Medicine. *J. Nanobiotechnology* **2004**, *2*, 1–6, doi:10.1186/1477-3155-2-3.
76. Jeevanandam, J.; Barhoum, A.; Chan, Y.S.; Dufresne, A.; Danquah, M.K. Review on Nanoparticles and Nanostructured Materials: History, Sources, Toxicity and Regulations. *Beilstein J. Nanotechnol.* **2018**, *9*, 1050–1074, doi:10.3762/bjnano.9.98.
77. Nasrollahzadeh, M.; Sajadi, S.M.; Sajjadi, M.; Issaabadi, Z. Chapter 4 - Applications of Nanotechnology in Daily Life. In *Interface Science and Technology*; Nasrollahzadeh, M., Sajadi, S.M., Sajjadi, M., Issaabadi, Z., Atarod, M., Eds.; An Introduction to Green Nanotechnology; Elsevier, 2019; Vol. 28, pp. 113–143.
78. Huang, L.; Lemos, H.P.; Li, L.; Li, M.; Chandler, P.R.; Baban, B.; McGaha, T.L.; Ravishankar, B.; Lee, J.R.; Munn, D.H.; et al. Engineering DNA Nanoparticles as

- Immunomodulatory Reagents That Activate Regulatory T Cells. *J. Immunol. Baltim. Md 1950* **2012**, *188*, 4913–4920, doi:10.4049/jimmunol.1103668.
79. Slavin, Y.N.; Asnis, J.; Häfeli, U.O.; Bach, H. Metal Nanoparticles: Understanding the Mechanisms behind Antibacterial Activity. *J. Nanobiotechnology* **2017**, *15*, 1–20, doi:10.1186/s12951-017-0308-z.
 80. Majhi, K.C.; Yadav, M. Chapter 5 - Synthesis of Inorganic Nanomaterials Using Carbohydrates. In *Green Sustainable Process for Chemical and Environmental Engineering and Science*; Inamuddin, Boddula, R., Ahamed, M.I., Asiri, A.M., Eds.; Elsevier, 2021; pp. 109–135, ISBN 978-0-12-821887-7.
 81. Roy, N.; Gaur, A.; Jain, A.; Bhattacharya, S.; Rani, V. Green Synthesis of Silver Nanoparticles: An Approach to Overcome Toxicity. *Environ. Toxicol. Pharmacol.* **2013**, *36*, 807–812, doi:10.1016/j.etap.2013.07.005.
 82. Li, Q.; Liu, F.; Li, M.; Chen, C.; Gadd, G.M. Nanoparticle and Nanomineral Production by Fungi. *Fungal Biol. Rev.* **2021**, *xx*, 1–14, doi:10.1016/j.fbr.2021.07.003.
 83. Banu, A.; Rathod, V. Biosynthesis of Monodispersed Silver Nanoparticles and Their Activity against Mycobacterium Tuberculosis. *J. Nanomedicine Biotherapeutic Discov.* **2013**, *3*, 1–5, doi:10.4172/2155-983X.1000110.
 84. Sivaraj, A.; Kumar, V.; Sunder, R.; Parthasarathy, K.; Kasivelu, G. Commercial Yeast Extracts Mediated Green Synthesis of Silver Chloride Nanoparticles and Their Anti-Mycobacterial Activity. *J. Clust. Sci.* **2020**, *31*, 287–291, doi:10.1007/s10876-019-01626-4.

85. Fan, Y.; Pauer, A.C.; Gonzales, A.A.; Fenniri, H. Enhanced Antibiotic Activity of Ampicillin Conjugated to Gold Nanoparticles on PEGylated Rosette Nanotubes. *Int. J. Nanomedicine* **2019**, *14*, 7281–7289, doi:10.2147/IJN.S209756.
86. Danaraj, J.; Periakaruppan, R.; Usha, R.; Venil, C.K.; Shami, A. Chapter 15 - Mycogenic Nanoparticles: Synthesis, Characterizations and Applications. In *Agri-Waste and Microbes for Production of Sustainable Nanomaterials*; Abd-Elsalam, K.A., Periakaruppan, R., Rajeshkumar, S., Eds.; Nanobiotechnology for Plant Protection; Elsevier, 2022; pp. 357–373, ISBN 978-0-12-823575-1.

Chapter 3

Anti-Myco**acterium tuberculosis** activity of marine derived *Clonostachys rogersoniana* methanol extract and virtual assessment of Bionectin F as a potential inhibitor of β -ketoacyl-ACP reductase (MabA)

Kudzanai Ian Tapfuma¹, Kudakwashe Nyambo¹, Francis Adu-Amankwaah¹, Lucinda Baatjies¹, Liezel Smith¹, Nasiema Allie¹, Marshall Keyster², Andre G. Loxton¹, Mkhusele Ngxande³, Rehana Malgas-Enus⁴ and Vuyo Mavumengwana^{1,*}

¹ DSI-NRF Centre of Excellence for Biomedical Tuberculosis Research; South African Medical Research Council Centre for Tuberculosis Research; Division of Molecular Biology and Human Genetics, Faculty of Medicine and Health Sciences, Stellenbosch University, Cape Town, South Africa.

² Environmental Biotechnology Laboratory (EBL), Department of Biotechnology, University of the Western Cape, Cape Town, South Africa.

³ Computer Science Division, Department of Mathematical Sciences, Faculty of Science University of Stellenbosch, Matieland, South Africa.

⁴ Department of Chemistry and Polymer Science, Faculty of Science, University of Stellenbosch, Matieland, South Africa.

* Corresponding author.

Email address: vuyom@sun.ac.za; Tel.: +27 21 938 9952.

3.0 Abstract

The number and diversity of drugs in the tuberculosis (TB) drug development process has increased over the years, yet the attrition rate remains very high, signaling the need for continued research in drug discovery. In this study, extracts from marine-derived fungi associated with ascidians were evaluated for antimycobacterial activity and their metabolites were tentatively identified through untargeted mass spectrometry-based metabolite profiling. *In silico* molecular docking and molecular dynamics simulations were performed to interpret the potential mechanisms of antimycobacterial activity of the bioactive fungal metabolites in extracts with mycobacterial proteins. The methanol extract from *Clonostachys rogersoniana* MGK33 was found to be a potent inhibitor of the growth of *Mycobacterium smegmatis* mc²155 and *Mycobacterium tuberculosis* H37Rv. Metabolite profiling of six marine fungal isolates led to the tentative identification of 65 metabolites, among them was bionectin F from *C. rogersoniana* MGK33 had a docking score of -11.17 kcal/mol against *M. tuberculosis* β -ketoacyl-acyl carrier protein reductase (MabA, PDB ID = 1UZN), an essential enzyme involved in mycolic acid biosynthesis. Molecular dynamics simulation of the bionectin F and MabA complex revealed that bionectin F binds with A: SER140, a residue vital for the transformation of MabA to a holo-form. The cumulative effects of some bioactive metabolites in the crude extracts, for instance, bionectin F, dehydrohistidyl-tryptophanyl-diketopiperazine, viridicatin, and cytoglobosin D provide an important pharmacological and biological effect to the fungal crude extracts. These findings provided strong evidence to conclude that metabolites from marine-derived fungi are potentially rich sources of bioactive metabolites with antimycobacterial activity.

Keywords: Tuberculosis; drug-discovery; marine fungi; MabA; bionectin F.

3.1 Introduction

Tuberculosis (TB) is a serious infectious disease caused by *Mycobacterium tuberculosis* and is among the top causes of death in HIV-positive individuals [1]. An estimated one quarter of the global population is thought to be infected by the pathogen, yet most of these individuals are not (yet) ill, a condition described as latent TB which is asymptomatic and non-infectious [2]. In 2020, an estimated 5.8 million new TB cases and 1.5 million TB-related deaths were reported worldwide [1]. The effects of both TB and HIV in South Africa are socially and economically catastrophic as the country has a high incidence for both diseases [1].

Of great concern is the occurrence and spread of multi-drug resistant-TB (MDR-TB, resistant to isoniazid and rifampicin) and extensively drug resistant TB (XDR-TB, resistant to isoniazid, rifampicin, some of the fluoroquinolones and at least one of the injectable second-line drugs), which are difficult to treat using available drugs [3]. Reported global cases of MDR- and XDR-TB are seemingly increasing every year, yet the rate of discovery of new TB drugs is still somewhat not sufficient to meet an impending TB pandemic [3]. Desirable properties for new TB drugs include novel antimycobacterial mechanisms of action, less toxicity, low production costs, limited drug/drug interactions, and high potency [4].

There is abundant evidence in literature that reports secondary metabolites derived from marine fungi as a rich source of bioactive compounds with potential therapeutic uses [5–7]. Currently, there is an approximate 1 901 documented marine fungal species [8] and more being discovered annually as interest in their natural products is surging. Marine fungi are commonly isolated as endobionts and/or epibionts of sea animals, plants, algae, corals, and sponges; and less commonly isolated as free-living microbes from sediments [9].

Of particular interest in this study are ascidians, also known as sea-squirts (Phylum: Chordata; Class: Ascidiacea) which are marine invertebrates found all over the world and abundantly in

harbors [10]. Ascidians proliferate in nutrient-rich environments and may host a wide diversity of microorganisms in their tissues as it has been shown by the barcoding of their microbiomes [11]. *Aspergillus clavatus* AS-107 and *Aspergillus candidus* KMM 4676 are amongst the many examples of fungi isolated from ascidians and were later on shown to produce novel bioactive compounds with antibacterial and cytotoxic activity, respectively [12,13]. However, studies involving bioprospecting of metabolites from ascidian-associated fungi to discover compounds with bioactivity against *M. tuberculosis*, are rarely reported.

An interesting example of a marine fungus (not associated with ascidians) that was shown to produce compounds with antimycobacterial activity includes *Nigrospora* sp., a mangrove endophyte that produced anthraquinone 4-deoxybostrycin [14]. It was observed that 4-deoxybostrycin had activity against *M. tuberculosis* H37Rv and MDR *M. tuberculosis* K2903531 in a Kirby-Bauer disk diffusion susceptibility assay (zone of inhibition = 25 mm) [14]. In an *in silico* study that investigated the antimycobacterial activity of 100 anthraquinones from marine fungi against essential enzymes from *M. tuberculosis* H37rv, namely *M. tuberculosis* β -ketoacyl-acyl carrier protein reductase (MabA) and polyketide synthase 18 (PKS18), averufin produced by *Aspergillus* sp., was actually found to be more bioactive than 4-deoxybostrycin [15,16].

Researchers in this study purposed to investigate the bioactivity of several marine fungi isolated from native and invasive ascidians found along the South African coastline. *In vivo* antimycobacterial activity of fungal crude extracts were determined against *Mycobacterium smegmatis* mc²155 and *M. tuberculosis* H37Rv and minimum inhibitory concentrations were determined. Untargeted liquid chromatography mass spectrometry (LC-MS) was performed, and annotation was done manually to tentatively identify the fungal metabolites. Finally, molecular docking and molecular dynamics simulations were performed to identify putative

fungal bioactive metabolites with antimycobacterial potential. This study will immensely contribute to the discovery of new drugs derived from marine fungi bioactive metabolites.

3.2 Methods and materials

3.2.1 Collection of ascidians and their identification

Different species of both native and invasive ascidians were collected from Saldanha Bay (33° 1' 36.06" S, 17° 57' 39.55" E) and from False Bay (34° 11' 28.40" S, 18° 26' 2.96" E) on the 9th and 11th of September 2019 respectively. The two sites serve as marinas for local and international yachts and small boats. Following a modified method outlined by Havenga [17], ascidians were harvested from Perspex® plates that had been tied to a rope and submerged in water for 23 weeks at a depth of 1.5 and 3.0 m. At the time of harvesting, various species of ascidians had settled and grown on the plates, with some species occurring on multiple plates. Due to the extensive overgrowth on the Perspex® plates, the organisms were transported the laboratory attached to their plates in large containers filled with chilled sea water. Upon arriving at the laboratory, the samples were kept at 4 °C until processed within 24 hours. Morphological identification of ascidians and their classification was done by marine biologists, Prof. Tamara Bridgett Robinson and Dr. Tainã Gonçalves Loureiro, who considered features such as color, shape, texture, individual and colony size, growth patterns and position of siphons.

3.2.2 Isolation of fungi from ascidians, DNA sequencing and species identification

Each ascidian sample was detached from the Perspex® plate and then rinsed at least three times with sterile distilled water. Using a sterile scalpel, ascidian samples were then sectioned into small pieces of approximately 0.5 x 0.5 cm and plated onto potato dextrose agar (PDA) in triplicates with four pieces in each plate. Inoculated PDA plates were then incubated at room temperature (approximately 23 °C) under constant monitoring for 14 days to promote growth

of fungi. Distinct fungal colonies from each PDA plate were then sub-cultured and purified for further experiments. Long term storage of purified fungal cultures was achieved by firstly culturing fungi in potato dextrose broth (PDB) and incubating at room temperature on a rotary shaker for 3 days (or until exponential phase was reached), followed by preparation of 50% culture-glycerol mixtures (v/v) which were stored at -80 °C.

3.2.3 Fungal DNA isolation, sequencing and phylogenetic analysis

Following a previously described method [18], fungal DNA was extracted and the ribosomal DNA inter-transcribed spacer regions 1 and 2 (ITS 1 and 2) were amplified using the primer pairs ITS1 (5'-TCCGTAGGTGAACCTGCGG-3') and ITS4 (5'-TCCTCCGCTTATTGATATGC-3'). Forward and reverse sequencing was then performed as previously described in Tapfuma et al., [18]. Nucleotide sequences were then visualized and edited using Geneious Prime software (version 2020, <http://www.geneious.com/>). Using the Nucleotide Basic Local Alignment Search (BLASTN) algorithm on the National Center for Biotechnology Information (NCBI) [19], nucleotide sequences from fungi in this study were compared with sequences from the NCBI database and statistical significance of matches was calculated and assignment of identities was performed. To confirm the assigned identities, maximum likelihood phylogenetic analysis was performed using MEGA X software (version 10, <https://www.megasoftware.net/>), with Kimura 2-parameter predicted as the best suitable model and *Allomyces macrogynus* ATCC 38327 used as the outgroup. A total of 1 000 replicate runs were performed, and bootstrap values were calculated. Fungal nucleotide sequences were then submitted to GenBank for curation and accession numbers were assigned (MT738573-MT738604).

3.2.4 Extraction of crude secondary metabolites from fungi

Fungi were cultured on PDA and incubated at room temperature for 28 days. PDA cultures were then dried in a vented oven blowing a warm stream of air at 30 °C. Dried cultures were then macerated into powder and added to methanol at a ratio of 100 mL of solvent for every 10 g of macerated fungal culture for metabolite extraction [20]. The mixtures were allowed to shake for 24 hours before re-extracting the residues with the same amount of solvent 2 more times. The solvent extracts were then filtered through a Whatman No. 1 filter paper and then concentrated using a rotary evaporator at 60 °C under reduced pressure. Concentrated extracts (powder/oil) were stored at – 80 °C.

3.2.5 Antimycobacterial activity screening and minimum inhibitory concentrations

(MICs) of fungal crude extracts

Methanol extracts from fungi were initially dissolved in 100% dimethyl sulfoxide (DMSO) and then subsequently diluted to 10% DMSO. Extracts for the actual tests were prepared in Middlebrook 7H9 broth medium containing 0.05% Tween 80, 0.5% glycerol and 10% oleic acid-albumin-dextrose-catalase (OADC) supplement, which was also used in the growth and maintenance of *Mycobacterium* cultures [21]. Antimycobacterial activity screening was performed at varying concentrations (Table 3.3) against *M. smegmatis* mc²155 and *M. tuberculosis* H37Rv in 96-well microplates for 19 selected fungi which had sufficient extract yields for subsequent experiments. Inoculum was prepared by firstly incubating the starter culture at 37 °C until an optical density (OD_{600nm}) of 0.8-1.0 was reached, followed by adjustment of the culture to OD_{600nm} of 0.01, subculturing and further incubation until an OD_{600nm} 0.2-0.3 was reached. These cells, at exponential phase were then diluted 100 times in Middlebrook 7H9 broth medium to prepare inoculum for use in screening. Aliquots of 100 µL of fungal extracts and 100 µL of inoculum were added to 96-well microplates and allowed to incubate for 3 days for *M. smegmatis* mc²155 and 6 days for *M. tuberculosis* H37Rv.

Antimycobacterial activity was determined by addition of 20 μL of 0.015% resazurin dye per well and allowed to incubate for a further 4 hours for *M. smegmatis* mc²155 and 24 hours for *M. tuberculosis* H37Rv [22]. In the presence of viable cells, resazurin (blue) is reduced by viable cells to form resorufin (pink). 96-well microplates were thus visualized after the incubation period and extracts with antimycobacterial activity were noted. Minimum inhibitory concentration (MIC) experiments were performed by serially diluting the extracts in 96-well microplates and then following the same procedure outlined for screening. The lowest concentration capable of inhibiting microbial growth after incubation was regarded as the MIC [23]. Isoniazid was used a positive control for antimycobacterial activity.

3.2.6 Metabolite profiling of fungal extracts

Untargeted metabolite profiling of fungal extracts was performed using tandem liquid chromatography quadrupole time-of-flight mass spectrometry (LC-QTOF-MS/MS), following previously described methods [24,25]. Briefly, 1 mg/mL of each fungal extract dissolved in LC-MS grade methanol was passed through a 0.22 μm nylon membrane syringe filter and then 200 μL of sample was added to LC-MS autosampler vials with inserts and pre-split septate leads. An injection volume of 2 μL per sample was selected for separation of analytes using a Waters Acquity ultraperformance liquid chromatography (UPLC) system, fitted with an Acquity photo-diode array (PDA) detector and an Acquity C18 column with the following dimensions: 130 \AA pore size, 1.7 μm particle size, 2.1 mm internal diameter and 100 mm length (Acquity, Waters Corp, Milford, MA, USA). Water acidified with 0.1% formic acid (v/v) (solvent A) and acetonitrile (solvent B) were selected for a gradient elution program set as follows: 0% solvent B between 0-0.5 min; 0-100% solvent B between 0.5-12.00 min; 100% solvent B between 12.00-12.50 min; 100-0% solvent B between 12.50-13.00 min; 0% solvent B between 13.00-15.00 min. Both mobile phases were pumped at a constant flow rate of 0.4 mL/min. The UPLC system was connected to a Waters Synapt G2 quadrupole time-of-flight

mass spectrometry system which acquired data under the following conditions: Centroid mode; positive electro-spray ionization (ESI+) MS/MS mode; nitrogen gas for desolvation at 275 °C at a flow rate of 650 L/hr; cone voltage at 15 V; capillary voltage at 3 kV; trap MS collision energy of 6 eV and survey scan of 150-1 500 m/z for MS1 data acquisition; trap MS collision energy of 20 eV (low energy) and 70 eV (high energy), and survey scan of 40-1 500 m/z for MS2 data acquisition. The .raw data files acquired from the Waters LC-QTOF-MS/MS system were then converted to .abf files and further analyzed using MS-Dial software (version 4.24) to identify metabolites [26]. Only $[M+H]^+$ adducts ions with a height of 1 000 were considered. Putative compound identifications were assigned to ions which found matches with error ppm < 7.0 in the following databases: FungalMet (<http://www.fungalmet.org/en/test/>), KNApSackK (http://www.knapsackfamily.com/KNApSackK_Family/) and Dictionary of Natural Products (<https://dnp.chemnetbase.com/faces/chemical/ChemicalSearch.xhtml>).

3.2.7 *Molecular docking*

The potential mechanism of anti-mycobacterial activity of the fungal metabolites against mycobacterial proteins was investigated using molecular docking studies. Molecular docking was performed to evaluate the potential association of fungal metabolites with *M. tuberculosis* β -ketoacyl-acyl carrier protein reductase A (MabA), β -lactamase (Blac), and β -ketoacyl-acyl carrier protein synthase (KasA). The 3D structure of MabA (PDB ID: 1UZN), Blac (PDB ID: 4Q8I) and KasA (PDB ID: 4Q8I) were retrieved from the protein data bank. The 3D structures of fungal compounds were obtained from PubChem (<https://pubchem.ncbi.nlm.nih.gov/>) and ChemSpider (<http://www.chemspider.com/>). The chemical structures were energy minimized using the OPLS 2005 force field in LigPrep (Schrödinger Release 2021-1 accessed via South African CHPC) [27]. Proteins were prepared using Protein Preparation Wizard (Schrödinger Release 2021-1 accessed via South African CHPC). The protein crystallographic structures were prepared by adding polar hydrogens, removing water molecules, co-crystallized

heterogeneous groups, and finally by performing an energy minimization using the OPLS 2005 force field [27,28]. The Sitemap application was utilized to predict possible binding pockets and the predictions were verified using CASTp (<http://sts.bioe.uic.edu/castp/index.html?1uzn>) [29]. Using the verified binding site predictions from the Sitemap application, dimensions for outer grid boxes were specified using the size of the Sitemap (1UZN = 56.355 Å³, 4Q8I = 43.208 Å³ and 6P9K = 61.396 Å³) while the inner grid boxes were 10 x 10 x 10 Å with the following grid center of dimensions (x, y, z): 1UZN = 14.896, -18.106, -3.669 Å; for 4Q8I = 28.632, -10.055, 43.208 Å; for 6P9K = 81.502, 49.119, 10.515 Å. The docking was then performed using the Glide application (Schrödinger Release 2021-1 accessed via South African CHPC). The 3D docked poses of the protein-ligand complexes were visualized in Maestro (Schrodinger 2021-1 suite). The ligands which exhibited the highest docking poses were considered for further analysis with molecular dynamics simulations.

3.2.8 *Molecular dynamics*

The best docking pose with the highest binding score from molecular docking was selected for molecular dynamics simulations. The stability of the protein-ligand complex was evaluated through 50 nanoseconds (ns) molecular dynamics simulations. Molecular dynamics simulation was performed using applications Desmond module (Schrödinger Release 2021-1 accessed via South African CHPC). The OPLS_2005 force field was used to perform the molecular dynamic simulation. The protein-ligand (1UZN-Bionectin F) complex was explicitly solvated using the TIP3P water model in a boundary condition orthorhombic box shape with boundary dimensions in angstrom units (15 Å × 15 Å × 15 Å) [27]. The system was neutralized by adding 0.15 M counter ions (Na⁺ and Cl⁻) to predict the physical properties of a realistic system precisely. The systems were energy minimized and equilibrated in an NPT ensemble at constant temperature and pressure (300 K and 1.01325 bar, respectively) using a default

protocol [28]. The equilibrated systems were subjected to a final production step of 50 ns with internal energy recording 1.2 picosecond (ps) intervals.

3.3 Results and Discussion

3.3.1 Culture-dependent isolation and identification of fungi associated with ascidians

A total of 16 ascidian samples were collected from Saldanha Bay and False Bay marinas and were identified using their morphological features (Table 3.1 and Appendix A). In most regions across the world, invasive marine species are introduced by fouling hulls on ships (propeller, rudder, sea chest, etc.), ballast water deposited in new regions and mariculture [29]. In the Cape coastal regions, a great proportion of invasive species originate from the North Atlantic Ocean as a result of shipping patterns (container ships, tour boats, fishing boats, yachts, etc.) and warmer temperatures that prevail [29].

Invasive ascidian species accounted for about 75% (6 out of 8) species collected from the False Bay marina, compared to 50% (4 out of 8) of species collected from the Saldanha Bay marina. The higher occurrence of invasive ascidians in False Bay was expected since this marina is a popular tourist site that hosts a higher number of luxury international and local yachts and boats as compared to the Saldanha Bay marina.

Ascidians are filter-feeders, their adult bodies are designed as branchial baskets connected to the digestive system while also opening to the exterior to allow for trapping organic matter as the water is filtered through the tissues [30]. Due to this method of feeding, inner tissues of ascidians host a diverse microbiome which is sometimes thought to assist invasive ascidians to adapt to new environments [11], and thus it is possible to isolate numerous microbial symbionts of diverse species. In this study, standard laboratory culture techniques allowed for the isolation of 46 fungi from 94% (15 out of 16) of the collected ascidians.

Table 3.1. List of sampled ascidians, their identities and number of fungi isolated.

Site	Ascidian code	Characteristics	Common name	Scientific name	Fungal isolates	No. of isolates (%) [†]
Saldanha Bay (33°1' 36.06" S, 17°57' 39.55" E)	SB1	Colonial, native	White ringed ascidian	<i>Botryllus magnicoecus</i>	MGK26	1 (2.17%)
	SB2	Colonial, native	White ringed ascidian	<i>Botryllus magnicoecus</i>	MGK02, MGK03, MGK06, MGK08, MGK20, MGK31	6 (13.04%)
	SB3	Solitary, invasive	Sea vase	<i>Ciona robusta</i>	MGK07, MGK09, MGK10, MGK34, MGK36, MGK51	6 (13.04%)
	SB4	Solitary, invasive	Waxy sea squirt	<i>Asterocarpa humilis</i>	-	0
	SB5	Colonial, native	White ringed ascidian	<i>Botryllus magnicoecus</i>	MGK25, MGK39, MGK49	3 (6.52%)
	SB6	Solitary, invasive	Waxy sea squirt	<i>Asterocarpa humilis</i>	-	0
	SB7	Solitary, invasive	Light bulb ascidian	<i>Clavelina lepadiformis</i>	MGK42, MGK48	2 (4.35%)
	SB8	Colonial, native	-	<i>Botryllus gregalis</i>	MGK47, MGK53	2 (4.35%)
False Bay (34°11' 28.40" S, 18°26' 2.96" E)	FB1	Colonial, invasive	Golden star ascidian	<i>Botryllus schlosseri</i>	MGK05, MGK21, MGK35	3 (6.52%)
	FB2	Solitary, invasive	European sea squirt	<i>Ascidrella aspersa</i>	MGK52, MGK55, MGK56, MGK57	4 (8.70%)
	FB3	Solitary, invasive	Light bulb ascidian	<i>Clavelina lepadiformis</i>	MGK14, MGK15, MGK30	3 (6.52%)
	FB4	Solitary, invasive	Orange-tipped sea squirt	<i>Corella eumyota</i>	MGK13, MGK16	2 (4.35%)
	FB5	Solitary, invasive	European sea squirt	<i>Ascidrella aspersa</i>	MGK17, MGK22, MGK33, MGK41	4 (8.70%)
	FB6	Colonial, invasive	Red-rust bryozoan	<i>Watersporia subtorquata</i>	MGK28, MGK46	2 (4.35%)
	FB7	Colonial, native	Meandering ascidian	<i>Botryllus meandrus</i>	MGK19, MGK24	2 (4.35%)
	FB8	Colonial, native	White ringed ascidian	<i>Botryllus magnicoecus</i>	MGK23, MGK43, MGK44, MGK49, MGK50, MGK54	6 (13.04%)

[†] Percentage contribution to the overall sum of 46 fungal isolates is shown in brackets () in each row.

Invasive *Ciona robusta* (SB3) and native *Botryllus magnicoecus* (SB1, SB2, SB5 and FB8) species yielded the highest numbers of culturable fungi, while no fungi were isolated from *Asterocarpa humilis* (SB4 and SB6) (Table 3.1). Using a culture-independent metagenomics approach could have given more comprehensive insight into the diversity of fungi which associate with ascidians [31,32], however the limitation of these methods is that they do not allow for *in vitro* and *in vivo* bioactivity investigations of compounds produced by the

identified fungi. Morphological identification of fungi was performed and identical isolates from the same individual host were eliminated, thus effectively reducing the number of isolates for further experiments to 32.

DNA sequence analysis of the amplified internal transcribed spacer regions 1 (ITS1) and ITS2 of the 32 fungal isolates resulted in the fungi being assigned to 10 genera and 14 species as shown in Table 3.2 and Figure 3.1. It was observed that filamentous fungi (*Penicillium* genus in particular) were predominant and consistent with literature where reports mention that most of the fungi identified from marine environments to date have been from the Ascomycota and Basidiomycota phyla [33]. The maximum likelihood phylogenetic tree of the 32 sequences fungal isolates in Figure 3.1 corroborated the BLAST results from GenBank (partly shown in Table 3.2) as organisms from the same genus and species formed clads together.

Marine fungal species which fall within the *Penicillium*, *Alternaria*, *Mucor*, *Fusarium*, *Galactomyces* and *Clonostachys* genera have been widely reported as associates of ascidians [34–36], while fungi of the *Saccharomycetales*, *Geotrichum*, *Galactomyces* and *Bartalinia* genera are reported as associates of ascidians for the first time in this study. Unfortunately, the sample size of different ascidian species utilized in this study was inadequate to conclude on whether the cultivable fungal microbiota isolated in this study associate with specific ascidian species or not.

3.3.2 Antimycobacterial activity of extracts from fungi associated with ascidians

The 32 fungi listed in Table 3.2 were cultured on potato dextrose agar (PDA) for 14 days and crude secondary metabolites were extracted using methanol. Some fungi which include *Alternaria* sp. MGK02, *Saccharomycetales* sp. MGK23, those from the *Galactomyces* and *Geotrichum* genera exhibited poor growth on PDA and thus very low extract-yields were obtained during methanol-solvent extraction.

Table 3.2. Percentage sequence similarity of fungal isolates and their closest relatives in the GenBank database.

Fungal isolate	Closest relative in NCBI (accession no.)	Similarity (%)	Assigned identity	GenBank accession no.
MGK02	<i>Alternaria</i> sp. D21 (MH029120)	99.47	<i>Alternaria</i> sp. MGK02	MT738573
MGK03	<i>Penicillium digitatum</i> CMV010G4 (MK450692)	100	<i>P. digitatum</i> MK03	MT738574
MGK05	<i>Galactomyces pseudocandidus</i> CBS:11392 (KY103457)	100	<i>G. pseudocandidus</i> MGK05	MT738575
MGK06	<i>P. digitatum</i> CMV010G4 (MK450692)	98.98	<i>P. digitatum</i> MK06	MT738576
MGK07	<i>Penicillium brevicompactum</i> (MH047201)	99.83	<i>P. brevicompactum</i> MGK07	MT738577
MGK08	<i>P. brevicompactum</i> kfb KR704880	100	<i>P. brevicompactum</i> MGK08	MT738578
MGK09	<i>Penicillium crustosum</i> DUCC5730 (MT582770)	99.81	<i>P. crustosum</i> MGK09	MT738579
MGK10	<i>Geotrichum candidum</i> M13 (MN007135.1)	97.86	<i>G. candidum</i> MGK10	MT738580
MGK13	<i>Fusarium oxysporum</i> A6-2 ()	100	<i>F. oxysporum</i> MGK13	MT738581
MGK14	<i>Mucor circinelloides</i> F1-01 (JN561250)	99.69	<i>M. circinelloides</i> MGK14	MT738582
MGK15	<i>G. candidum</i> GAD1 (MN638741)	99.2	<i>G. candidum</i> MGK15	MT738583
MGK16	<i>Mucor circinelloides</i> CMRC 573 (MT603954)	99.83	<i>M. circinelloides</i> MGK16	MT738584
MGK17	<i>Bartalinia robillardoides</i> CBS 122705 (NR_126145)	100	<i>B. robillardoides</i> MGK17	MT738585
MGK19	<i>P. crustosum</i> MBRU_F899 (MZ541868)	99.83	<i>P. crustosum</i> MGK19	MT738586
MGK20	<i>Curvularia eragrosticola</i> BRIP 12538 (NR_158446)	98.92	<i>C. eragrosticola</i> MGK20	MT738587
MGK21	<i>P. crustosum</i> MBRU_F899 (MZ541868)	99.63	<i>P. crustosum</i> MGK21	MT738588
MGK23	<i>Saccharomycetales</i> sp. A2 (KC310808)	99.73	<i>Saccharomycetales</i> sp. MGK23	MT738589
MGK25	<i>Penicillium rubens</i> DTO269E3 (MN413181)	99.32	<i>P. rubens</i> MGK25	MT738590
MGK28	<i>P. crustosum</i> MBRU_F899 (MZ541868)	100	<i>P. expansum</i> MGK28	MT738591
MGK30	<i>P. crustosum</i> strain DUCC5730 (MT582770)	100	<i>P. crustosum</i> MGK30	MT738592
MGK31	<i>Penicillium antarcticum</i> CBS 116939 (KP016829)	99.83	<i>P. antarcticum</i> MGK31	MT738593
MGK33	<i>Clonostachys rogersoniana</i> YFCC 899 (MW199073)	99.3	<i>C. rogersoniana</i> MGK33	MT738594
MGK34	<i>P. crustosum</i> MBRU_F899 (MZ541868)	100	<i>P. crustosum</i> MGK34	MT738595
MGK41	<i>Penicillium commune</i> CSK2_3 (MK460792)	98.98	<i>P. commune</i> MGK41	MT738596
MGK42	<i>Penicillium expansum</i> 19-14 (MT872092)	100	<i>P. expansum</i> MGK42	MT738597
MGK44	<i>P. crustosum</i> MBRU_F899 (MZ541868)	99.49	<i>P. crustosum</i> MGK44	MT738598
MGK47	<i>Penicillium</i> sp. isolate CLE41 MN544011	86.65	<i>Penicillium</i> sp. MGK47	MT738599
MGK48	<i>G. candidum</i> strain GC1 KY009607	98.66	<i>G. candidum</i> MGK48	MT738600
MGK49	<i>G. candidum</i> DBMY703 (KJ706920)	99.47	<i>G. candidum</i> MGK49	MT738601
MGK51	<i>G. candidum</i> M13 (MN007135)	98.93	<i>G. candidum</i> MGK51	MT738602
MGK52	<i>P. crustosum</i> MBRU_F899 (MZ541868)	100	<i>P. expansum</i> MGK52	MT738603
MGK54	<i>P. expansum</i> 19-14 (MT872092)	99.66	<i>P. expansum</i> MGK54	MT738604

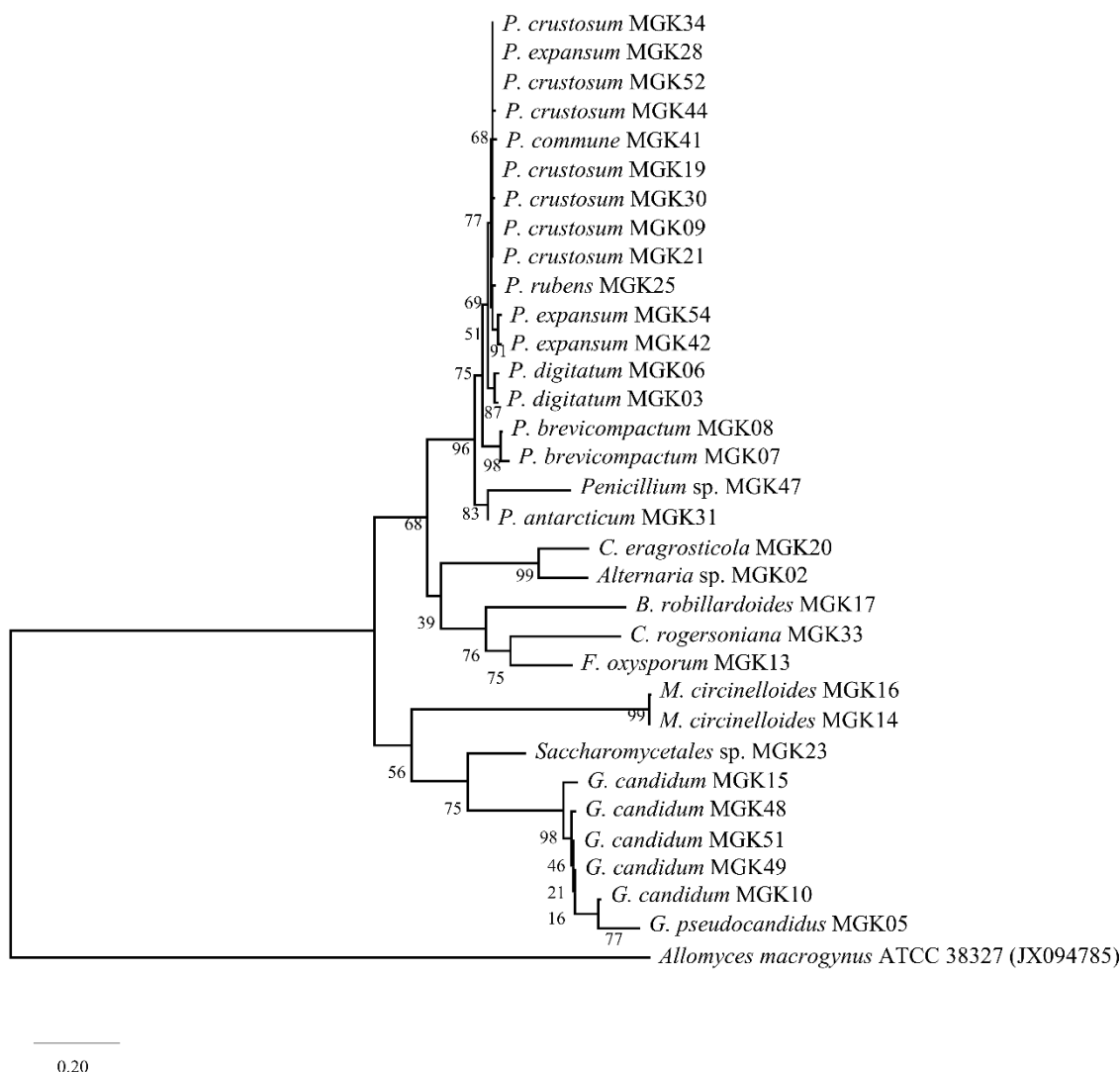


Figure 3.1. The evolutionary history was inferred by using the maximum likelihood method and Kimura 2-parameter model. The tree with the highest log likelihood (-6061.78) is shown. The percentage of trees in which the associated taxa clustered together is shown next to the branches, while GenBank accession numbers are also displayed next to the respective sequences. *Allomyces macrogynus* was used as an outgroup.

An observed limitation leading to this occurrence was that PDA does not mimic the chemical composition of sea water, the natural environment for the marine fungi in this study, which perhaps negatively impacted the growth of some isolates. In another study, powdered *Ciona intestinalis* was used as a supplement for growth media with sea water chemical composition and effectively led to the exclusive isolation of *Acrostalagmus*, *Arthopyrenia*, *Cordyceps* and *Sporosarcina* fungal species from the gut tissues of *C. intestinalis* [34]. Even though it was understood that different fungal species may have unique nutritional requirements as shown in

some studies [34], it was beyond the scope of this study to investigate the response of fungal isolates to different culture media and growth conditions.

A total of 19 fungal cultures exhibited excellent growth on PDA and thus were prioritized for crude metabolite extraction using methanol. The crude extracts were tested *in vitro* for antimycobacterial activity against *M. smegmatis* mc²155 and *M. tuberculosis* H37Rv, and the minimum inhibitory concentrations (MICs) observed are listed in Table 3.3.

Table 3.3. Minimum inhibitory concentration (MIC) values of fungal extracts tested against *M. smegmatis* mc²155 and *M. tuberculosis* H37Rv.

Fungal crude extract	<i>M. smegmatis</i> mc ² 155 MIC (mg/mL)	<i>M. tuberculosis</i> H37Rv MIC (mg/mL)
<i>P. digitatum</i> MGK03	> 10	Not tested
<i>P. brevicompactum</i> MGK07	> 5	Not tested
<i>P. brevicompactum</i> MGK08	10	Not tested
<i>P. crustosum</i> MGK09	> 10	Not tested
<i>F. oxysporum</i> MGK13	> 1	> 0.33
<i>M. circinelloides</i> MGK14	> 2.50	>1.67
<i>M. circinelloides</i> MGK16	> 2.50	> 1.67
<i>P. commune</i> MGK19	> 5	> 3.33
<i>C. eragrosticola</i> MGK20	> 2.50	> 1.67
<i>P. rubens</i> MGK25	> 1	> 0.33
<i>P. expansum</i> MGK28	> 2.50	> 1.67
<i>P. crustosum</i> MGK30	> 10	Not tested
<i>P. antarcticum</i> MGK31	> 2.50	> 1.67
<i>C. rogersoniana</i> MGK33	0.125	0.20
<i>P. crustosum</i> MGK34	> 10	Not tested
<i>P. commune</i> MGK41	> 5	> 3.33
<i>P. expansum</i> MGK42	> 5	> 1.67
<i>P. crustosum</i> MGK44	> 5	> 3.3
<i>P. crustosum</i> MGK52	> 5	> 3.33
Isoniazid	0.031	< 0.31

According to Awouafack et al., the MIC of crude extracts are considered to be significant if they are below 0.1 mg/mL, moderate if between 0.1-0.625 mg/mL and weak if greater than 0.625 mg/mL [37]. The methanol extract from *C. rogersoniana* MGK33 therefore exhibited moderate activity against *M. smegmatis* mc²155 and *M. tuberculosis* H37Rv with MIC values

of 0.125 and 0.20 mg/mL respectively. No data was found for antitubercular activity of *C. rogersoniana* extracts in literature to make comparisons. Methanol extracts from *Penicillium*, *Fusarium*, *Galactomyces*, *Geotrichum* and *Mucor* showed poor inhibitory activity against *M. smegmatis* mc²155 and *M. tuberculosis* H37Rv.

Poor activity from extracts of multiple fungi was unsurprising because *Mycobacteria* are known to possess intrinsic and extrinsic resistance to many antibiotics currently available. Drug-resistance mechanisms utilized by *Mycobacteria* include the use of a thick, waxy and hydrophobic cell envelope on the pathogen's surface to limit penetration of compounds [38]. Drugs that may possibly make past the cell wall defense system may be met with degrading enzymes such as rifampin inactivating ADP ribosyltransferase, penicillin inactivating β -lactamase, erythromycin ribosome methyltransferase and aminoglycoside acetyltransferase [38–40]. Protein pumps such as the ATP-binding cassette (ABC) transporters (e.g., Rv1819c, Rv0194, Rv0933, Rv1473, Rv2477c, etc.) are known to facilitate the efflux of β -lactams, macrolides, isoniazid, rifampicin and several other antibiotics [41].

Since some fungal secondary metabolite biosynthetic gene clusters (BGCs) are understood to be silent in standard culture conditions [42], activating these genes in fungal isolate cultures could promote the production of antimycobacterial compounds by the fungi. Some interesting techniques utilized in the stimulation of silent BGCs include the co-culturing of fungi and *Mycobacteria* to promote cross-talk and activation of silent-pathways in fungi [43,44]. In one study, researchers observed that there was selective production of aurasperone, desmethylkotanin, TMC-256A1 and malformin C by marine *Aspergillus niger* when co-cultured with *M. smegmatis* [45].

More recently, a CRISPR-based transcriptional activation methodology has been developed for filamentous fungi and promises to expand the exploration of silent genes in fungi [46]. Thus said, fungi which did produce bioactive extracts against *Mycobacteria* may very well have their

BGC-induction studies re-explored to assess metabolites which are not observed in standard culture conditions that were used in this study.

3.3.3 Metabolite profiling of fungal isolates

Six fungal isolates which include *F. oxysporum* MGK13, *M. circinelloides* MGK14, *C. eragrosticola* MGK20, *P. antarcticum* MGK31, *C. rogersoniana* MGK33 and *P. expansum* MGK42 were prioritized for metabolite profiling using tandem liquid chromatography quadrupole time-of-flight mass spectrometry (LC-QTOF-MS/MS) in positive mode. MSFinder was used to calculate molecular formulas for the detected $[M+H]^+$ ions. After manually searching in several public and subscription databases, peaks were annotated with predicted compound IDs as shown in Tables 3.4 and 3.5.

Among the metabolites identified, a total of 55 metabolites were found to be unique (Table 3.4), and whose occurrence was observed in a single individual fungal isolate in this study. Of these unique metabolites, five were identified from the methanol crude extract of *F. oxysporum* MGK13 as follows: Dehydrofusaric acid (1), fusarinolic acid (2), fusaric acid (3), 3-dehydrosphinganine (4) and beauvericin (5). Against *M. tuberculosis*, fusaric acid (2) at a concentration of 60 μ M was found to cause 14.9% growth inhibition [47], while beauvericin (5) exhibited a MIC of 0.8–1.6 mg/mL [48].

The weak antimycobacterial activity of fusaric acid (2) and beauvericin (5) help explain the poor activity observed from *F. oxysporum* MGK13 methanol crude extract in this study. Metabolites from *M. circinelloides* MGK14 were very challenging to identify as there are a limited number of reports on pure compounds from the *Mucor* genus. Bioprospecting studies utilizing extracts from this genus are also rare.

Table 3.4. Unique metabolites identified from extracts of six selected fungi and their docking scores.

No.	Proposed ID	Predicted Formula	Precursor m/z [M+H] ⁺	Err ppm	RT (min)	Docking scores (kcal/mol)*		
						1UZN	4Q8I	6P9K
<i>F. oxysporum</i> MGK13 metabolites								
1	Dehydrofusaric acid	C ₁₀ H ₁₁ NO ₂	178.0860	1.44	4.69	-4.80	-3.71	-2.62
2	Fusarinolic acid	C ₁₀ H ₁₃ NO ₃	196.0966	1.13	4.69	-6.01	-4.60	-5.06
3	Fusaric acid	C ₁₀ H ₁₃ NO ₂	180.1017	1.15	5.42	-5.40	-3.48	-3.64
4	3-Dehydrosphinganine	C ₁₈ H ₃₇ NO ₂	300.2885	4.03	11.49	-2.65	-2.85	-4.96
5	Beauvericin	C ₄₅ H ₅₇ N ₃ O ₉	784.4191	-2.99	11.92	-4.15	-1.49	-2.88
<i>M. circinelloides</i> MGK14 metabolites								
6	Pantothenic acid	C ₉ H ₁₇ NO ₅	220.1183	-1.60	4.69	-5.49	-1.68	-1.92
<i>C. eragrosticola</i> MGK20								
7	L-Arginine	C ₆ H ₁₄ N ₄ O ₂	175.1188	0.87	0.72	-4.23	-4.44	-5.33
8	L-Phenylalanine	C ₉ H ₁₁ NO ₂	166.0859	2.15	4.57	-5.34	-3.77	-5.61
9	N-Acetylsphinganine	C ₂₀ H ₄₁ NO ₃	344.3154	1.52	9.06	-4.83	-4.57	-4.54
10	Sphingosine	C ₁₈ H ₃₇ NO ₂	300.2911	-4.66	11.40	-4.50	-3.63	-4.20
11	Antibiotic BK230	C ₅₇ H ₉₁ N ₉ O ₁₄	1126.678	-1.93	12.16	n.d.	n.d.	n.d.
<i>P. antarcticum</i> MGK31 metabolites								
12	Arohynapene A	C ₁₈ H ₂₂ O ₃	287.1631	3.74	0.78	-6.87	-4.36	-5.59
13	Chrysogine	C ₁₀ H ₁₀ N ₂ O ₂	191.0812	1.60	5.31	-6.90	-5.27	-7.00
14	L-Phe-L-His	C ₁₅ H ₁₈ N ₄ O ₃	303.1452	-0.11	5.41	-7.37	-4.89	-4.96
15	Cyclo(L-Phe-L-Pro)	C ₁₄ H ₁₆ N ₂ O ₂	245.1286	-0.60	5.77	-6.02	-4.30	-5.06
16	Penicitrinol P	C ₁₆ H ₂₀ O ₆	309.1328	1.51	6.25	-5.43	-4.90	-4.67
17	Trans-Resorcylide	C ₁₆ H ₁₈ O ₅	291.1227	0.00	6.25	-6.20	-2.81	-6.16
18	Penexanthone B	C ₁₉ H ₂₀ O ₈	377.1257	-6.93	6.42	-5.32	n.d.	-4.78
19	Cladosporin	C ₁₆ H ₂₀ O ₅	293.1385	-0.51	8.17	-6.19	-4.80	-5.29
20	Penicisochroman A	C ₁₆ H ₁₈ O ₄	275.1273	1.80	8.17	-6.44	-4.53	-4.97
21	Antibiotic TAN 1446A	C ₁₇ H ₂₂ O ₅	307.154	0.00	9.60	-5.14	-3.85	-4.81
22	Chrysogeside C	C ₄₀ H ₇₃ NO ₉	712.5357	0.15	11.98	-5.69	-5.20	-5.59
<i>C. rogersoniana</i> MGK33 metabolites								
23	Gadusol	C ₈ H ₁₂ O ₆	205.0693	6.69	0.67	-6.22	-3.65	-4.67
24	Bionectin F	C₅₀H₉₆O₈	825.7189	-1.34	9.08	-11.17	-8.19	-8.94
25	C16 Phytosphingosine	C ₁₆ H ₃₅ NO ₃	290.2702	-4.25	7.85	-2.16	-1.15	-3.23
26	L-Ile-L-Pro	C ₁₁ H ₂₀ N ₂ O ₃	229.1556	-4.08	2.82	-5.30	-3.64	-4.81
27	L-Tryptophan	C ₁₁ H ₁₂ N ₂ O ₂	205.0977	-2.67	2.82	-6.46	-5.73	-4.55
28	L-Tyrosine	C ₉ H ₁₁ NO ₃	182.0810	0.94	1.67	-5.98	-5.24	-4.11
<i>P. expansum</i> MGK42								
29	Dihydrovermistatin	C ₁₈ H ₁₈ O ₆	331.1161	4.59	0.78	-5.22	-2.82	-4.89
30	Sativan	C ₁₇ H ₁₈ O ₄	287.1266	4.14	0.78	-5.75	-4.24	-5.16
31	Canadensolide	C ₁₁ H ₁₄ O ₄	211.0957	3.74	5.22	-4.69	-3.85	-4.12

*Abbreviations represent protein receptors as follows: **1UZN** = *M. tuberculosis* β-ketoacyl-acyl carrier protein reductase A (MabA); **4Q8I** = β-lactamase (Blac) and **6P9K** = β-ketoacyl-acyl carrier protein synthase (KasA). In the table, n.d. means not docked.

Table 3.4 (Continued). Unique metabolites identified from extracts of six selected fungi and their docking scores.

No.	Proposed ID	Predicted Formula	Precursor m/z [M+H] ⁺	Err ppm	RT (min)	Docking scores (kcal/mol)*		
						1UZN	4Q8I	6P9K
<i>P. expansum</i> MGK42								
32	Aurantioclavine	C ₁₅ H ₁₈ N ₂	227.1532	4.75	5.42	-4.05	-5.43	-5.36
33	Clavicipitic acid	C ₁₆ H ₁₈ N ₂ O ₂	271.1438	1.13	5.48	-6.59	-4.70	-5.77
34	Roquefortine C	C ₂₂ H ₂₃ N ₅ O ₂	390.1931	-1.67	5.75	-9.36	-3.48	-4.98
35	Roquefortine D	C ₂₂ H ₂₅ N ₅ O ₂	392.2077	1.03	5.76	-5.31	-3.66	-4.48
36	(16R)-Hydroxyroquefortine C	C ₂₂ H ₂₃ N ₅ O ₃	406.1877	-0.82	6.07	-5.80	-4.04	-4.98
37	Cyclo(L-Phe-L-Phe)	C ₁₈ H ₁₈ N ₂ O ₂	295.1449	-2.71	6.36	-6.05	-3.87	-6.08
38	Dehydrohistidyl-tryptophanyl-diketopiperazine	C ₁₇ H ₁₅ N ₅ O ₂	322.1298	0.16	6.37	-8.25	-6.13	-6.15
39	Communesin E	C ₂₇ H ₃₀ N ₄ O ₂	443.2454	-2.82	6.55	-5.60	-2.91	-5.37
40	Commnesin 470	C ₂₇ H ₃₄ O ₇	471.2389	0.36	7.06	-6.25	-4.02	-5.17
41	24-Oxocyclocitrinol	C ₂₅ H ₃₄ O ₄	399.2537	-1.79	7.13	-6.03	-4.69	-5.36
42	Chaetoglobosin E	C ₃₂ H ₃₈ N ₂ O ₅	531.2850	0.66	7.50	-4.47	-3.25	-6.27
43	Communesin B	C ₃₂ H ₃₆ N ₄ O ₂	509.2880	6.10	7.50	-3.80	-2.66	-2.58
44	Citrinin	C ₁₃ H ₁₄ O ₅	251.0912	0.80	7.65	-5.80	-2.23	-5.02
45	Viridicatin	C ₁₅ H ₁₁ NO ₂	238.0862	0.23	7.65	-6.49	-4.75	-4.72
46	Chaetoglobosin A	C ₃₂ H ₃₆ N ₂ O ₅	529.2690	1.32	8.28	-5.73	-0.76	-4.03
47	Deformylcalbistrin A	C ₃₀ H ₄₀ O ₇	513.2877	-5.90	8.43	-5.32	-3.38	-4.49
48	Chaetoglobosin F	C ₃₂ H ₃₈ N ₂ O ₅	531.2851	0.47	8.43	-6.12	-1.35	-3.61
49	Communesin D	C ₃₂ H ₃₄ N ₄ O ₃	523.2708	-0.83	8.49	-4.75	-2.80	-3.94
50	Andrastin A	C ₂₈ H ₃₈ O ₇	487.2703	-2.61	9.07	-4.66	n.d.	-1.45
51	Chaetoglobosin D	C ₃₂ H ₃₆ N ₂ O ₅	529.2690	1.32	9.10	-4.53	-2.88	-4.16
52	Cytoglobosin D	C ₃₂ H ₃₈ N ₂ O ₄	515.2919	-2.85	9.88	-7.14	-1.94	-4.37
53	Chaetoglobosin J	C ₃₂ H ₃₆ N ₂ O ₄	513.2749	-0.23	10.36	-5.96	-2.97	-4.44
54	Chrysogeside A	C ₄₀ H ₇₃ NO ₉	712.5344	1.98	11.51	-5.99	-6.41	-6.71

*Abbreviations represent protein receptors as follows: **1UZN** = *M. tuberculosis* β -ketoacyl-acyl carrier protein reductase A (MabA); **4Q8I** = β -lactamase (Blac) and **6P9K** = β -ketoacyl-acyl carrier protein synthase (KasA). In the table, n.d. means not docked.

However, *M. circinelloides* has been reported to accumulate β -carotene (Vitamin A) [49], which perhaps explains the identification of pantothenic acid (Vitamin B5) (**6**) using the MS/MS fragmentation data of m/z 220.1183 [M+H]⁺. *M. circinelloides* is also known to be an oleaginous fungus capable of producing γ -linolenic [50]. Among the metabolites identified from *C. eragrosticola* MGK20, two were amino acids, L-arginine (**7**) and L-phenylalanine (**8**). These naturally occurring amino acids participate in various metabolic processes in cells, and thus are not expected to possess antimicrobial effect.

Extracts from *P. antarcticum* MGK31 and *P. expansum* MGK42 had greatest number of database hits (compounds **12-22** and **29-54** respectively) as the *Penicillium* genus is one of the widely explored natural source of bioactive agents. It was interesting to observe that even though extracts from the *Penicilliums* evidently harbored chemically diverse metabolites, the extracts showed poor inhibition of *Mycobacterial* growth in culture. This was not surprising as *Mycobacteria* are known to possess intrinsic resistance against a wide range of antibiotics as previously mentioned [38].

Metabolite profiling of the methanol extract from *C. eragrosticola* MGK20 resulted in the identification of gadusol (**23**), bionectin F (**24**), C16 phytosphingosine (**25**), L-Ile-L-Pro (**26**), L-Tryptophan (**27**) and L-Tyrosine (**28**). Among these compounds, the polyprenol polyterpenoid bionectin F (**24**) was first isolated from *Bionectria* sp. Y1085 (*Clonostachys* and *Bionectria* genera belong to the Bionectriaceae family) [51]. Unfortunately, the researchers in the previously mentioned study did not investigate any bioactivity of bionectin F. C16 phytosphingosine is a fatty acid which belongs to the family of sphingolipids, compounds abundant in fungi, plants and animal [52]. Başpınar et al., investigated the antimicrobial activity of commercially obtained phytosphingosine and found strong activity against *Enterococcus faecalis* (MIC = 4 µg/mL) and *Bacillus subtilis* (MIC = 8 µg/mL), but poor activity against *Pseudomonas aeruginosa*, *Salmonella enterica* and *Escherichia coli* (MIC ≥ 1 024 µg/mL) [53].

Gadusol (**23**), a metabolite of fungi, algae, bacteria and animals [54], plays a role as an ultra-violet (UV) photo-protectant that absorbs maximally at 268 nm in acidic pH, and as an antioxidant [55,56]. Reports on metabolites from *C. rogersoniana* are very limited and thus most ion peaks could not be annotated with database IDs. Bioactivity-guided fractionation and purification may help to isolate and characterize previously unidentified pure compounds.

Table 3.5. Metabolites common to fungal isolates and their molecular docking scores.

No.	Proposed ID	Predicted Formula	Metabolite occurrence [‡]	Precursor m/z [M+H] ⁺	Err ppm	RT (min)	Docking scores (kcal/mol)*		
							1UZN	4Q8I	6P9K
55	Choline sulfate	C ₅ H ₁₃ NO ₄ S	MGK13	184.0633	1.67	0.78	-4.51	-3.94	-3.37
			MGK20	184.0629	4.95	0.78			
			MGK31	184.0633	2.76	0.78			
56	L-Carnitine	C ₇ H ₁₅ NO ₃	MGK13	162.1123	1.67	0.78	-4.13	-3.46	-3.69
			MGK14	162.1124	0.43	0.81			
			MGK20	162.1123	1.05	0.78			
			MGK31	162.1127	-1.43	0.78			
			MGK42	162.1117	4.78	0.78			
57	Adenosine	C ₁₀ H ₁₃ N ₅ O ₄	MGK20	268.1043	4.61	4.56	-6.77	-4.43	-4.45
			MGK33	268.1028	-1.01	2.06			
58	Cyclo(L-Leu-L-Pro)	C ₁₁ H ₁₈ N ₂ O ₂	MGK31	211.1441	0.02	5.62	-5.57	-4.78	-5.67
			MGK33	211.1448	-3.31	3.85			
59	Cyclo(L-Pro-L-Val)	C ₁₀ H ₁₆ N ₂ O ₂	MGK20	197.1287	-1.25	4.86	-5.92	-4.07	-5.55
			MGK31	197.1288	-1.76	5.18			
60	Pyridoxamine	C ₈ H ₁₂ N ₂ O ₂	MGK20	169.0970	0.92	4.59	-5.26	-5.30	-6.20
			MGK31	169.0970	0.92	4.88			
61	Phytosphingosine	C ₁₈ H ₃₉ NO ₃	MGK13	318.3001	0.54	7.71	-3.77	-2.72	-6.20
			MGK14	318.3000	0.85	7.68			
			MGK20	318.3007	-1.35	7.59			
			MGK31	318.2993	3.06	8.63			
			MGK42	318.2998	1.48	7.63			
62	Sphinganine	C ₁₈ H ₃₉ NO ₂	MGK13	302.3053	0.19	8.49	-4.21	-3.44	-3.95
			MGK14	302.3050	1.18	8.46			
			MGK20	302.3059	-1.81	8.37			
			MGK31	302.3046	2.51	8.60			
			MGK42	302.3045	2.84	8.40			
63	Citrosprosteroide	C ₂₈ H ₄₄ O ₄	MGK31	445.3283	6.61	12.12	-4.70	-2.43	-3.02
			MGK42	445.3310	0.53	11.96			
64	Chrysogesinde B	C ₄₁ H ₇₅ NO ₉	MGK31	726.5522	-1.02	12.53	-6.91	-6.63	-6.98
			MGK42	726.5524	-1.30	12.22			
65	Ergosta-4,6,8(14),22-tetraen-3-one	C ₂₈ H ₄₀ O	MGK13	393.3153	-0.27	12.23	-5.13	-3.30	-4.80
			MGK31	393.3164	-3.08	12.49			

[‡]Abbreviations represent fungal isolates as follows: **MGK13** = *F. oxysporum* MGK13; **MGK14** = *M. circinelloides* MGK14; **MGK20** = *C. eragrosticola* MGK20; **MGK31** = *P. antarcticum* MGK31; **MGK33** = *C. rogersoniana* MGK33 and **MGK42** = *P. expansum* MGK42.

*Abbreviations represent protein receptors as follows: **1UZN** = *M. tuberculosis* β-ketoacyl-acyl carrier protein reductase A (MabA); **4Q8I** = β-lactamase (Blac) and **6P9K** = β-ketoacyl-acyl carrier protein synthase (KasA). In the table, n.d. means not docked.

3.3.4 Molecular docking and molecular dynamics simulation of fungal metabolites

The *in silico* molecular docking study demonstrated that the investigated ligands interacted with active site residues of *M. tuberculosis* H37Rv target proteins (1UZN, 4Q8I, and 6P9K) with docking scores presented in Tables 3.4 and 3.5. The values of the docking scores revealed

that bionectin F has the highest affinity to the selected target proteins (1UZN = -11.17 kcal/mol, 6P9K = -8.94 kcal/mol and 4Q8I = -8.19 kcal/mol). The molecular interactions of bionectin F with residues of the 1UZN and the binding pocket are both depicted in Figure 3.2. The strong interaction of bionectin F with the critical binding cavity of 1UZN was through hydrogen bonding MET A:190, ASP A:189, ASP A:94, LYS A:157, ASN A:88, ASN A:24, ILE A:31 and LYC A:184. Hydrophobic residues in the binding cavity of 1UZN also interacted with bionectin F, thus contributing to the ligand's observed affinity. The 1UZN and bionectin F complex was selected for further analysis in molecular dynamics simulations because of the interestingly high docking affinity.

The 1UZN and bionectin F (protein-ligand) complex was subjected to 50 ns molecular dynamics simulations to virtually evaluate in real-time, the structural stability and dynamic behavior of the protein-ligand complex system. The molecular dynamics simulations also determined which amino acids residues of 1UZN interact with the atoms of the bionectin F. The stability of the bionectin F and 1UZN complex was analyzed from the root mean square deviation (RMSD) plot depicted in Figure 3.3. The RMSD trajectory of the bionectin F and 1UZN complex, sharply augmented from 0 Å to approximately 2.8 Å from the onset until approximately 6 ns, remained constant until around 38 ns and then gradually fluctuated around 2 Å and 2.5 Å. The RMSD of (1UZN) backbone gradually rose from 0 Å to around 2.8 Å from 0 ns until the end of the 50 ns simulation. The RMSD plots show that the bionectin F and 1UZN complex is stable and there were no significant conformational changes in the structure of bionectin F (ligand). The systemic fluctuations along the 1UZN protein chain residues were analyzed based on the Root Mean Square Fluctuation (RMSF) plot presented in Figure 3.4.

The results showed low residual fluctuations in residues which interacted with the ligand while larger fluctuations were observed in residues which were not interacting with the ligand.

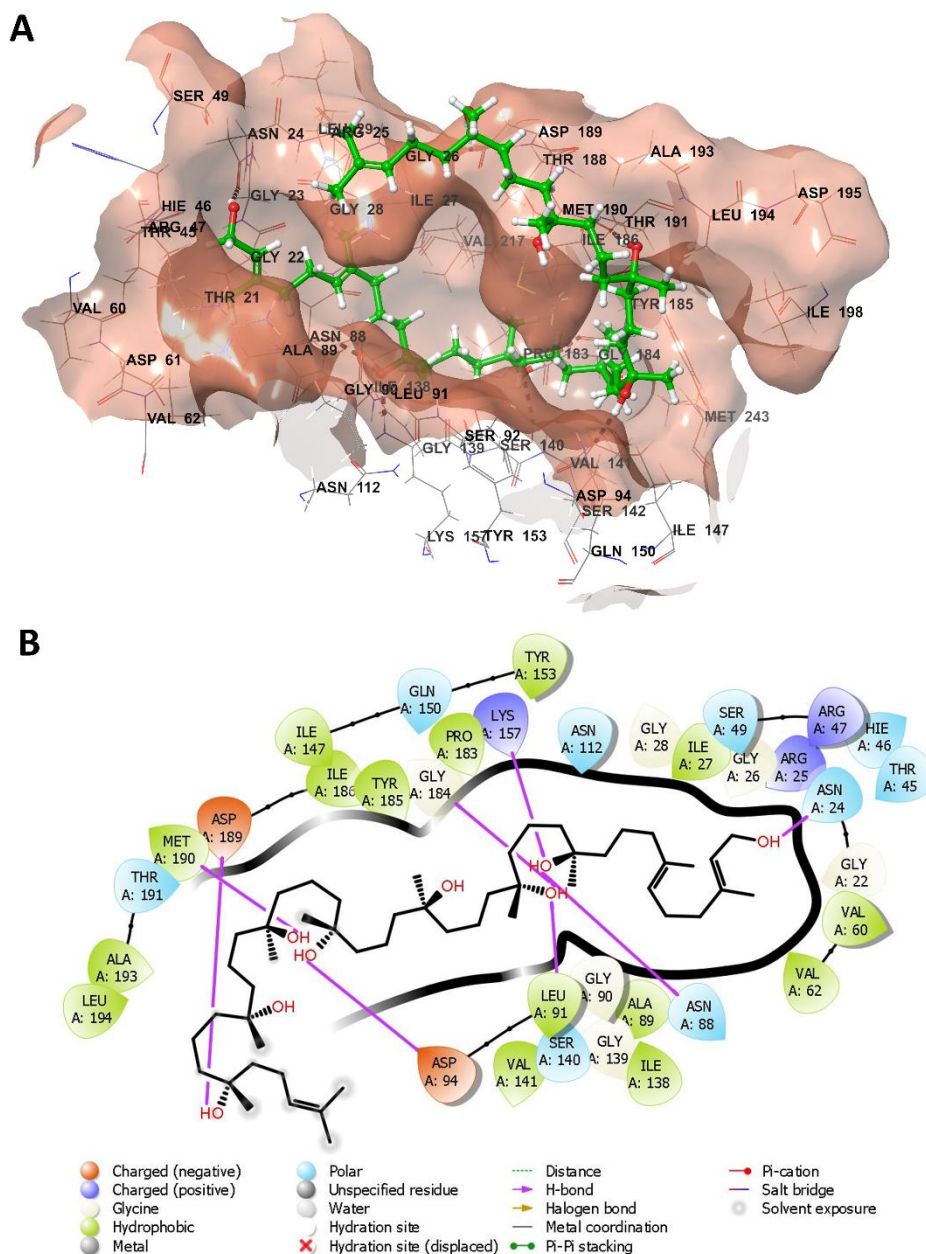


Figure 3.2. Three-dimensional representation of the binding pocket of 1UZN docked with bionectin F (**A**), and the two-dimensional representation of the molecular interactions observed between bionectin F and the binding site residues of 1UZN docked (**B**).

Trajectory analysis of the 0-50 ns simulation showed that bionectin F was bound to the cavity of 1UZN through hydrogen bonds (24 residues), ionic interactions (6 residues), water bridges (36 residues) and hydrophobic interactions (13 residues) along Chain A (Figure 3.5).

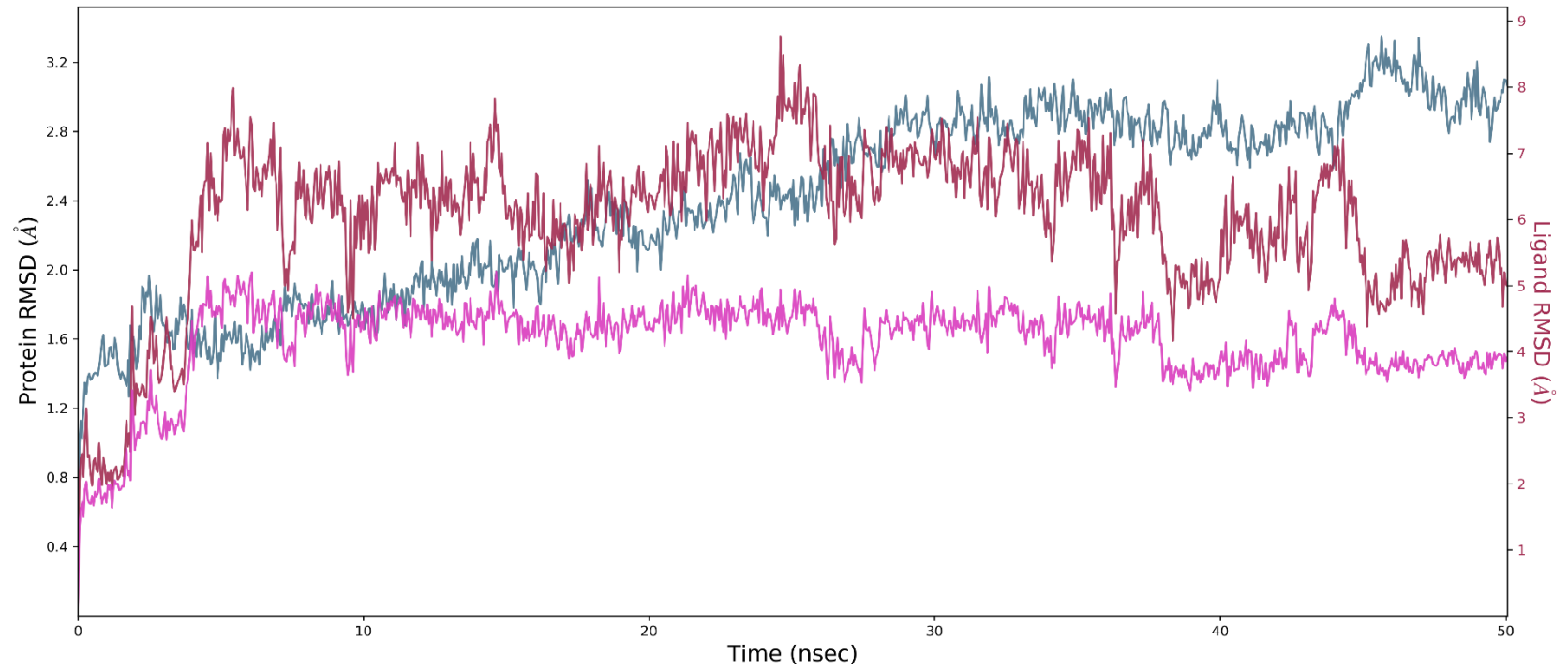
A

Figure 3.3. RMSD plots of the protein-ligand (1UZN and bionectin F) complex, ligand, and the protein back-bone for a 50 ns simulation.

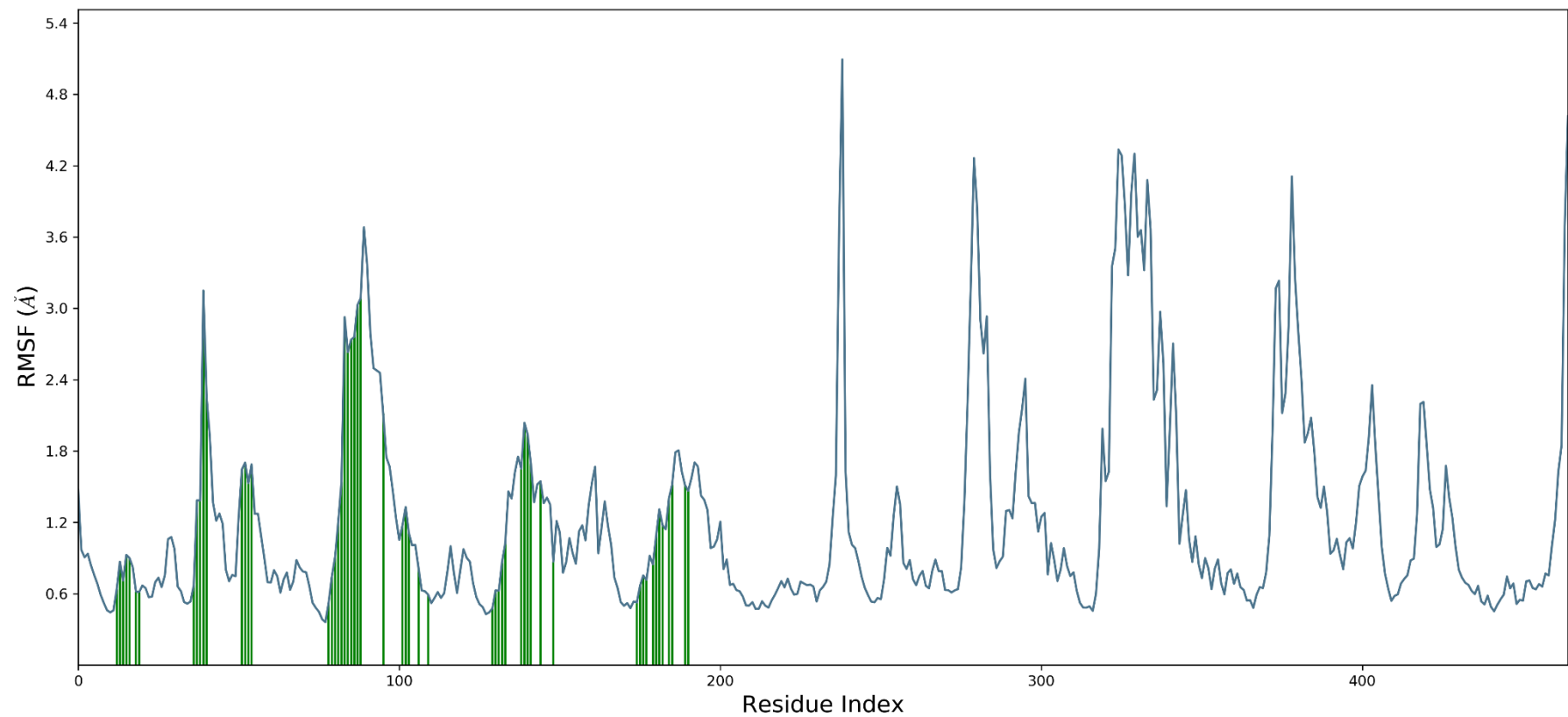


Figure 3.4. RMSF plot showing conformational fluctuations of the residues during the simulation, where interaction incidences are depicted by vertical green lines (**B**). The binding interactions of bionectin F with 1UZN during the simulation (**C**).

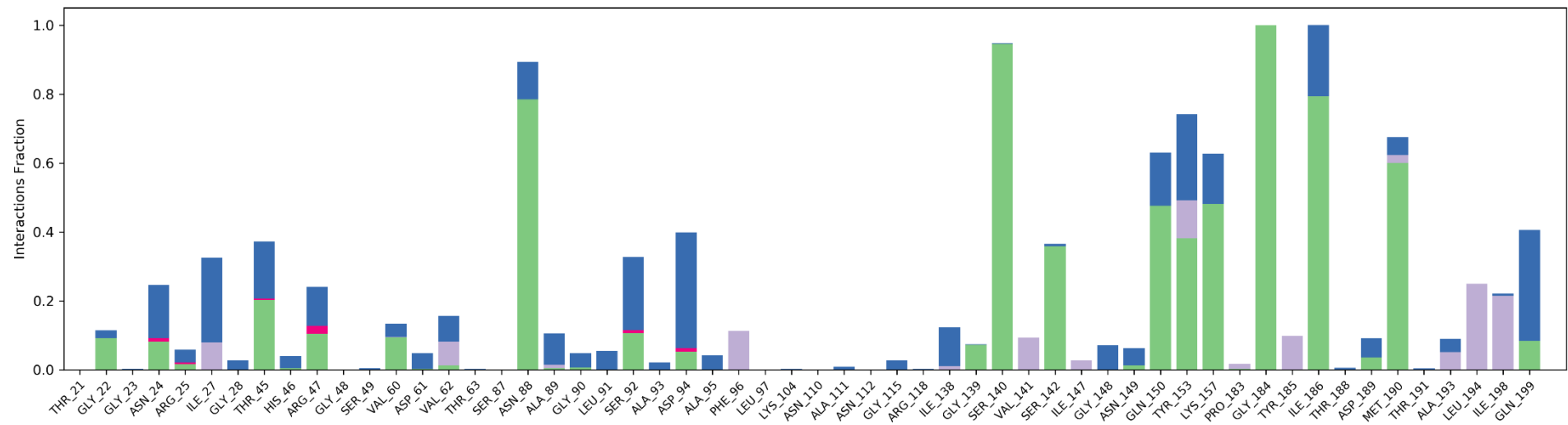


Figure 3.5. The binding interactions of bionectin F with 1UZN during the simulation.

After using CASTp to determine the binding pocket in 1UZN [57], it was noted that A:SER140 forms part of the substrate (β -ketoacyl-acyl carrier protein) binding site, while A:ASN88 and A:ILE186 form part of the binding site of the cofactor (NADPH). In a recent study, site-directed mutagenesis on A:SER140 led to complete loss of binding affinity for NADPH which is required by the enzyme to change the conformation the apo-form with a “closed” active site to an open conformation in the holo-form [58,59].

3.4 Conclusions

There is growing interest in discovering potent and novel antimycobacterial drugs which will overcome the limitations of presently used TB-drugs. Secondary metabolites from filamentous fungi have been regarded as an inexhaustible reservoir of diverse compounds for consideration in TB-drug discovery programs. In this study, the methanol crude extract from *C. rogersoniana* MGK33 was found to possess considerable antimicrobial activity against *M. smegmatis* mc²155 and *M. tuberculosis* H37Rv. Mass spectrometry-based metabolite profiling of this crude extract led to the tentative identification of bionectin F, a compound with very few biological activities described in literature. The potential Mycobacterial activity of 66 fungal metabolites identified in this study was evaluated by molecular docking against MabA (PDB ID = 1UZN), Blac (PDB ID = 4Q8I) and KasA (PDB ID = 6P9K). The results showed that bionectin F had the highest docking score (-11.17 kcal/mol) to MabA. The molecular dynamics simulations were used to gain a deeper insight of the conformational behaviors of the bionectin F and MabA complex. The analysis of the molecular dynamics simulations trajectories revealed that bionectin F interacted well with the protein and the complex was stable. The hydrogen bonding of bionectin F with A:SER140 could be play a role in inhibition of activity of MabA. Thus, the authors suggest that bionectin F can potentially be further investigated as an antimycobacterial compound for TB-drug discovery.

3.5 References

1. WHO *Global Tuberculosis Report 2021*; World Health Organization: Geneva, 2021.
2. WHO Tuberculosis (TB) Available online: <https://www.who.int/news-room/fact-sheets/detail/tuberculosis> (accessed on 30 May 2021).
3. WHO *Global Tuberculosis Report 2020*; World Health Organization: Geneva, 2020.
4. Quan, D.; Nagalingam, G.; Payne, R.; Triccas, J.A. New Tuberculosis Drug Leads from Naturally Occurring Compounds. *Int. J. Infect. Dis.* **2017**, *56*, 212–220, doi:10.1016/j.ijid.2016.12.024.
5. Duarte, K.; Rocha-Santos, T.A.P.; Freitas, A.C.; Duarte, A.C. Analytical Techniques for Discovery of Bioactive Compounds from Marine Fungi. *TrAC Trends Anal. Chem.* **2012**, *34*, 97–110, doi:10.1016/j.trac.2011.10.014.
6. Deshmukh, S.K.; Prakash, V.; Ranjan, N. Marine Fungi: A Source of Potential Anticancer Compounds. *Front. Microbiol.* **2018**, *8*, doi:10.3389/fmicb.2017.02536.
7. Wang, C.; Tang, S.; Cao, S. Antimicrobial Compounds from Marine Fungi. *Phytochem. Rev.* **2021**, *20*, 85–117, doi:10.1007/s11101-020-09705-5.
8. Marine Fungi Available online: <https://www.marinefungi.org/> (accessed on 31 May 2021).
9. El-Bondkly, E.A.M.; El-Bondkly, A.A.M.; El-Bondkly, A.A.M. Marine Endophytic Fungal Metabolites: A Whole New World of Pharmaceutical Therapy Exploration. *Heliyon* **2021**, *7*, e06362, doi:10.1016/j.heliyon.2021.e06362.

10. Watters, D.J. Ascidian Toxins with Potential for Drug Development. *Mar. Drugs* **2018**, *16*, 162, doi:10.3390/md16050162.
11. Evans, J.S.; Erwin, P.M.; Shenkar, N.; López-Legentil, S. Introduced Ascidians Harbor Highly Diverse and Host-Specific Symbiotic Microbial Assemblages. *Sci. Rep.* **2017**, *7*, 11033, doi:10.1038/s41598-017-11441-4.
12. Song, Q.; Li, X.-M.; Hu, X.-Y.; Li, X.; Chi, L.-P.; Li, H.-L.; Wang, B.-G. Antibacterial Metabolites from Ascidian-Derived Fungus *Aspergillus clavatus* AS-107. *Phytochem. Lett.* **2019**, *34*, 30–34, doi:10.1016/j.phytol.2019.09.004.
13. Yurchenko, A.N.; Ivanets, E.V.; Smetanina, O.F.; Pivkin, M.V.; Dyshlovoi, S.A.; von Amsberg, G.; Afiyatullof, Sh.Sh. Metabolites of the Marine Fungus *Aspergillus candidus* KMM 4676 Associated with a Kuril Colonial Ascidian. *Chem. Nat. Compd.* **2017**, *53*, 747–749, doi:10.1007/s10600-017-2108-y.
14. Wang, C.; Wang, J.; Huang, Y.; Chen, H.; Li, Y.; Zhong, L.; Chen, Y.; Chen, S.; Wang, J.; Kang, J.; et al. Anti-Mycobacterial Activity of Marine Fungus-Derived 4-Deoxybostrycin and Nigrosporin. *Molecules* **2013**, *18*, 1728–1740, doi:10.3390/molecules18021728.
15. Sharma, A.; Islam, M.H.; Fatima, N.; Upadhyay, T.K.; Khan, M.K.A.; Dwivedi, U.N.; Sharma, R. Elucidation of Marine Fungi Derived Anthraquinones as Mycobacterial Mycolic Acid Synthesis Inhibitors: An *in silico* Approach. *Mol. Biol. Rep.* **2019**, *46*, 1715–1725, doi:10.1007/s11033-019-04621-0.
16. Hu, J.; Li, Z.; Gao, J.; He, H.; Dai, H.; Xia, X.; Liu, C.; Zhang, L.; Song, F. New Diketopiperazines from a Marine-Derived Fungus Strain *Aspergillus versicolor* MF180151. *Mar. Drugs* **2019**, *17*, 262, doi:10.3390/md17050262.

17. Havenga, B.S. Fouling by Non-Indigenous Marine Species – Impacts on Biodiversity and Mariculture, Stellenbosch University: Stellenbosch, 2014.
18. Tapfuma, K.I.; Uche-Okereafor, N.; Sebola, T.E.; Hussan, R.; Mekuto, L.; Makatini, M.M.; Green, E.; Mavumengwana, V. Cytotoxic Activity of Crude Extracts from *Datura stramonium*'s Fungal Endophytes against A549 Lung Carcinoma and UMG87 Glioblastoma Cell Lines and LC-QTOF-MS/MS Based Metabolite Profiling. *BMC Complement. Altern. Med.* **2019**, *19*, 330, doi:10.1186/s12906-019-2752-9.
19. McGinnis, S.; Madden, T.L. BLAST: At the Core of a Powerful and Diverse Set of Sequence Analysis Tools. *Nucleic Acids Res.* **2004**, *32*, W20–W25, doi:10.1093/nar/gkh435.
20. Song, R.; Wang, J.; Sun, L.; Zhang, Y.; Ren, Z.; Zhao, B.; Lu, H. The Study of Metabolites from Fermentation Culture of *Alternaria oxytropis*. *BMC Microbiol.* **2019**, *19*, 35, doi:10.1186/s12866-019-1408-8.
21. Kanehiro, Y.; Tomioka, H.; Pieters, J.; Tatano, Y.; Kim, H.; Iizasa, H.; Yoshiyama, H. Identification of Novel Mycobacterial Inhibitors Against Mycobacterial Protein Kinase G. *Front. Microbiol.* **2018**, *9*, 1517, doi:10.3389/fmicb.2018.01517.
22. Elshikh, M.; Ahmed, S.; Funston, S.; Dunlop, P.; McGaw, M.; Marchant, R.; Banat, I.M. Resazurin-Based 96-Well Plate Microdilution Method for the Determination of Minimum Inhibitory Concentration of Biosurfactants. *Biotechnol. Lett.* **2016**, *38*, 1015, doi:10.1007/s10529-016-2079-2.
23. Andrews, J.M. Determination of Minimum Inhibitory Concentrations. *J. Antimicrob. Chemother.* **2001**, *48 Suppl 1*, 5–16, doi:10.1093/jac/48.suppl_1.5.

24. Tapfuma, K.I.; Sebola, T.E.; Uche-Okereafor, N.; Koopman, J.; Hussan, R.; Makatini, M.M.; Mekuto, L.; Mavumengwana, V. Anticancer Activity and Metabolite Profiling Data of *Penicillium janthinellum* KTMT5. *Data Brief* **2020**, *28*, 104959, doi:10.1016/j.dib.2019.104959.
25. Magangana, T.P.; Stander, M.A.; Masondo, N.A.; Makunga, N.P. Steviol Glycoside Content and Essential Oil Profiles of *Stevia rebaudiana* Bertoni in Response to NaCl and Polyethylene Glycol as Inducers of Salinity and Drought Stress *in vitro*. *Plant Cell Tissue Organ Cult. PCTOC* **2021**, *145*, 1–18, doi:10.1007/s11240-020-01972-6.
26. Tsugawa, H.; Cajka, T.; Kind, T.; Ma, Y.; Higgins, B.; Ikeda, K.; Kanazawa, M.; VanderGheynst, J.; Fiehn, O.; Arita, M. MS-DIAL: Data Independent MS/MS Deconvolution for Comprehensive Metabolome Analysis. *Nat. Methods* **2015**, *12*, 523, doi:10.1038/nmeth.3393.
27. Mark, P.; Nilsson, L. Structure and Dynamics of the TIP3P, SPC, and SPC/E Water Models at 298 K. *J. Phys. Chem. A* **2001**, *105*, 9954–9960, doi:10.1021/jp003020w.
28. Chinnathambi, S.; Karthikeyan, S.; Hanagata, N.; Shirahata, N. Molecular Interaction of Silicon Quantum Dot Micelles with Plasma Proteins: Hemoglobin and Thrombin. *RSC Adv.* **2019**, *9*, 14928–14936, doi:10.1039/C9RA02829C.
29. Robinson, T.B.; Peters, K.; Brooker, B. Coastal Invasions: The South African Context. In *Biological Invasions in South Africa*; van Wilgen, B.W., Measey, J., Richardson, D.M., Wilson, J.R., Zengeya, T.A., Eds.; Invading Nature - Springer Series in Invasion Ecology; Springer International Publishing: Cham, 2020; pp. 229–247 ISBN 978-3-030-32394-3.
30. Gordon, T.; Roth, L.; Caicci, F.; Manni, L.; Shenkar, N. Spawning Induction, Development and Culturing of the Solitary Ascidian *Polycarpa mytiligera*, an Emerging

- Model for Regeneration Studies. *Front. Zool.* **2020**, *17*, 19, doi:10.1186/s12983-020-00365-x.
31. Baeza, M.; Barahona, S.; Alcaíno, J.; Cifuentes, V. Amplicon-Metagenomic Analysis of Fungi from Antarctic Terrestrial Habitats. *Front. Microbiol.* **2017**, *0*, doi:10.3389/fmicb.2017.02235.
 32. Biller, S.J.; Berube, P.M.; Dooley, K.; Williams, M.; Satinsky, B.M.; Hackl, T.; Hogle, S.L.; Coe, A.; Bergauer, K.; Bouman, H.A.; et al. Marine Microbial Metagenomes Sampled across Space and Time. *Sci. Data* **2018**, *5*, 180176, doi:10.1038/sdata.2018.176.
 33. Amend, A.; Burgaud, G.; Cunliffe, M.; Edgcomb, V.P.; Ettinger, C.L.; Gutiérrez, M.H.; Heitman, J.; Hom, E.F.Y.; Ianiri, G.; Jones, A.C.; et al. Fungi in the Marine Environment: Open Questions and Unsolved Problems. *mBio* **2019**, *10*, e01189-18, doi:10.1128/mBio.01189-18.
 34. Utermann, C.; Echelmeyer, V.A.; Oppong-Danquah, E.; Blümel, M.; Tasdemir, D. Diversity, Bioactivity Profiling and Untargeted Metabolomics of the Cultivable Gut Microbiota of *Ciona intestinalis*. *Mar. Drugs* **2021**, *19*, 6, doi:10.3390/md19010006.
 35. López-Legentil, S.; Erwin, P.M.; Turon, M.; Yarden, O. Diversity of Fungi Isolated from Three Temperate Ascidiaceans. *Symbiosis* **2015**, *66*, 99–106, doi:10.1007/s13199-015-0339-x.
 36. Menezes, C.B.A.; Bonugli-Santos, R.C.; Miqueletto, P.B.; Passarini, M.R.Z.; Silva, C.H.D.; Justo, M.R.; Leal, R.R.; Fantinatti-Garboggini, F.; Oliveira, V.M.; Berlinck, R.G.S.; et al. Microbial Diversity Associated with Algae, Ascidiaceans and Sponges from the North Coast of São Paulo State, Brazil. *Microbiol. Res.* **2010**, *165*, 466–482, doi:10.1016/j.micres.2009.09.005.

37. Awouafack, M.D.; McGaw, L.J.; Gottfried, S.; Mbouangouere, R.; Tane, P.; Spiteller, M.; Eloff, J.N. Antimicrobial Activity and Cytotoxicity of the Ethanol Extract, Fractions and Eight Compounds Isolated from *Eriosema robustum* (Fabaceae). *BMC Complement. Altern. Med.* **2013**, *13*, 289, doi:10.1186/1472-6882-13-289.
38. Gygli, S.M.; Borrell, S.; Trauner, A.; Gagneux, S. Antimicrobial Resistance in *Mycobacterium tuberculosis*: Mechanistic and Evolutionary Perspectives. *FEMS Microbiol. Rev.* **2017**, *41*, 354–373, doi:10.1093/femsre/fux011.
39. Baysarowich, J.; Koteva, K.; Hughes, D.W.; Ejim, L.; Griffiths, E.; Zhang, K.; Junop, M.; Wright, G.D. Rifamycin Antibiotic Resistance by ADP-Ribosylation: Structure and Diversity of Arr. *Proc. Natl. Acad. Sci.* **2008**, *105*, 4886–4891, doi:10.1073/pnas.0711939105.
40. Sanz-García, F.; Anoz-Carbonell, E.; Pérez-Herrán, E.; Martín, C.; Lucía, A.; Rodrigues, L.; Aínsa, J.A. Mycobacterial Aminoglycoside Acetyltransferases: A Little of Drug Resistance, and a Lot of Other Roles. *Front. Microbiol.* **2019**, *10*, 46, doi:10.3389/fmicb.2019.00046.
41. Machado, D.; Lecorche, E.; Mougari, F.; Cambau, E.; Viveiros, M. Insights on *Mycobacterium leprae* Efflux Pumps and Their Implications in Drug Resistance and Virulence. *Front. Microbiol.* **2018**, *9*, 3072, doi:10.3389/fmicb.2018.03072.
42. Boruta, T. Uncovering the Repertoire of Fungal Secondary Metabolites: From Fleming's Laboratory to the International Space Station. *Bioengineered* **2018**, *9*, 12–16, doi:10.1080/21655979.2017.1341022.

43. Tomm, H.A.; Ucciferri, L.; Ross, A.C. Advances in Microbial Culturing Conditions to Activate Silent Biosynthetic Gene Clusters for Novel Metabolite Production. *J. Ind. Microbiol. Biotechnol.* **2019**, *46*, 1381–1400, doi:10.1007/s10295-019-02198-y.
44. Silva, K.P.T.; Chellamuthu, P.; Boedicker, J.Q. Quantifying the Strength of Quorum Sensing Crosstalk within Microbial Communities. *PLOS Comput. Biol.* **2017**, *13*, 1–16, doi:10.1371/journal.pcbi.1005809.
45. Jomori, T.; Hara, Y.; Sasaoka, M.; Harada, K.; Setiawan, A.; Hirata, K.; Kimishima, A.; Arai, M. *Mycobacterium smegmatis* Alters the Production of Secondary Metabolites by Marine-Derived *Aspergillus Niger*. *J. Nat. Med.* **2020**, *74*, 76–82, doi:10.1007/s11418-019-01345-0.
46. Mózsik, L.; Hoekzema, M.; de Kok, N.A.W.; Bovenberg, R.A.L.; Nygård, Y.; Driessen, A.J.M. CRISPR-Based Transcriptional Activation Tool for Silent Genes in Filamentous Fungi. *Sci. Rep.* **2021**, *11*, 1118, doi:10.1038/s41598-020-80864-3.
47. Emani, C.S.; Williams, M.J.; Wiid, I.J.; Baker, B.; Carolis, C. Compounds with Potential Activity against *Mycobacterium tuberculosis*. *Antimicrob. Agents Chemother.* **2018**, *62*, e02236-17, doi:10.1128/AAC.02236-17.
48. Nilanonta, C.; Isaka, M.; Kittakoop, P.; Trakulnaleamsai, S.; Tanticharoen, M.; Thebtaranonth, Y. Precursor-Directed Biosynthesis of Beauvericin Analogs by the Insect Pathogenic Fungus *Paecilomyces tenuipes* BCC 1614. *Tetrahedron* **2002**, *58*, 3355–3360, doi:10.1016/S0040-4020(02)00294-6.
49. Naz, T.; Nosheen, S.; Li, S.; Nazir, Y.; Mustafa, K.; Liu, Q.; Garre, V.; Song, Y. Comparative Analysis of β -Carotene Production by *Mucor circinelloides* Strains CBS

- 277.49 and WJ11 under Light and Dark Conditions. *Metabolites* **2020**, *10*, doi:10.3390/metabo10010038.
50. Tang, X.; Zhao, L.; Chen, H.; Chen, Y.Q.; Chen, W.; Song, Y.; Ratledge, C. Complete Genome Sequence of a High Lipid-Producing Strain of *Mucor circinelloides* WJ11 and Comparative Genome Analysis with a Low Lipid-Producing Strain CBS 277.49. *PLOS ONE* **2015**, *10*, 1–11, doi:10.1371/journal.pone.0137543.
51. Yang, Y.-H.; Yang, D.-S.; Li, G.-H.; Pu, X.-J.; Mo, M.-H.; Zhao, P.-J. Antibacterial Diketopiperazines from an Endophytic Fungus *Bionectria* sp. Y1085. *J. Antibiot. (Tokyo)* **2019**, *72*, 752–758, doi:10.1038/s41429-019-0209-5.
52. Singh, A.; Del Poeta, M. Sphingolipidomics: An Important Mechanistic Tool for Studying Fungal Pathogens. *Front. Microbiol.* **2016**, *7*, 501, doi:10.3389/fmicb.2016.00501.
53. Başpınar, Y.; Kotmakçı, M.; Öztürk, İ. Antimicrobial Activity of Phytosphingosine Nanoemulsions against Bacteria and Yeasts. *Celal Bayar Univ. J. Sci.* **2018**, *14*, 223–228, doi:10.18466/cbayarfbe.403152.
54. Osborn, A.R.; Almabruk, K.H.; Holzwarth, G.; Asamizu, S.; LaDu, J.; Kean, K.M.; Karplus, P.A.; Tanguay, R.L.; Bakalinsky, A.T.; Mahmud, T. De Novo Synthesis of a Sunscreen Compound in Vertebrates. *eLife* **2015**, *4*, doi:10.7554/eLife.05919.
55. Orallo, D.E.; Lores, N.J.; Arbeloa, E.M.; Bertolotti, S.G.; Churio, M.S. Sensitized Photo-Oxidation of Gadusol Species Mediated by Singlet Oxygen. *J. Photochem. Photobiol. B* **2020**, *213*, 112078, doi:10.1016/j.jphotobiol.2020.112078.

56. Arbeloa, E.M.; Uez, M.J.; Bertolotti, S.G.; Churio, M.S. Antioxidant Activity of Gadusol and Occurrence in Fish Roes from Argentine Sea. *Food Chem.* **2010**, *119*, 586–591, doi:10.1016/j.foodchem.2009.06.061.
57. Tian, W.; Chen, C.; Lei, X.; Zhao, J.; Liang, J. CASTp 3.0: Computed Atlas of Surface Topography of Proteins. *Nucleic Acids Res.* **2018**, *46*, W363–W367, doi:10.1093/nar/gky473.
58. Rosado, L.A.; Caceres, R.A.; de Azevedo, W.F.; Basso, L.A.; Santos, D.S. Role of Serine140 in the Mode of Action of *Mycobacterium tuberculosis* β -Ketoacyl-ACP Reductase (MabA). *BMC Res. Notes* **2012**, *5*, 526, doi:10.1186/1756-0500-5-526.
59. Küssau, T.; Flipo, M.; Van Wyk, N.; Viljoen, A.; Olieric, V.; Kremer, L.; Blaise, M. Structural Rearrangements Occurring upon Cofactor Binding in the *Mycobacterium smegmatis* β -Ketoacyl-Acyl Carrier Protein Reductase MabA. *Acta Crystallogr. Sect. Struct. Biol.* **2018**, *74*, 383–393, doi:10.1107/S2059798318002917.

Chapter 4

Antimycobacterial activity of metal-coated iron oxide nanoparticles and their functionalization with an extract from *Clonostachys rogersoniana* MGK33

Kudzanai Ian Tapfuma¹, Annamé Geldenhuys², Lucinda Baatjies¹, Nasiema Allie¹, Andre G. Loxton¹, Vuyo Mavumengwana¹ and Rehana Malgas-Enus^{1,*}

^a DSI-NRF Centre of Excellence for Biomedical Tuberculosis Research; South African Medical Research Council Centre for Tuberculosis Research; Division of Molecular Biology and Human Genetics, Faculty of Medicine and Health Sciences, Stellenbosch University, Cape Town.

^b Department of Chemistry and Polymer Science, Faculty of Science, University of Stellenbosch, Matieland, South Africa.

* Corresponding author.

Email address: rehana@sun.ac.za; Tel.: +27 21 808 2801.

4.0 Abstract

Anti-tuberculosis (TB) drug discovery studies are essential for the discovery of new antimycobacterial agents to support efforts of eradicating this epidemic. The current drugs available for the treatment of TB are susceptible to resistance by *Mycobacterium tuberculosis*, hence a need for novel classes of new drugs is eminent. In this study, mono- and bi-metallic super-paramagnetic iron oxide nanoparticles (SPIONs) were investigated for potential use as anti-TB agents. SPIONs were synthesized through chemical co-precipitation of Fe(II) and Fe(III), followed by surface modification using Ni, Zn, Au, Cu and Ag, to form core-shell coated SPIONs. These NPs were characterized by Fourier-transform infrared spectroscopy

(FTIR) and ultraviolet visible spectroscopy (UV-Vis). High-resolution transmission electron microscopy (HRTEM) was used to determine the spherical shape and size of the nanoparticles with a diameter in the range of 20-32 nm. Thereafter, mono- and bi-metallic SPIONs were functionalized with a crude fungal extract from *Clonostachys rogersoniana* MGK33. Evidence of functionalization was confirmed by performing liquid chromatography mass spectrometry (LCMS) analysis. In particular, extraction efficiency of bionectin F by the nanoparticles was calculated and found to be highest for Ni-SPIONs@MGK33 (22.94%). Antimycobacterial assays against *Mycobacterium smegmatis* mc²155 showed that the Cu-SPIONs and Ag-SPIONs had the strongest activity, exhibiting total growth inhibition at concentrations as low as 15.63 and 7.81 µg/mL respectively. Functionalized Cu-SPIONs@MGK33 and Ag-SPIONs@MGK33 exhibited weaker activity, leading to the assumption that the adsorbed metabolites reduced the bioactive surface area of the nanoparticles and thus limited contact with targets. Thus, it was concluded that future drug development studies should focus on enhancing the safety and efficacy of Ag-SPIONs and Cu-SPIONs as leads for future anti-TB agents.

Keywords: Iron oxide nanoparticles; Tuberculosis; Fungal metabolites; Drug discovery.

4.1 Introduction

Tuberculosis (TB) is an infectious disease caused by *Mycobacterium tuberculosis* in humans [1]. Estimates suggest that more than one-third of the global population is infected with the disease, thus presenting a major global health problem as the TB pandemic can turn into an epidemic disease if not well managed [2]. TB is mainly transmitted when pathogen-laden bioaerosols (< 5 µm) generated in lower respiratory tract of infected individuals are exhaled and consequently inhaled by other individuals, where the infection establishes primarily in the lungs [3]. Treatment is achieved by the administration of a 6-month multi-drug regimen containing a combination of the four first-line drugs for drug-susceptible TB, while multi-drug

resistant and extensively-drug resistant TB (MDR- and XDR-TB) requires use of second-line TB drugs whose regimens may comprise of injectable drugs to be taken daily for periods that may exceed 24 months [4]. The long duration of currently approved TB treatment, adverse effects of the first- and second-line drugs and their susceptibility to resistance by the pathogen, necessitates the need for the discovery of a new class of antimicrobials which will overcome the limitations of the presently used TB-drugs.

Application of metallic NPs as antimicrobial agents for treatment of infectious diseases is an area of intensive research. Successful utilization of Au, Ag, Cu, Al, Zn, Fe and several other metallic nanoparticles against microbial pathogens in general has been widely reported and their mechanisms of action have been proposed [5]. Furthermore, the use of nanoparticles presents a number of benefits as they are likely to be taken up by cells due to their small size (1-100 nm), and thus in some cases, allowing delivery of antibiotic ligands to their targets [6]. Inhalation of aerosols laden with active nanoparticles is a proposed technique that may allow effective introduction of nanoparticles into the lungs which are the site of primary infection for TB [7]. However, nanoparticles may fail to achieve sufficient residence time to penetrate granulomas, which are an aggregate of immune cells containing *M. tuberculosis*.

The use of SPIONs is a potential technique that may allow nanoparticles with antimycobacterial activity to be guided by an external magnet to a specific site of infection in the lungs or any other site/organ. SPIONs are already being successfully employed in penetrating solid, deep-seeded cancer tumors with the aid of oppositely-polarized magnets [8–10]. In addition, SPIONs are capable of inducing magnetic hyperthermia in TB treatment, which is localized and sustained heating at 42 °C or above, resulting from the application of a specific external magnetic frequency [11]. This technique has been proven to cause cell death.

In this study, the aim was to investigate the *in vitro* antimycobacterial activity of SPIONs coated with various metals and functionalized with a bioactive extract from the marine derived fungus, *Clonostachys rogersoniana* MGK33, whose minimum inhibitory concentration (MIC) was found to be 125 µg/mL against *Mycobacterium smegmatis* mc²155 in a previous study [12]. SPIONs were chemically synthesized, and their surfaces were modified using Ni, Zn, Au, Cu and Ag. The fungal extract used is a potential enhancer of the antimycobacterial activity of the nanoparticles. This study followed the design outline in Figure 4.1.

4.2 Methods and materials

4.2.1 Synthesis naked superparamagnetic iron oxide nanoparticles (SPIONs)

SPIONs were synthesized using the chemical co-precipitation of Fe(III) and Fe(II) [13]. FeSO₄·7H₂O (2.330 g, 8.381 mmol) and FeCl₃·6H₂O, (4.521 g, 16.726 mmol) were dissolved in distilled deionized water (100 mL) in a 1:2 molar ratio. Dropwise addition of an excess amount of ammonium hydroxide (NH₄OH, 33%, 26 mL) resulted in the formation of a black precipitate (SPIONs). At this point, the reaction was allowed to continue for a further 30 min to ensure complete precipitation of metal ions. Using magnetic decantation, SPIONs were then separated from the solution and washed several times using deionized water until a pH of 7 was reached. The product was then washed twice with 50 mL of ethanol and allowed to dry overnight in an oven at 40 °C. The yield of SPIONs was 3.560 g.

4.2.2 Synthesis of nickel coated SPIONs (Ni-SPIONs)

Ni-SPIONs were synthesized by initially suspending 0.4 g of SPIONs and 0.2 g of Ni(NO₃)₂·6H₂O (0.688 mmol) in 40 mL of distilled deionized water and stirred for 30 min. NaBH₄, (0.391 g, 10.333 mmol) was then slowly added. The reaction was then allowed to continue stirring for a further two hours to ensure complete reduction. The NPs was again

isolated by magnetic decantation followed by ethanol washing (3 x 10 mL) to isolate Ni-SPIONs which were then dried at 60 °C in an oven. The yield of Ni-SPIONs was 0.556 g.

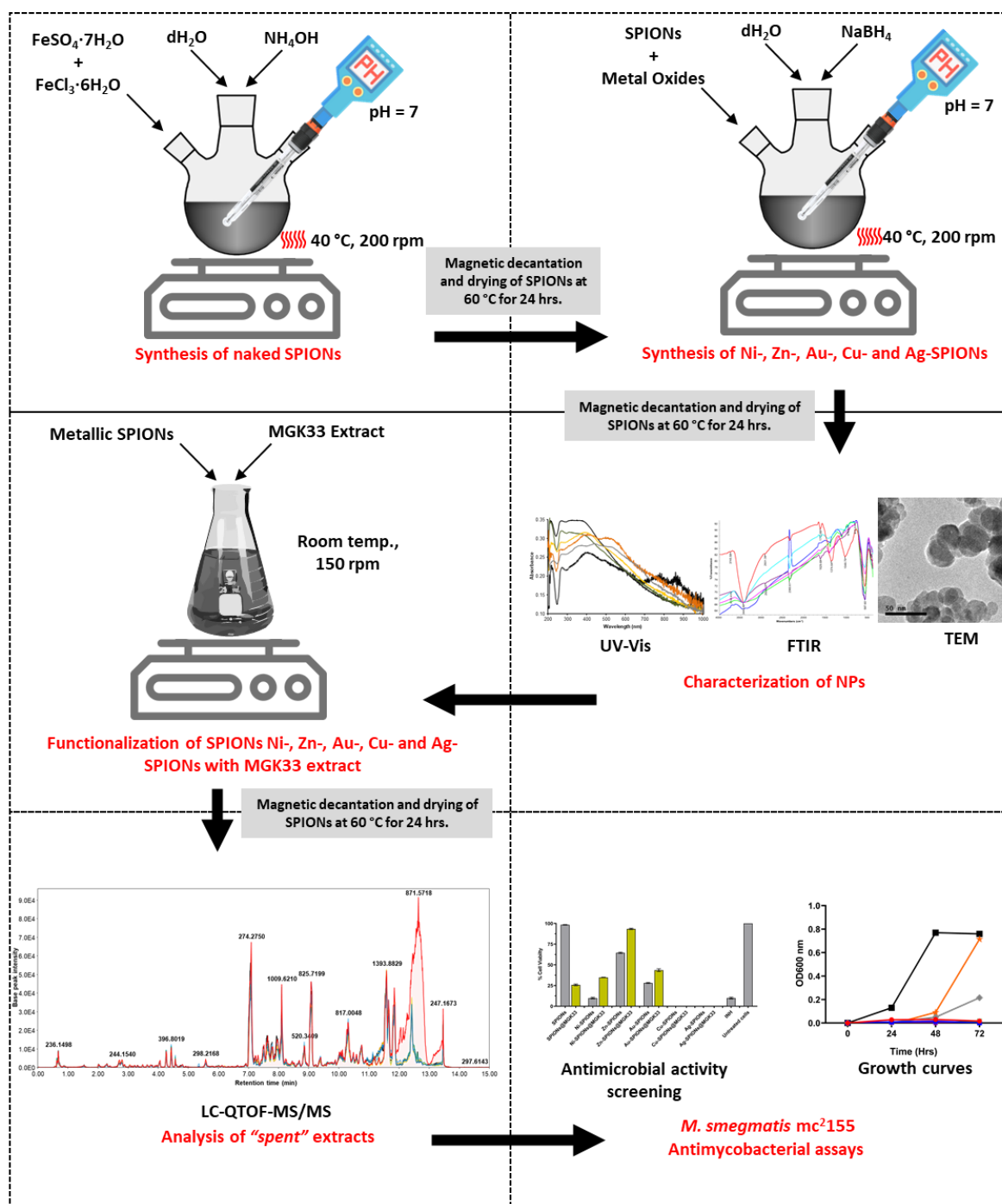


Figure 4.1. Figurative representation of the study design.

4.2.3 Synthesis of zinc coated SPIONs (Zn-SPIONs)

Zn-SPIONs were synthesized by initially suspending 0.4 g of SPIONs and 0.2 g of ZnCl_2 (1.467 mmol) in 40 mL of distilled deionized water and stirred for 30 min. NaBH_4 (0.833 g,

22.014 mmol) was then slowly added. The reaction was then allowed to continue stirring for a further two hours to ensure complete reduction. The NPs was again isolated by magnetic decantation followed by ethanol washing (3 x 10 mL) to isolate Zn-SPIONs which were then dried at 60 °C in an oven. The yield of Zn-SPIONs was 0.526 g.

4.2.4 Synthesis of gold coated SPIONs (Au-SPIONs)

Au-SPIONs were synthesized by initially suspending 0.2 g of SPIONs and 0.1 g of HAuCl₄ (0.294 mmol) in 20 mL of distilled deionized water and stirred for 30 min. NaBH₄ (0.096 g, 2.537 mmol) was then slowly added. The reaction was then allowed to continue stirring for a further two hours to ensure complete reduction. The NPs was again isolated by magnetic decantation followed by ethanol washing (3 x 10 mL) to isolate Au-SPIONs which were then dried at 60 °C in an oven. The yield of Au-SPIONs was 0.220 g.

4.2.5 Synthesis of copper coated SPIONs (Cu-SPIONs)

Cu-SPIONs were synthesized by initially suspending 0.2 g of SPIONs and 0.1 g of CuNO₃ (0.796 mmol) in 20 mL of distilled deionized water and stirred for 30 min. NaBH₄ (0.243 g, 6.422 mmol) was then slowly added. The reaction was then allowed to continue stirring for a further two hours to ensure complete reduction. The NPs was again isolated by magnetic decantation followed by ethanol washing (3 x 10 mL) to isolate Cu-SPIONs which were then dried at 60 °C in an oven. The yield of Cu-SPIONs was 0.207 g.

4.2.6 Synthesis of silver coated SPIONs (Ag-SPIONs)

Ag-SPIONs were synthesized by initially suspending 0.2 g of SPIONs and 0.1 g of AgNO₃ (0.589 mmol) in 20 mL of distilled deionized water and stirred for 30 min. NaBH₄ (0.220 g, 5.814 mmol) was then slowly added. The reaction was then allowed to continue stirring for a further two hours to ensure complete reduction. The NPs was again isolated by magnetic

decantation followed by ethanol washing (3 x 10 mL) to isolate Ag-SPIONs which were then dried at 60 °C in an oven. The yield of Ag-SPIONs was 0.246 g.

4.2.7 Ultraviolet–visible (UV-Vis) spectroscopy

Ultraviolet–visible (UV-Vis) spectral data for nanoparticles were gathered using a MultiScan Sky spectrophotometer (Thermo Fisher Scientific). Absorbance of a small amount of nanoparticle sample dispersed in methanol was measured over a continuous wavelength range of 200-1000 nm using the fast mode set at 1 nm per step.

4.2.8 Fourier transform infrared (FTIR) spectroscopy

FTIR spectroscopy was performed using a PerkinElmer Spectrum Two Infra-Red spectrometer as previously described [13]. Approximately 100 mg of dry potassium bromide (KBr) was mixed with a small amount nanoparticle sample, ground into fine powder using a mortar and pestle, then subsequently pressed into a pellet using a manual hydraulic pellet-press. A KBr pellet was also prepared as a background noise control. Spectral data were collected between 4000 and 400 cm^{-1} using 32 scans at a nominal resolution of 4.0 cm^{-1} [13].

4.2.9 High resolution transmission electron microscopy (HRTEM)

The JEOL-1200EXII high resolution transmission electron microscope (JEOL Ltd, MA, USA) was utilized to capture images of nanoparticles and measure their sizes at an accelerating voltage of 250 kV. Samples of nanoparticles were initially dispersed in deionized water, following by placing a drop of the sample on carbon-coated 200 mesh copper grid. Drying was then performed using a UV lamp before submitting the samples for analysis [13]. ImageJ, a free image analysis software available online [14], was used to determine the average size of approximately 200 individual nanoparticles from each sample. The software, SPSS Statistics 27 (IBM Corporation, NY, USA), was then utilized to draw histogram plots.

4.2.10 Functionalization of nanoparticles with a crude extract from *Clonostachys rogersoniana* MGK33 and liquid chromatography mass spectrometry

The methanolic crude extract from the marine fungus, *C. rogersoniana* MGK33, was utilized in this study to functionalize synthetic nanoparticles. The MGK33 extract was isolated, tested for antimycobacterial activity and profiled using tandem liquid chromatography quadrupole time-of-flight mass spectrometry (LC-QTOF-MS/MS) in a previous study [12]. Each sample of nanoparticles (naked SPIONs, Ni-SPIONs, Zn-SPIONs, Au-SPIONs, Cu-SPIONs and Ag-SPIONs), measuring 10 mg was mixed with 1 mL of a filter-sterilized MGK33 extract, dissolved in methanol at 5 mg/mL. The mixtures were sonicated for 15 minutes and allowed to shake at 150 rpm at room temperature for 4 hours to allow metabolites from the extract to bind to the nanoparticles. Magnetic separation was then performed, and the nanoparticles functionalized with metabolites from the MGK33 extract (SPIONs@MGK33, Ni-SPIONs@MGK33, Zn-SPIONs@MGK33, Au-SPIONs@MGK33, Cu-SPIONs@MGK33 and Ag-SPIONs@MGK33) were allowed to stand in a biosafety cabinet overnight to evaporate residual methanol. The 'spent' fraction of the MGK33 which was a by-product of magnetic decantation was analyzed using LC-QTOF-MS/MS, following a previously described method [12].

4.2.11 Antimycobacterial activity of nanoparticles

Before performing antimycobacterial assays, each sample of nanoparticles weighing 10 mg was suspended in 5 mL of sterile distilled water (dH₂O) and then sonicated for 1 hour. Test concentrations for treatments were prepared in Middlebrook 7H9 broth supplemented with 0.085% (w/v) sodium chloride, 0.2% (w/v) glucose, 0.5% (v/v) glycerol and 0.05% (v/v) Tween 80. Antimycobacterial activity was investigated using *Mycobacterium smegmatis* mc²155. Bacterial cultures were initially grown in Middlebrook 7H9 broth until the optical density measured at 600 nm (OD_{600nm}) was equal to 0.2-0.3. This was then followed by the

preparation of inoculum by diluting the culture down to an OD_{600nm} of 0.002. of the synthesized nanoparticles were screened for antimycobacterial activity at 62.5 $\mu\text{g/mL}$ for 72 hours, followed by broth macro-dilution of bioactive samples to obtain 31.25, 15.63, 7.82, 3.91 and 1.95 $\mu\text{g/mL}$ for the determination of the minimum inhibitory concentration (MIC). All treatment of cultures was performed in 10 mL of Middlebrook 7H9 broth in 50 mL tubes incubated at 37 °C, shaking at 150 rpm. To obtain growth curves, OD_{600nm} was measured at 24-hour intervals using the MultiSkan Sky spectrophotometer. GraphPad Prism 8 (GraphPad Software, NY, USA) was used to analyze growth curve data and to plot line graphs.

4.3 Results and discussion

4.3.1 Synthesis and characterization of SPIONs

In this study, naked SPIONs were synthesized using the chemical co-precipitation method of mixing $\text{FeSO}_4 \cdot 7\text{H}_2\text{O}$ and $\text{FeCl}_3 \cdot 6\text{H}_2\text{O}$ and then adding NH_4OH as a reducing agent. The resulting black precipitate was isolated and washed with ethanol. Using UV-Vis spectroscopy, the surface plasmon resonance (SPR) band of the newly formed nanoparticles was observed as an absorption peak with a maxima at 270 nm (Figure 4.2), consistent with previous studies which place the characteristic SPR absorption peak of magnetite between 250-300 nm [15,16].

Surface modification of naked SPIONs using Ni, Zn, Au, Cu and Ag was then performed to form the bi-metallic core shell SPIONs. The formation of bi-metallic SPIONs meant that the surface of the precursor (mono-metallic SPIONs) was now completely/in part covered by the secondary metal. The commonly reported SPR absorption bands for each metal were observed as individual and continuous absorption peaks, thus showing the successful formation of the bi-metallic nanoparticles [17]. Thus, all the bi-metallic nanoparticles were observed to show the presence of the SPR absorption peak of magnetite, with a maxima between the 250-300 nm wavelength band, and additional characteristic SPR absorption peaks for each added metal as follows: a peak at 401 nm for Ni-SPIONs [18,19], a broad peak between 300-380 nm for Zn-

SPIONs [20,21], a broad peak between 513-526 nm for Au-SPIONs [22], a strong peak at 405 nm for Cu-SPIONs [23], and a peak at 440 nm for Ag-SPIONs [24].

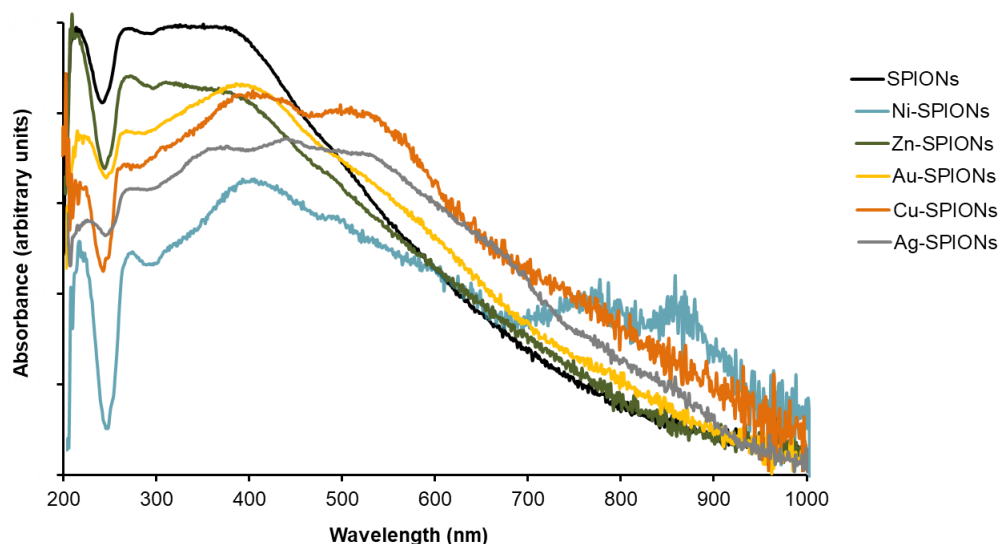


Figure 4.2. UV-Vis spectra of mono- and bi-metallic SPIONs synthesized in this study.

Besides the commonly reported characteristic plasmonic wavelength bands for each metal, additional peaks were observed for some of the bi-metallic nanoparticles and could be attributed to the uneven size distribution of nanoparticles within samples, which potentially can cause shifts in the SPR maximum absorbance wavelength [22].

The FTIR spectrum of mono-metallic SPIONs is shown in Figure 4.3, overlaid with spectra obtained from analysis of bi-metallic SPIONs. Absorption bands which appeared approximately at 3444 cm^{-1} and 1630 cm^{-1} on all spectra were due to water absorption by the samples during preparation, while absorption bands appearing at approximately 2361 cm^{-1} were assigned to CO_2 [13,25]. A strong absorption band at approximately 580 cm^{-1} observed in all spectra was assigned to the Fe-O bond, characteristic of SPIONs [13].

Analysis of FTIR spectra also revealed significant absorbance bands at 1375 cm^{-1} and at 1045 cm^{-1} (prominent on the spectra of Zn-SPIONs) which were attributed to O-H bending and CO-O-CO stretching. Other than the absorption of water and CO_2 during preparation, SPIONs may

have acquired some of the carbon and oxygen moieties observed in the FTIR analysis from the ethanol used during synthesis.

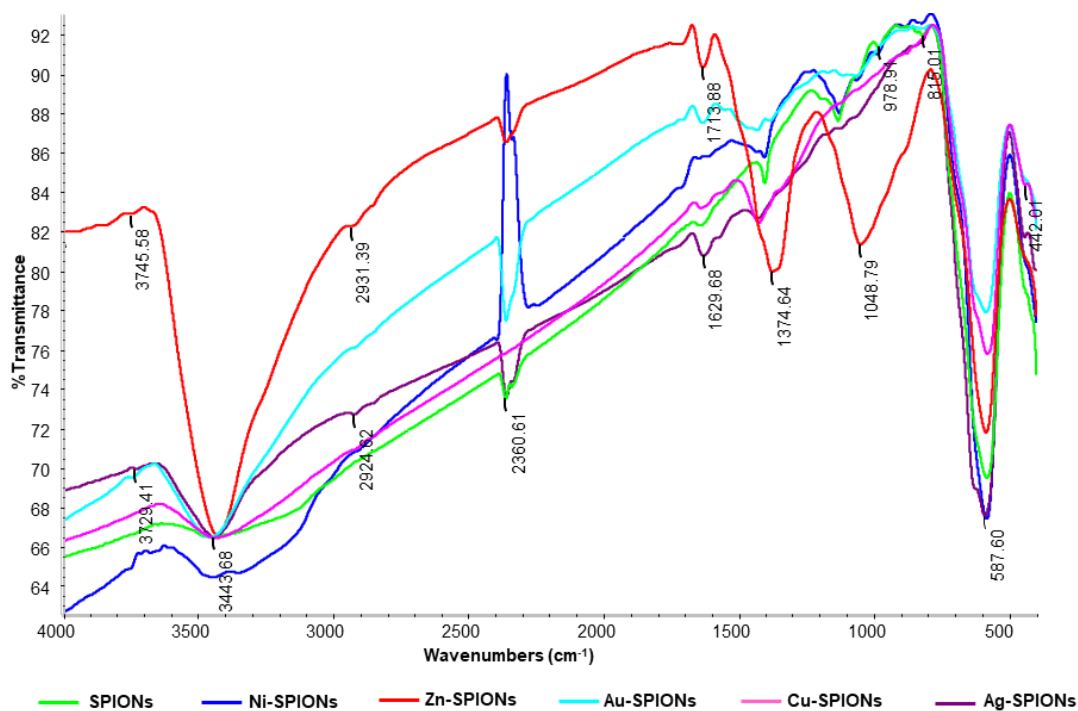


Figure 4.3. FTIR spectra of mono- and bi-metallic SPIONs synthesized in this study.

HRTEM was performed to determine the shapes and sizes of SPIONs and the results are shown in Table 4.1 and Figure 4.4. All samples were mostly characterized by spherical nanoparticles with the average diameter ranging between 20-31 nm. Interestingly, bi-metallic SPIONs did not differ significantly in average diameter compared to their precursor, mono-metallic SPIONs.

Table 4.1. Average sizes of SPIONs

Sample	Average size in nm (\pm standard deviation)
SPIONs	24.27 \pm 9.46
Ni-SPIONs	31.67 \pm 14.92
Zn-SPIONs	26.43 \pm 9.77
Au-SPIONs	31.84 \pm 9.95
Cu-SPIONs	25.21 \pm 13.24
Ag-SPIONs	20.53 \pm 7.26

Since the magnetic decantation technique was used throughout the synthesis steps, the possibility of carrying over unintentionally formed nanoparticles of Ni, Zn, Au, Cu and Ag during synthesis was eliminated. Therefore, surface modification of mono-metallic SPIONs using the aforementioned metals resulted in the formation surface layers which were less than 10 nm in thickness. Statistical analysis also revealed that the size (diameter) of nanoparticles in each sample was not normally distributed, and thus may have impacted on the shifting of SPR absorbance bands of each metal as previously discussed.

4.3.2 Functionalization of mono- and bi-metallic SPIONs with the MGK33 fungal extract

Both mono- and bi-metallic were functionalized with an extract from *C. rogersoniana* MGK33, which was previously shown to be bioactive against *M. smegmatis* mc²155 (MIC = 125 µg/mL) [12]. Since the MGK33 crude extract was previously shown to contain bioactive compound(s) against *M. smegmatis* mc²155, it was hypothesized that using various types of bi-metallic SPIONs synthesized in this study would result in the extraction of active compounds in the crude extract, and thus enhance the bi-metallic SPIONs stability and/or bioactivity against *M. smegmatis* mc²155.

Evidence of successful extraction was shown by the untargeted LC-QTOF-MS/MS analysis of the “spent” crude extract obtained as a by-product of magnetic decantation, following the extraction process (Figure 4.5). A comparison of the base peak chromatograms of the MGK33 extract in Figure 4.5A, and that of the “spent” extracts from mono- and bi-metallic SPIONs in Figure 4.5B, showed a visibly significant “region of high extraction” between the retention time of 12-13.5 minutes.

However, comparing the base peak intensities of spectra within Figure 4.5B alone showed minor differences, signifying that the adsorption of compounds from the MGK33 was largely non-selective by the mono- and bi-metallic SPIONs.

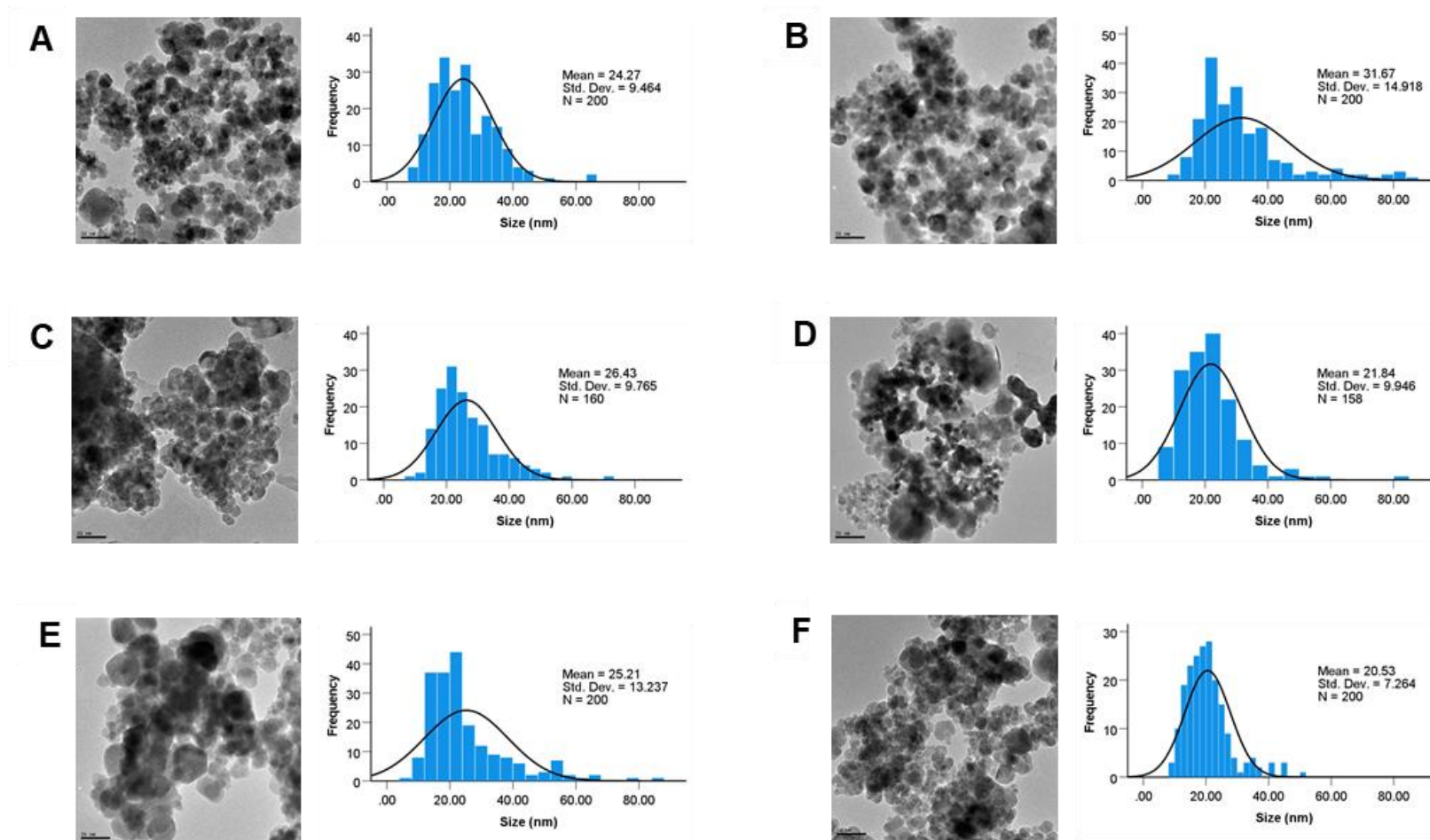


Figure 4.4. HRTEM analysis of mono- and bi-metallic SPIONs synthesized in this study. In the figure, mono-metallic SPIONs are shown in **A**, Ni-SPIONs are shown in **B**, Zn-SPIONs are shown in **C**, Au-SPIONs are shown in **D**, Cu-SPIONs are shown in **E**, and Ag SPIONs are shown in **F**. Within each sample, the area of 150-200 individual nanoparticles was measured and the calculated average diameter was then assigned to each respective sample in nanometers (nm).

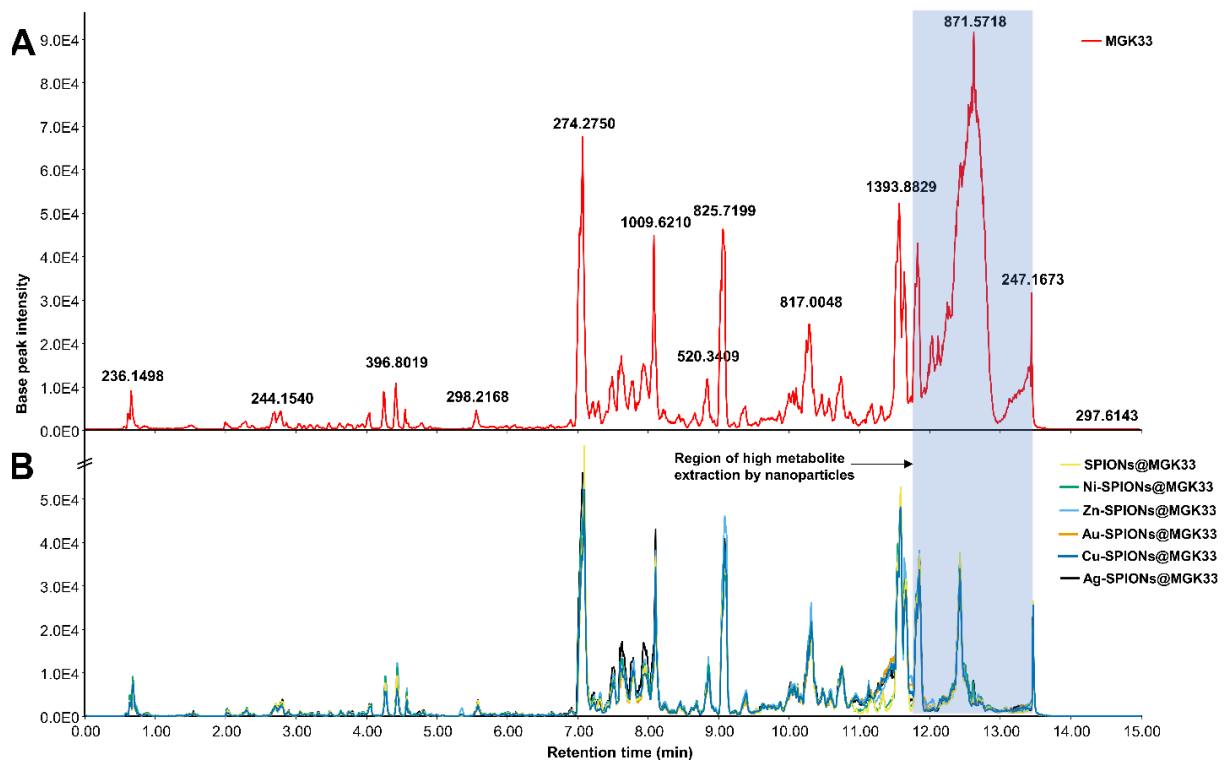


Figure 4.5. Base peak chromatograms obtained after performing untargeted LC-QTOF-MS/MS. In the figure, **A** shows the base peak chromatogram of the MGK33 extract, while **B** shows chromatograms from the “spent” extracts of mono-metallic SPIONs (SPIONs@MGK33) and bi-metallic SPIONs (Ni-SPIONs@MGK33, Zn-SPIONs@MGK33, Au-SPIONs@MGK33, Cu-SPIONs@MGK33 and Ag-SPIONs@MGK33). Aligned spectral data is available in Appendix **B1** (<https://www.scidb.cn/s/ni6Jby>).

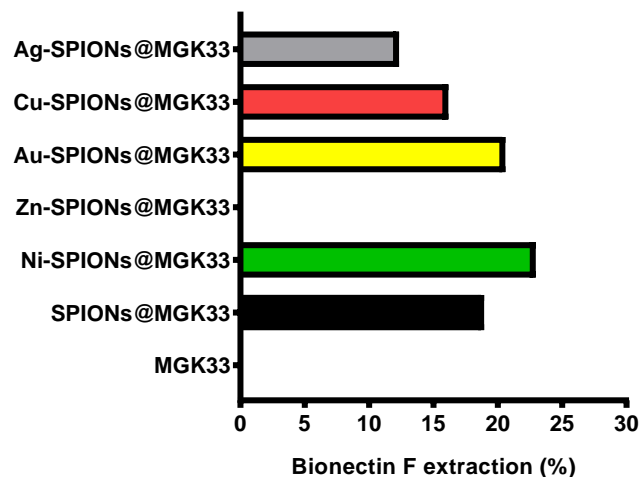


Figure 4.6. Bionectin F extraction efficiency by nanoparticles. The original MGK33 extract was used as a standard (0%), while extraction by the mono- and bi-metallic SPIONs was as follows: Zn-SPIONs@MGK33 = 0%, Ag-SPIONs@MGK33 = 12.32%, Cu-SPIONs@MGK33 = 16.15%, SPIONs@MGK33 = 18.34%, Au-SPIONs@MGK33 = 20.58% and Ni-SPIONs@MGK33 = 22.94%. Base peak intensities of bionectin F were used in the calculations.

In the previous study involving the isolation of *C. rogersoniana* MGK33 and the manual annotation of metabolites after performing LC-QTOF-MS/MS untargeted profiling, metabolites that fell within the “region of high extraction” were not identified in public databases [12].

A total of 78 ion peaks were observed from the MGK33 extract between 12-13.5 minutes and are presented in Appendix B2 with predicted molecular formula. However, among the six fungal compounds that were identified from the extract of *C. rogersoniana* MGK33 in the previous study [12], the authors in this study sought to determine the extent to which the nanoparticles were able to adsorb and extract bionectin F ($C_{50}H_{96}O_8$, $m/z = 825.7199$, $RT = 9.06$ min) from the MGK33 extract. The percentage extraction efficiencies of nanoparticles utilized in this study are shown in Figure 4.6 while the supporting data is shown in Appendix B3.

Since bionectin F is a highly hydroxylated (eight OH groups) polyprenol polyterpenoid as shown in Figure 4.7, coordination with nanoparticles may have occurred through the OH groups. It is tempting to assume that the length of bionectin F which is approximately 51.6 Å (5.16 nm), may have contributed negatively to coordination with nanoparticles and thus became a limiting factor. Since the bionectin F molecule is capable of folding, it is likely that some of the individual compounds coordinated with a single nanoparticle at multiple points along the compound's length.

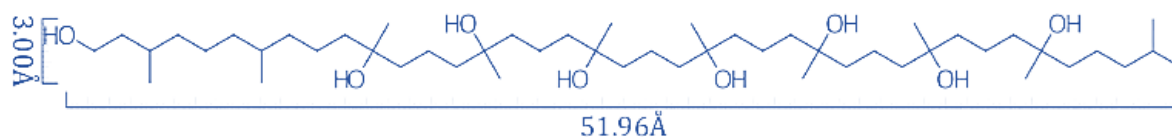


Figure 4.7. Length and width of bionectin F measured in angstroms (Å).

4.3.3 Antimycobacterial activity of mono- and bi-metallic SPIONs

In this study, antimicrobial activity of mono- and bi-metallic SPIONs was determined against *M. smegmatis* mc²155. Initially, screening was performed by treating *M. smegmatis* mc²155 with 62.5 µg/mL of each sample for 72 hours. Afterwards, percentage cell viability was determined by measuring the OD_{600nm}. As shown in Figure 4.8, Cu-SPIONs, Cu-SPIONs@MGK33, Ag-SPIONs and Ag-SPIONs@MGK33 were all capable of inhibiting the growth of the bacterium. Appendix B3 shows images of various treatments of culture flasks during experimental optimization, with Appendix B4 Figure B4-8 providing evidence of sterilizing of cultures by Cu-SPIONs and Ag-SPIONs at 31.25 µg/mL.

It was interesting to observe that mono-metallic SPIONs had the least activity against *M. smegmatis* mc²155, with cell viability of the treated culture almost a 100%. Iron (Fe³⁺) is essential for the growth of *Mycobacteria* as they are known to synthesize siderophores (mycobactin and carboxymycobactin) specific for chelating and translocating of Fe³⁺ [26]. Therefore, magnetite in the form of Fe₃O₄ (SPIONs), rather than being an antimicrobial, became a supplementary source of iron to *M. smegmatis* mc²155. Since excess intracellular iron is likely to cause formation of free radicals and thus causing toxicity, levels of intracellular iron are regulated by the global iron-dependent transcriptional regulator (IdeR) in *Mycobacteria* [27]. Therefore, although the naked (Fe) SPIONs extracted a good amount of metabolites from the crude sample, they have limited activity against *M. smegmatis* mc²155. This implies that the naked SPIONs need to be coated with a more suitable metal to keep the magnetic activity while inhibiting bacterial growth.

After observing the strong antimycobacterial activity of Cu-SPIONs, Cu-SPIONs@MGK33, Ag-SPIONs and Ag-SPIONs@MGK33 at 62.5 µg/mL, growth curves of *M. smegmatis* mc²155 treated with the four samples at seven concentrations ranging from 62.5-1.96 µg/mL were performed and are shown in Figure 4.9. OD_{600nm} measurements showed that all tested

concentrations (62.5-1.96 $\mu\text{g/mL}$) of Cu-SPIONs were capable of inhibiting *M. smegmatis* mc²155 growth during the first 24 hours of incubation. Thereafter, partial growth inhibition was observed at 7.81 $\mu\text{g/mL}$ at 48 and 72 hours, while *M. smegmatis* mc²155 developed resistance to Cu-SPIONs at 3.91 and 1.96 from the 24-hour time point.

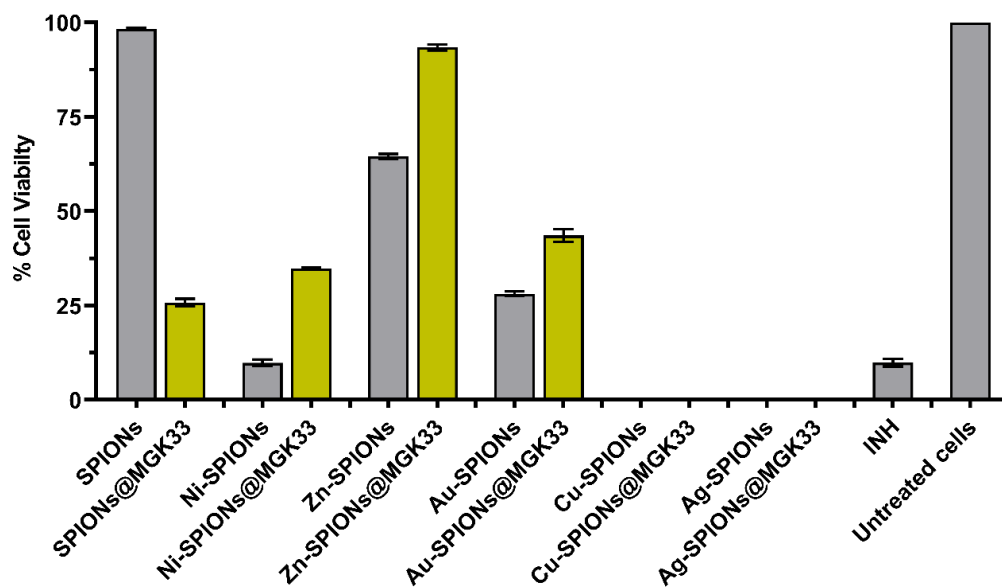


Figure 4.8. Percentage cell viability of cultures after treatment with mono-metallic, bi-metallic and functionalized nanoparticles. INH (isoniazid) was used as a positive control while untreated cells were used as a negative control. Treatment with nanoparticles was done at a concentration of 62.5 $\mu\text{g/mL}$ for 72 hours. Cell viability was determined from optical density measurements at 600 nm.

Even though *Mycobacteria* produce a specific P-type ATPase Cu transporter referred to as CtpB [29], responsible for conferring tolerance to Cu^+ and Cu^{2+} , assays in this study fall short of explaining the reason for susceptibility of *M. smegmatis* mc²155 to concentrations of Cu-SPIONs as low as 7.81 $\mu\text{g/mL}$. It was observed that the functionalized nanoparticles (Cu-SPIONs@MGK33) were less potent than their counterparts, Cu-SPIONs (A1 in Figure 4.9). The coating of the surfaces Cu-SPIONs reduced the surface area available for reactions, thus rendering the Cu-SPIONs@MGK33 less effective in this study.

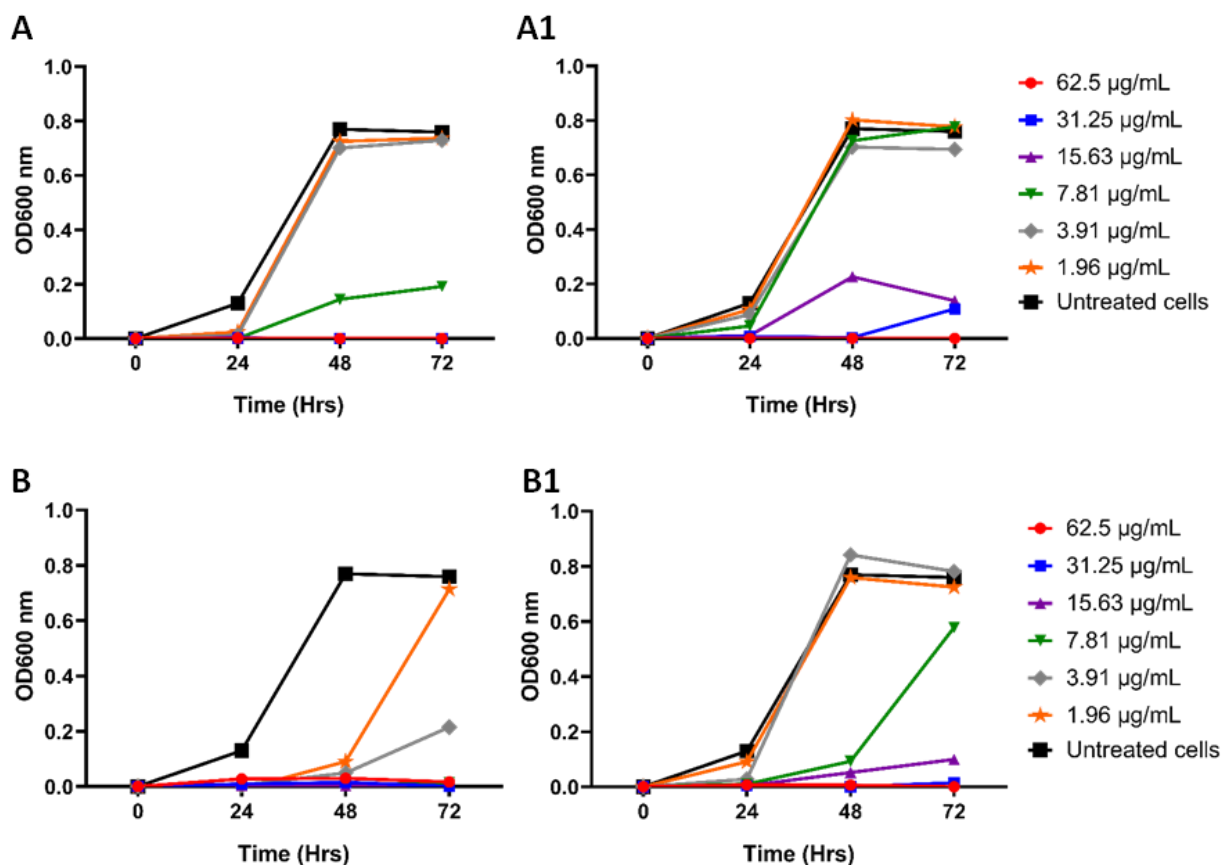


Figure 4.9. Growth curves of *M. smegmatis* mc²155 after treatment with Cu-SPIONs (A), Cu-SPIONs@MGK33 (A1), Ag-SPIONs (B) and Ag-SPIONs@MGK33 (B1) for 72 hours. Cell growth was determined by measuring optical density at 600 nm (OD600 nm) while untreated cells were used as a negative control.

Ag-SPIONs exhibited the strongest activity observed in this study. Significant growth inhibition of *M. smegmatis* mc²155 was observed at 1.96 µg/mL for up to 24 hours (B in Figure 4.9). While *M. smegmatis* mc²155 developed some resistance to 1.96 and 3.91 µg/mL after 24 hours, little to no resistance was observed at a concentration of 7.81 µg/mL until the end of the incubation period at 72 hours. The antimycobacterial effect of Ag-SPIONs against *M. smegmatis* mc²155 is comparable to that of the second line drug streptomycin, whose reported MIC against *M. tuberculosis* ranges from 2-8 µg/mL [30].

As was observed with Cu-SPIONs@MGK33, Ag-SPIONs@MGK33 were less bioactive compared to Ag-SPIONs (B1 in Figure 4.9). In a recent study, the MICs of Ag nanoparticles

with an average size of 50 nm were found to be 1, 4 and 16 $\mu\text{g/mL}$ *M. tuberculosis*, *Mycobacterium bovis* and MDR-*M. tuberculosis*, respectively [31]. The most important mechanisms of action exhibited by Ag nanoparticles have been carefully summarized in a recent review article [32].

4.5 Conclusions

This study evaluated the potential use of bi-metallic SPIONs as anti-TB agents. SPIONs modified with Ni, Zn, Au, Cu and Ag on the surface, were synthesized and further modified using a crude fungal extract obtained from *C. rogersoniana* MGK33. It was observed that mono-metallic SPIONs are ineffective inhibitors against *M. smegmatis* mc²155 as no significant inhibition of cell growth was observed at 62.5 $\mu\text{g/mL}$ after 72 hours of treatment. On the other hand, Cu-SPIONs and Ag-SPIONs showed the strongest activity among all the samples tested in this study. Growth of *M. smegmatis* mc²155 was inhibited for 72 hours by Ag-SPIONs at a concentration of 7.81 $\mu\text{g/mL}$, while it took a concentration of 15.63 $\mu\text{g/mL}$ for Cu-SPIONs to exhibit the same effect. Interesting to note was that functionalization of mono- and bi-metallic SPIONs had a negative impact on bioactivity. Thus, it was concluded that Ag-SPIONs and Cu-SPIONs are the preferred candidates for lead development in future TB-drug discovery studies.

4.6 References

1. WHO *Global Tuberculosis Report 2021*; World Health Organization: Geneva, 2021.
2. Tăbăran, A.-F.; Matea, C.T.; Mocan, T.; Tăbăran, A.; Mihaiu, M.; Iancu, C.; Mocan, L. Silver Nanoparticles for the Therapy of Tuberculosis. *Int. J. Nanomedicine* **2020**, *15*, 2231, doi:10.2147/IJN.S241183.
3. Wurie, F.B.; Lawn, S.D.; Booth, H.; Sonnenberg, P.; Hayward, A.C. Bioaerosol Production by Patients with Tuberculosis during Normal Tidal Breathing: Implications for Transmission Risk. *Thorax* **2016**, *71*, 549–554, doi:10.1136/thoraxjnl-2015-207295.
4. Nasiruddin, M.; Neyaz, M.K.; Das, S. Nanotechnology-Based Approach in Tuberculosis Treatment. *Tuberc. Res. Treat.* **2017**, *2017*, e4920209, doi:10.1155/2017/4920209.
5. Lee, N.-Y.; Ko, W.-C.; Hsueh, P.-R. Nanoparticles in the Treatment of Infections Caused by Multidrug-Resistant Organisms. *Front. Pharmacol.* **2019**, *10*, 1153, doi:10.3389/fphar.2019.01153.
6. Tăbăran, A.-F.; Matea, C.T.; Mocan, T.; Tăbăran, A.; Mihaiu, M.; Iancu, C.; Mocan, L. Silver Nanoparticles for the Therapy of Tuberculosis. *Int. J. Nanomedicine* **2020**, *15*, 2231–2258, doi:10.2147/IJN.S241183.
7. Moreno-Sastre, M.; Pastor, M.; Salomon, C.J.; Esquisabel, A.; Pedraz, J.L. Pulmonary Drug Delivery: A Review on Nanocarriers for Antibacterial Chemotherapy. *J. Antimicrob. Chemother.* **2015**, *70*, 2945–2955, doi:10.1093/jac/dkv192.
8. Liu, J.F.; Lan, Z.; Ferrari, C.; Stein, J.M.; Higbee-Dempsey, E.; Yan, L.; Amirshaghghi, A.; Cheng, Z.; Issadore, D.; Tsourkas, A. Use of Oppositely-Polarized External Magnets

- to Improve the Accumulation and Penetration of Magnetic Nanocarriers into Solid Tumors. *ACS Nano* **2020**, *14*, 142–152, doi:10.1021/acsnano.9b05660.
9. Singh, N.; Jenkins, G.J.S.; Asadi, R.; Doak, S.H. Potential Toxicity of Superparamagnetic Iron Oxide Nanoparticles (SPION). *Nano Rev.* **2010**, *1*, 5358, doi:10.3402/nano.v1i0.5358.
 10. Revia, R.A.; Zhang, M. Magnetite Nanoparticles for Cancer Diagnosis, Treatment, and Treatment Monitoring: Recent Advances. *Mater. Today* **2016**, *19*, 157–168, doi:10.1016/j.mattod.2015.08.022.
 11. Lachowicz, D.; Kaczyńska, A.; Wirecka, R.; Kmita, A.; Szczerba, W.; Bodzoń-Kułakowska, A.; Sikora, M.; Karewicz, A.; Zapotoczny, S. A Hybrid System for Magnetic Hyperthermia and Drug Delivery: SPION Functionalized by Curcumin Conjugate. *Materials* **2018**, *11*, 2388, doi:10.3390/ma11122388.
 12. Tapfuma, K.I.; Nyambo, K.; Baatjies, L.; Smith, L.; Keyster, M.; Loxton, A.G.; Ngxande, M.; Malgas-Enus, R.; Mavumengwana, V. Anti-*Mycobacterium tuberculosis* Activity of Marine Derived *Clonostachys rogersoniana* Methanol Extract and Virtual Assessment of Bionectin F as a Potential Inhibitor of β -Ketoacyl-ACP Reductase (MabA). Unpublished research article, Stellenbosch University: Cape Town, 2022.
 13. Khutlane, J.T.; Koch, K.R.; Malgas-Enus, R. Competitive Removal of PGMs from Aqueous Solutions via Dendrimer Modified Magnetic Nanoparticles. *SN Appl. Sci.* **2020**, *2*, 1125, doi:10.1007/s42452-020-2922-x.
 14. Schneider, C.A.; Rasband, W.S.; Eliceiri, K.W. NIH Image to ImageJ: 25 Years of Image Analysis. *Nat. Methods* **2012**, *9*, 671–675, doi:10.1038/nmeth.2089.

15. Justin, C.; Philip, S.A.; Samrot, A.V. Synthesis and Characterization of Superparamagnetic Iron-Oxide Nanoparticles (SPIONs) and Utilization of SPIONs in X-Ray Imaging. *Appl. Nanosci.* **2017**, *7*, 463–475, doi:10.1007/s13204-017-0583-x.
16. Farhana, A.; Jenifer Selvarani, A.; Samrot, A.V.; Alsrhani, A.; Raji, P.; Sahithya, C.S.; Jane Cypriyana, P.J.; Senthilkumar, P.; Ling, M.P.; Yishak, S. Utilization of Superparamagnetic Iron Oxide Nanoparticles (SPIONs) Impregnated Activated Carbon for Removal of Hexavalent Chromium. *J. Nanomater.* **2022**, *2022*, e4326939, doi:10.1155/2022/4326939.
17. Calagua, A.; Alarcon, H.; Paraguay, F.; Rodriguez, J. Synthesis and Characterization of Bimetallic Gold-Silver Core-Shell Nanoparticles: A Green Approach. *Adv. Nanoparticles* **2015**, *04*, 116, doi:10.4236/anp.2015.44013.
18. Ganjali, M.; Ganjali, M.; Vahdatkhah, P.; Marashi, S.M.B. Synthesis of Ni Nanoparticles by Pulsed Laser Ablation Method in Liquid Phase. *Procedia Mater. Sci.* **2015**, *11*, 359–363, doi:10.1016/j.mspro.2015.11.127.
19. Imran Din, M.; Rani, A. Recent Advances in the Synthesis and Stabilization of Nickel and Nickel Oxide Nanoparticles: A Green Adeptness. *Int. J. Anal. Chem.* **2016**, *2016*, e3512145, doi:10.1155/2016/3512145.
20. Bulcha, B.; Leta Tesfaye, J.; Anatol, D.; Shanmugam, R.; Dwarampudi, L.P.; Nagaprasad, N.; Bhargavi, V.L.N.; Krishnaraj, R. Synthesis of Zinc Oxide Nanoparticles by Hydrothermal Methods and Spectroscopic Investigation of Ultraviolet Radiation Protective Properties. *J. Nanomater.* **2021**, *2021*, e8617290, doi:10.1155/2021/8617290.

21. Guidelli, E.J.; Baffa, O.; Clarke, D.R. Enhanced UV Emission From Silver/ZnO And Gold/ZnO Core-Shell Nanoparticles: Photoluminescence, Radioluminescence, And Optically Stimulated Luminescence. *Sci. Rep.* **2015**, *5*, 14004, doi:10.1038/srep14004.
22. Huang, X.; El-Sayed, M.A. Gold Nanoparticles: Optical Properties and Implementations in Cancer Diagnosis and Photothermal Therapy. *J. Adv. Res.* **2010**, *1*, 13–28, doi:10.1016/j.jare.2010.02.002.
23. Thamer, N.A.; Muftin, N.Q.; Al-Rubae, S.H.N. Optimization Properties and Characterization of Green Synthesis of Copper Oxide Nanoparticles Using Aqueous Extract of *Cordia myxa* L. Leaves. *Asian J. Chem.* **2018**, *30*, doi:10.14233/AJCHEM.2018.21242.
24. Talabani, R.F.; Hamad, S.M.; Barzinjy, A.A.; Demir, U. Biosynthesis of Silver Nanoparticles and Their Applications in Harvesting Sunlight for Solar Thermal Generation. *Nanomaterials* **2021**, *11*, 2421, doi:10.3390/nano11092421.
25. Coenen, K.; Gallucci, F.; Mezari, B.; Hensen, E.; van Sint Annaland, M. An In-Situ IR Study on the Adsorption of CO₂ and H₂O on Hydrotalcites. *J. CO₂ Util.* **2018**, *24*, 228–239, doi:10.1016/j.jcou.2018.01.008.
26. Sritharan, M.; Margolin, W. Iron Homeostasis in Mycobacterium Tuberculosis: Mechanistic Insights into Siderophore-Mediated Iron Uptake. *J. Bacteriol.* **2016**, *198*, 2399–2409, doi:10.1128/JB.00359-16.
27. Pandey, R.; Rodriguez, G.M. IdeR Is Required for Iron Homeostasis and Virulence in *Mycobacterium tuberculosis*. *Mol. Microbiol.* **2014**, *91*, 98–109, doi:10.1111/mmi.12441.

28. Chen, L.; Li, X.; Xu, P.; He, Z.-G.; Lamichhane, G. A Novel Zinc Exporter CtpG Enhances Resistance to Zinc Toxicity and Survival in *Mycobacterium bovis*. *Microbiol. Spectr.* **2022**, *0*, e01456-21, doi:10.1128/spectrum.01456-21.
29. León-Torres, A.; Arango, E.; Castillo, E.; Soto, C.Y. CtpB Is a Plasma Membrane Copper (I) Transporting P-Type ATPase of *Mycobacterium tuberculosis*. *Biol. Res.* **2020**, *53*, 6, doi:10.1186/s40659-020-00274-7.
30. Tapfuma, K.I.; Nyambo, K.; Baatjies, L.; Keyster, M.; Mekuto, L.; Smith, L.; Allie, N.; Loxton, A.G.; Malgas-Enus, R.; Mavumengwana, V. Fungal-Derived Compounds and Mycogenic Nanoparticles with Antimycobacterial Activity: A Review. *SN Appl. Sci.* **2022**, *4*, 134, doi:10.1007/s42452-022-05010-2.
31. Selim, A.; Elhaig, M.M.; Taha, S.A.; Nasr, E.A. Antibacterial Activity of Silver Nanoparticles against Field and Reference Strains of *Mycobacterium tuberculosis*, *Mycobacterium bovis* and Multiple-Drug-Resistant Tuberculosis Strains. *Rev. Sci. Tech. Int. Off. Epizoot.* **2018**, *37*, 823–830, doi:10.20506/rst.37.3.2888.
32. Tăbăran, A.-F.; Matea, C.T.; Mocan, T.; Tăbăran, A.; Mihaiu, M.; Iancu, C.; Mocan, L. Silver Nanoparticles for the Therapy of Tuberculosis. *Int. J. Nanomedicine* **2020**, *15*, 2231–2258, doi:10.2147/IJN.S241183.

Chapter 5

Bioactivity of bi-metallic SPIONs and a *Clonostachys rogersoniana* MGK33 crude extract on RAW 264.7 macrophage cells infected with *Mycobacterium smegmatis* mc²155

Kudzanai Ian Tapfuma¹, Francis Adu-Amankwaah¹, Maano Valerie Masiphephethu^{1,2}, Lucinda Baatjies¹, Liezel Smith¹, Nasiema Allie¹, Andre G. Loxton¹, Rehana Malgas-Enus³ and Vuyo Mavumengwana^{1,*}

¹ DSI-NRF Centre of Excellence for Biomedical Tuberculosis Research; South African Medical Research Council Centre for Tuberculosis Research; Division of Molecular Biology and Human Genetics, Faculty of Medicine and Health Sciences, Stellenbosch University, Cape Town, South Africa.

² Department of Biochemistry, Faculty of Science, Engineering and Agriculture, University of Venda, Thohoyandou, South Africa.

³ Department of Chemistry and Polymer Science, Faculty of Science, University of Stellenbosch, Matieland, South Africa.

* Corresponding author.

Email address: vuyom@sun.ac.za; Tel.: +27 21 938 9952.

5.0 Abstract

Host-directed therapy modulating the response of the innate immune system to tuberculosis (TB) infection is one of the newly proposed approaches for the treatment of TB. In this study, the bioactivity of bi-metallic superparamagnetic iron oxide nanoparticles (SPIONs) and the fungal extract, MGK33, derived from *Clonostachys rogersoniana* MGK33, were investigated on RAW 264.7 macrophage cells infected with *Mycobacterium smegmatis* mc²155. Initially,

bi-metallic copper- and silver-superparamagnetic iron oxide nanoparticles (Cu-SPIONs and Ag-SPIONs) were investigated for cytotoxic activity on RAW 264.7 macrophage cells to determine the non-cytotoxic concentrations. RAW 264.7 macrophage cells were then infected with *M. smegmatis* mc²155 and treatments were performed for 24 hours using Cu-SPIONs, Ag-SPIONs, SPIONs modified with the MGK33 extract (Cu-SPIONs@MGK33 and Ag-SPIONs@MGK33), and MGK33. Colony forming units (CFUs) were enumerated at 6-hour intervals, while flow cytometry was performed only after 24 hours. Results from the cytotoxicity assay showed that RAW 264.7 macrophage cells treated with Cu-SPIONs and Ag-SPIONs at a concentration of 1.96 µg/mL exhibited cell viability percentages of 70.82% and 84.63%, respectively. After infecting RAW 264.7 macrophage cells treating them with various agents for 24 hours, MGK33 exhibited the highest early apoptosis activity (9.61%), followed by Cu-SPIONs@MGK33 (3.34%). Cu-SPIONs were found to induce higher levels of late apoptosis when compared with the Cu-SPIONs@MGK33, Ag-SPIONs and Ag-SPIONs@MGK33 treatments. Furthermore, MGK33 was found to be the most potent against intracellular bacteria after recording 11 ± 3 CFU/mL after 24 hours of treatment. Cu-SPIONs and Ag-SPIONs coated with the MGK33 fungal extract showed reduced cytotoxic activity and bactericidal effects against intracellular bacteria. Surface modification of the Cu-SPIONs and Ag-SPIONs with the MGK33 extract resulted in the nanoparticles exhibiting a cell protective effect as cell viabilities were highest in the Cu-SPIONs@MGK33 and Ag-SPIONs@MGK33 treatments. Surprisingly, the MGK33 fungal extract was found to be the most potent against intracellular bacteria. Further studies should be done to isolate and purify compounds from the MGK33 crude extract to identify the compound(s) with immunomodulatory activities.

Keywords: RAW 264.7 macrophage cells; nanoparticles; host-directed therapy; apoptosis; necrosis.

5.1. Introduction

Tuberculosis (TB) is an epidemic that has caused mortalities, morbidities and economic losses of immense magnitude globally. One third of the global population is thought to be infected by *Mycobacterium tuberculosis* which is the causative agent of TB [1]. The successful persistence of tuberculosis as an epidemic is mostly linked to the clinical behavior of *M. tuberculosis* inside the host. This pathogen has the ability to infect, survive and modulate cell death of several major players of the innate immune system, including macrophages, neutrophils and dendritic cells [2,3]. Disarmament of the innate immune system allows *M. tuberculosis* to actively evade death and also establish within the host during the lag phase of priming of the adaptive immune system for establishment of a specific T-cell response [4].

The primary site of infection for *M. tuberculosis* is the lungs. The pathogen primarily enters the host through inhalation of aerosolized infectious droplets liberated from infected patients with active TB when they cough [5]. Pathogen-laden droplets $< 5 \mu\text{m}$ are capable of reaching the alveolus while those $> 5 \mu\text{m}$ are likely trapped by mucus and cilia in the upper respiratory system [6]. Upon reaching the alveolus, *M. tuberculosis* will first likely encounter alveolar macrophages, or alveolar type I epithelial cells (AT-I cells) which cover about 95% of the surface and are largely responsible for gaseous exchange, or alveolar type II epithelial cells (AT-II cells) which are best known for synthesis surfactant protein A (SP-A) [7]. SP-A is a self-stimulant that drives AT-II cells to produce chemotactic factors which include monocyte chemoattractant 1 (MCP-1/CCL2), IL-8 and granulocyte macrophage colony-stimulating factor (GM-CSF) chemotaxis of phagocytic cells such as macrophages

Resident alveolar macrophages express a wide variety of receptors that are capable of recognizing *M. tuberculosis*. Also known as pattern recognition receptors (PRR), they include the T C-type lectin receptors (CLRs) and Toll-like receptors (TLRs) which recognize mycolic acids, lipoarabinomannan (LAM) and mannosylated-LAM (ManLAM) [8]. After being

engulfed by macrophages through phagocytosis, *M. tuberculosis* either promote apoptosis or inhibit it to lead the cell to necrotic. Weakly virulent *M. tuberculosis* induce the macrophages to produce pro-inflammatory cytokines such as MCP-1, IL-6 and TNF- α [9]. The P19 lipoprotein located on the surface of weakly virulent Mycobacteria and the of apoptosis of macrophages has been shown to cause caspase-8 activation through TLR-2 signaling, thus effecting apoptosis in a time and does dependent mechanism [9]. The P19 lipoprotein has also been shown to promote the differentiation of CD4⁺ cells and the release of cytokines like IL-6, IL-12 and IFN- γ [10].

Strongly virulent *M. tuberculosis* employs various strategies to inhibit apoptosis, including the production and secretion of Rv3654c and Rv3655c proteins in the cytoplasm which are known to block the extrinsic pathway [11], production of ESAT-6 which increases intracellular Ca²⁺ and subsequent calpain activation while also modulating anti-apoptotic mechanisms [12], and the serine threonine protein kinase PknE which is known to modulate the expression of pro-apoptotic factors which include TNF- α , P53 and Bax [13]. *M. tuberculosis* also subverts death inside macrophages by inhibiting bactericidal cellular mechanisms such as phagosome maturation which would otherwise result in the formation of an acidic phagolysosome containing oxidative and hydrolytic agents that are capable of neutralizing the pathogen [9].

In physiological conditions, viable cells display a set of “don’t eat me” (referring to phagocytosis) signals which include CD31, CD47 and numerous other self-associated molecular patterns (SAMPs) [14]. On the other hand, cells undergoing cell death by apoptosis or necrosis also display various sets of “eat me” signals on their surfaces which include apoptotic cell-associated molecular patterns (ACAMPs) and pathogen-associated molecular patterns (PAMPs), respectively [15]. In *in vitro* studies, these markers can be used to distinguish apoptotic and necrotic cell populations. Using flow cytometry, two standard fluorescent stains are employed as follows: Fluorescein isothiocyanate conjugated Annexin V

(Annexin V-FITC) which binds to extracellular phosphatidylserine, a biomarker that exposed on the surface of apoptotic cells, and propidium iodine (PI) which is able to bind to DNA by permeating into dying cells with compromised cell membranes and distinguishing stained cells as necrotic [16,17]. When a dying cell exposes phosphatidylserine on an intact cell membrane, it is described as early (primary) apoptotic and can be stained only by Annexin V-FITC [16]. If phagocytosis of early apoptotic cells does not occur, cells may undergo late apoptosis/secondary necrosis, whereby the cell membrane is permeabilized to allow PI intake while phosphatidylserine is exposed [18]. Necrotic (primary necrotic) cells are recognized as those that stain PI positive and Annexin V-FITC negative, signifying considerable cell membrane damage that arise from chemical and mechanical insults [16].

Currently, treatment of tuberculosis is mainly achieved by use of antimicrobials which target unique physiological processes in *M. tuberculosis* (pathogen-directed therapies, PDTs) using isoniazid, rifampicin, pyrazinamide and ethambutol as first line drugs [19]. The pathogen however has the capacity to acquire resistance against the mentioned drugs and thus necessitating the use of second line drugs [20]. Several studies have shown the mild to fatal side effects of some of the second-line anti-TB, these effects often lead to increased treatment discontinuation, morbidity and mortality among patients and thus impede efforts to completely eliminate tuberculosis globally [21,22].

Use of host-directed therapies (HDTs) as a way of augmenting PDTs have been proposed as one of the ways to provide an innovative approach that may reduce emergence of resistant tuberculosis, duration of treatment, lung tissue damage, drug induced side effects and other iatrogenic conditions [23]. Since the modulation of cells of the innate immune system by *M. tuberculosis* results in the establishment of the pathogen in the host, the cells should therefore be targeted for TB HDT. In this study, murine derived RAW 264.7 macrophage cells were infected with avirulent *Mycobacterium smegmatis* mc²155 and then subsequently treated with

bi-metallic nanoparticles, namely copper and silver superparamagnetic iron oxide nanoparticles (Cu-SPIONs and Ag-SPIONs). Time-dependent apoptosis and necrosis measurements of treated RAW 264.7 macrophage cells were performed using flow cytometry. Both Cu-SPIONs and Ag-SPIONs were previously found to possess significant antimycobacterial activity in Chapter 4.

5.2 Methods and materials

5.2.1 Cytotoxic activity of bi-metallic SPIONs on RAW 264.7 macrophage cells

RAW 264.7 macrophage cells maintained in RPMI 1640 medium supplemented with 10% fetal bovine serum (FBS) were seeded at 6 000 cells/well in 96 well plates and allowed to attach overnight in a humidified incubator (CelCulture[®] CO₂ Incubator, ESCO, Singapore) at 37 °C, with 5% CO₂. Cu-SPIONs and Ag-SPIONs were prepared RPMI 1640 medium and added to the wells at various concentrations ranging from 0.98-15.63 µg/mL, while isoniazid was tested at 31.25-250 µg/mL. Treatments were allowed to incubate for 48 hours before removing the media and adding 100 µL of 0.5 mg/mL 3-(4,5-Dimethylthiazol-2-yl)-2,5-diphenyltetrazolium bromide (MTT), and allowing for a further incubation of 4 hours. Absorbance was measured using a spectrophotometer (FLUOstar Omega, BMG Labtech, Germany) at 540 nm.

5.2.2 Infection of RAW 264.7 macrophage cells with *M. smegmatis mc²155* and subsequent treatment with bi-metallic SPIONs

M. smegmatis mc²155 in Middlebrook 7H9 broth supplemented with 0.085% (w/v) sodium chloride, 0.2% (w/v) glucose, 0.5% (v/v) glycerol and 0.05% (v/v) Tween 80, cultured overnight to reach an OD_{600nm} of 1-1.5 (whereby OD_{600nm} of 1.0 = 1 x 10⁸) was used for infection experiments. The bacterial culture was then passed through 40 µm filter to remove clumps in preparation for infection.

RAW 264.7 macrophage cells maintained in RPMI 1640 medium supplemented with 10% fetal bovine serum (FBS) were seeded at 3.5×10^5 cells/well in 24 well plates and allowed to incubate overnight to allow for attachment. After removing media from the wells, a culture of *M. smegmatis* mc²155 diluted in RPMI 1640 medium was added to the wells to achieve a multiplicity of infection (MOI) of 5:1. RAW 264.7 macrophage cells were then incubated for 3 hours before removing the bacterial culture and incubating for a further 60 minutes with 1 mL of penicillin-streptomycin (10 000 U/ml) to kill extracellular bacteria. Afterwards, the cells were washed twice with phosphate buffered saline (PBS) and then treated with various agents at 1.96 $\mu\text{g/mL}$ (Cu-SPIONs, Cu-SPIONs@MGK33, Ag-SPIONs, Ag-SPIONs@MGK33, MGK33 extract and isoniazid) before being allowed to incubate for 24 hours.

5.2.3 Flow cytometry Annexin V-FITC and PI-stained cells

Following treatment and incubation of infected RAW 264.7 macrophage cells for 24 hours, detachment of cells was performed using AccutaseTM and cells were allowed to recover in fresh RPMI 1640 medium for 1 hour in the incubator. The Annexin V-FITC/PI apoptosis detection kit (Invitrogen, ThermoFisher Scientific, USA) was used to stain cells for flow cytometry following the manufacturer's instructions. The stained cells were then analysed using the BC DxFlex (Beckman Coulter, Inc., USA) with about 20 000 events collected for each sample. Data analysis was performed using CytExpert version 2.0.2.18 (Beckman Coulter, Inc., USA).

5.2.4 Enumeration of colony forming units

Since the enumeration of colony forming units (CFUs) was to be performed every 6 hours, the treatment of infected RAW 264.7 macrophage cells was performed in quintuple for each agent tested. After every 6 hours, one set of 24 well plates containing the treated cells was washed 3 times with PBS and then lysed with 1 mL of sterile added to the wells, followed by serial dilutions of up to 10^{-5} in PBS containing 0.05% Tween 80. Aliquots of 50 μL of the dilutions

were plated out in triplicate on Middlebrook 7H10 supplemented with 0.085% (w/v) sodium chloride, 0.2% (w/v) glucose and 0.5% (v/v) glycerol, and then incubated for 72 hours with constant monitoring. Colonies counted from the 10^{-1} dilutions were eventually used in calculations and results were expressed as CFUs/mL.

5.3 Results and discussion

5.3.1 Cytotoxic activity of Cu-SPIONs and Ag-SPIONs on RAW 264.7 macrophage cells

Cytotoxic activity of Cu-SPIONs and Ag-SPIONs on RAW 264.7 macrophage cells was investigated to determine non-lethal concentrations for consideration in further experiments. Figure 5.1 shows the cell viability percentages obtained after treating RAW 264.7 macrophage cells with varying concentrations of Cu-SPIONs, Ag-SPIONs and isoniazid.

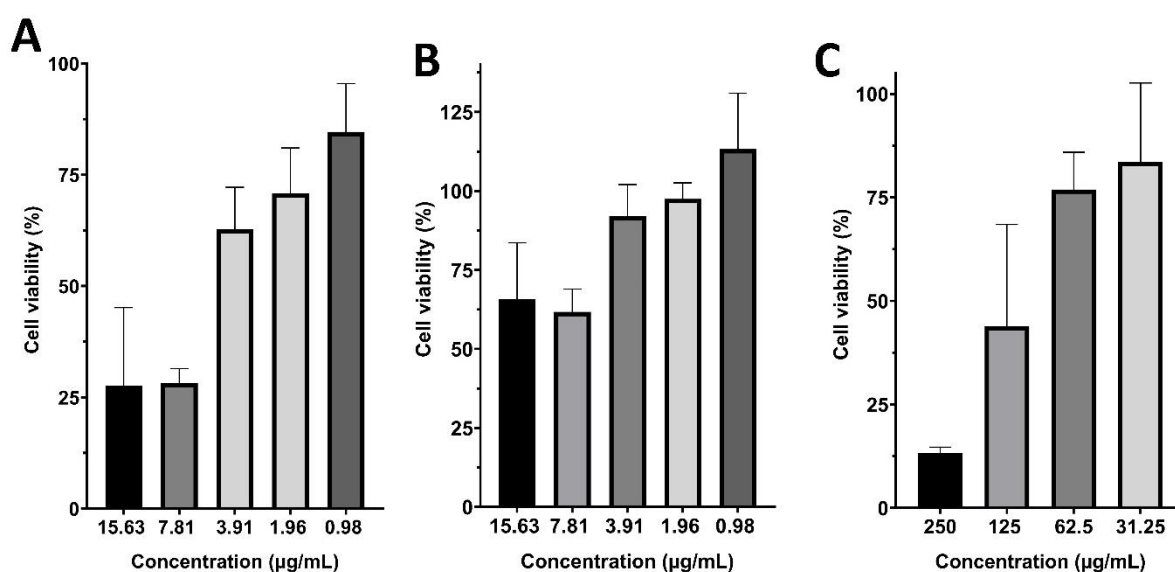


Figure 5.1. Cell viability percentages of RAW 264.7 macrophage cells obtained after treatment with various agents for 48 hours. In the figure, Cu-SPIONs and Ag-SPIONs are represented by **A** and **B** respectively, while **C** represents isoniazid which was used as a control. Error bars represent standard deviation where $n = 3$. Cell viability is expressed as a percentage of untreated cells.

When cell viability after treatment with an agent is $< 70\%$, the agent is considered as cytotoxic, while cell viability percentage of $> 70\%$ would mean that the agent is non-cytotoxic [24]. In this regard, Cu-SPIONs were found to be non-cytotoxic at a concentration of 1.96 and

0.98 $\mu\text{g/mL}$, with corresponding cell viability percentages being found to be 70.82% and 84.63%, respectively. The cytotoxic activity of Cu-SPIONs in this study was found to be comparatively stronger than that of Cu and CuO nanoparticles which were previously tested on the same cell line. After exposing RAW 264.7 macrophage cells to Cu and CuO nanoparticles for 24 hours, cell viability percentages of $> 80\%$ were recorded for treatments of 10 $\mu\text{g/mL}$ for both types of nanoparticles [25].

Ag-SPIONs were found to be non-cytotoxic at 3.91, 1.96 and 0.98 $\mu\text{g/mL}$, with corresponding cell viability being found to be 92.00%, 97.47% and 113.26%, respectively. These results were more comparable to those from a previous study where biogenic Ag nanoparticles were evaluated for cytotoxicity on RAW 264.7 macrophage cells and were found to be cytotoxic at concentrations $\geq 3 \mu\text{g/mL}$ [26]. Interestingly in another study, exposure of RAW 264.7 macrophage cells to Ag nanoparticles to concentrations between 6.25-100 $\mu\text{g/mL}$ did not result in a dramatic reduction of cell after 24 hours of treatment, and thus were found non-cytotoxic in the mentioned concentration range [27]. The differences in the findings can be attributed to the differences in synthesis techniques and reagents used in generation of nanoparticles. Thus, variations in size, shape and organic/inorganic coatings are likely to lead to the differences in bioactivity the from the different studies.

As a first-line TB drug, isoniazid was used as a control in this study. Isoniazid showed the least cytotoxic activity with treatments of 62.5 and 31.25 $\mu\text{g/mL}$ exhibiting cell viability percentages of 76.88% and 83.49%, respectively. It is worth mentioning that isoniazid is a pro-drug that is activated by a multifunctional catalase-peroxidase enzyme known as KatG in Mycobacteria to form isonicotinoyl acyl radical, which in turn reacts with NAD^+/NADH to form at the potent inhibitor of InhA, isoniazid-NADH [28,29]. It is thought that the cytotoxic activity profile of isoniazid-NADH may be hypothetically different from that of isoniazid, reports on the subject are scarce and thus conclusions are difficult to make.

In this study, cytotoxicity was found to be concentration dependent. It can further be stated that the extent of cytotoxicity was material dependent. The physical and chemical properties determine the extent to which metallic nanoparticles exhibit cytotoxicity. However, the non-cytotoxic concentrations observed for RAW 264.7 macrophages may not stay the same when the Cu-SPIONs and Ag-SPIONs are tested on numerous other cell line which are models of various body organs, such as the intestines. Thus, before proceeding to *in vivo* studies, the safety profile of these afore mentioned nanoparticles have to be thoroughly investigated in order to avoid undesirable side effects.

5.3.2 Apoptosis and necrosis of infected RAW 264.7 macrophage cells after treatment with bi-metallic SPIONs

After evaluating the cytotoxic activity of Cu-SPIONs and Ag-SPIONs on RAW 264.7 macrophage cells, it was observed that the 1.96 and 3.91 $\mu\text{g/mL}$ were the highest concentrations respectively to be regarded as non-cytotoxic for the two types of nanoparticles. For treatment of RAW 264.7 macrophage cells infected with *M. smegmatis* mc²155, 1.96 $\mu\text{g/mL}$ for both Cu-SPIONs and Ag-SPIONs was selected as the testing concentration. Additionally, this concentration of 1.96 $\mu\text{g/mL}$ was also chosen for the fungal extract from *Clonostachys rogersoniana* MGK33, and also bi-metallic SPIONs surface modified using the fungal extract (Cu-SPIONs@MGK33 and Ag-SPIONs@MGK33). Figure 5.2 shows the flow-cytometry dot-plots obtained after analyzing cells treated for 24 hours with various agents mentioned previously. A summary of the percentage number of cells determined as viable, early apoptotic, late apoptotic and necrotic after 24 hours of treatment is shown in Figure 5.3.

Treatment of infected RAW 264.7 macrophage cells with Cu-SPIONs resulted in 2.28% early apoptotic cells, 20.67% late apoptotic cells and 25.91% necrotic cells. In the Ag-SPIONs treatment, 2.51 early apoptotic cells, 12.22% late apoptotic cells and 35.44% necrotic cells

were observed. It was evident that the Ag-SPIONs induced less apoptosis and more necrosis compared to Cu-SPIONs.

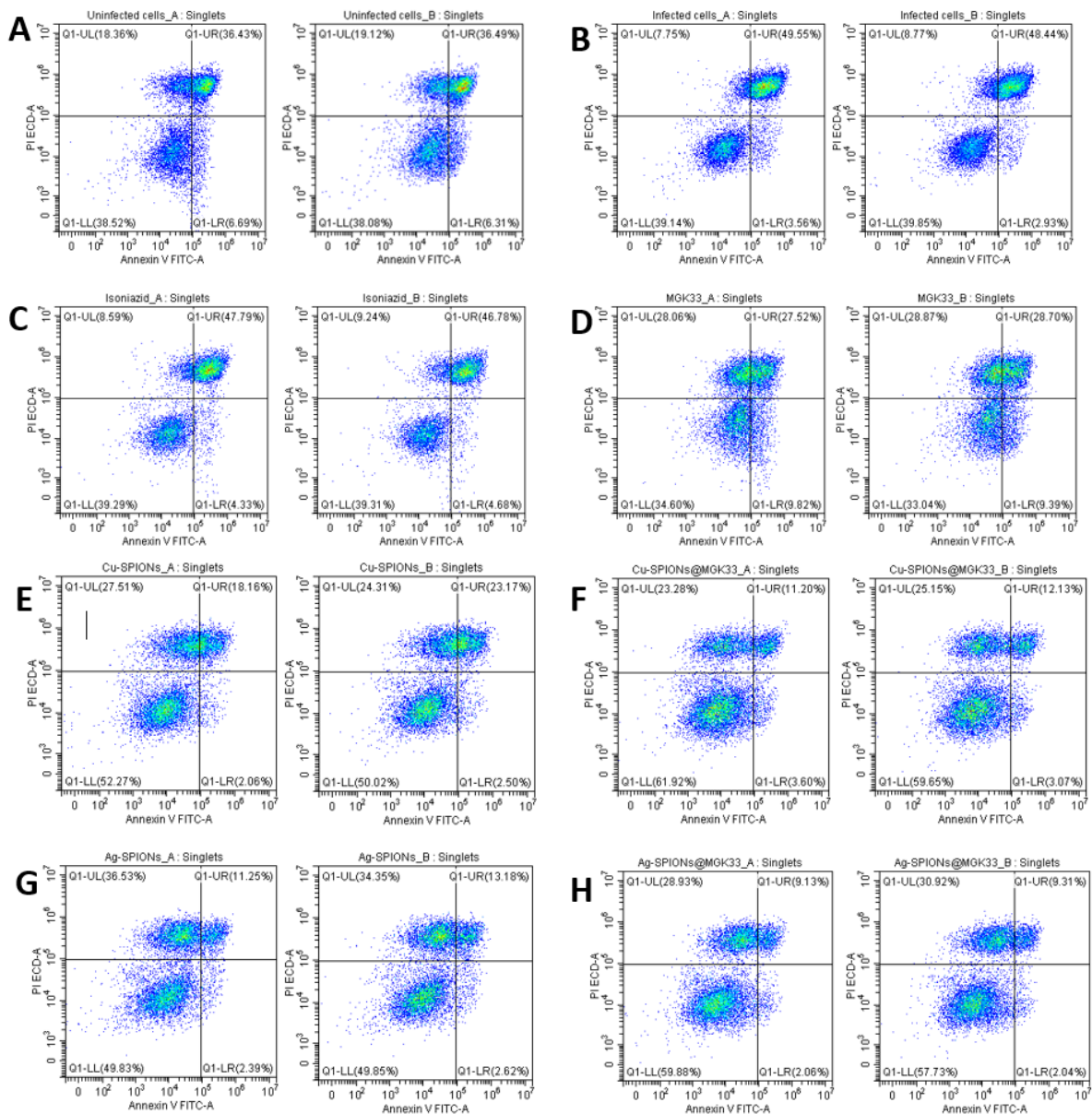


Figure 5.2. Flow cytometry dot-plots obtained after 24 hours of treatment of RAW 264.7 macrophage cells. In the figure, samples are presented as follows: Uninfected cells (A), infected cells (B), isoniazid (C), MGK33 (D), Cu-SPIONs (E), Cu-SPIONs@MGK33 (F), Ag-SPIONs (G) and Ag SPIONs@MGK33 (H). Isoniazid was used as a control for antimycobacterial activity while $n = 2$. Appendix C shows the Annexin V-FITC and PI gates for each sample displayed in this figure.

Bi-metallic SPIONs modified with the MGK33 fungal extract, namely Cu-SPIONs@MGK33 and Ag-SPIONs@MGK33, were observed to exhibit a protective effect on cells as evidenced by the high cell viability (60.79% and 58.81%, respectively), reduced late apoptosis (11.67%

and 9.22%, respectively) and reduced necrosis (24.22% and 29.93%, respectively), were observed, compared to the naked Cu-SPIONs and Ag-SPIONs. The highest percentage of cells in early apoptosis was observed from the MGK33 extract which recorded 9.61%, with an approximately equal effect on apoptosis (28.11%) and necrosis (28.47%).

High amounts of late apoptotic cells in the isoniazid treatment (47.29%) and the untreated infected cells (49.00%) were unsurprisingly observed. It has been previously reported that *M. smegmatis* is naturally capable of inducing apoptosis in macrophages, that is in somewhat similar mechanisms as *M. tuberculosis*. In a recent study, it was shown that infection of RAW 264.7 macrophage cells with *M. smegmatis* leads to an increase ROS production in bacteria-containing phagosomes, which in turn leads to an upregulation in the production of pro-inflammatory cytokines, namely tumor necrosis factor alpha (TNF α), interleukin 6 (IL-6) and monocyte chemoattractant protein-1 (MCP-1) which are associated with clearance of pathogens [30]. The increase in the production of ROS induces an increase in unfolded or misfolded proteins in the endoplasmic reticulum (ER) and thus causing an ER stress [30]. ER stress results in the activation of the unfolded protein response (UPR) signaling pathway which results in apoptosis [31].

It is also worthwhile mentioning that higher levels of macrophage-apoptotic cell death are expected upon infection with avirulent bacteria such as *M. smegmatis*, compared to virulent strains with *M. tuberculosis* which express proteins capable of inhibiting host apoptosis, such as the Mycobacterial protein-tyrosine phosphatase A (MtpA), which dephosphorylates host proteins in the cytoplasm [32].

Since metallic nanoparticles are known to be capable of inducing ROS dependent oxidative stress, it is tempting to suggest that ER stress and the activation of the UPR signaling pathway may have resulted in the observed apoptosis from both Cu-SPIONs and Ag-SPIONs and their

fungus-extract coated counterparts. It is also plausible that apoptosis induced by Cu-SPIONs and Ag-SPIONs may have resulted from the activation of caspase-dependent pathways, a recent study involving the use of CuO nanoparticles on MCF-7 cells reported an upregulation of caspases 3 and 9, and a downregulation of caspase 8 [33]. Activation of caspase 3 could have led to the activation of other caspases and thus set the path for irrecoverable apoptosis.

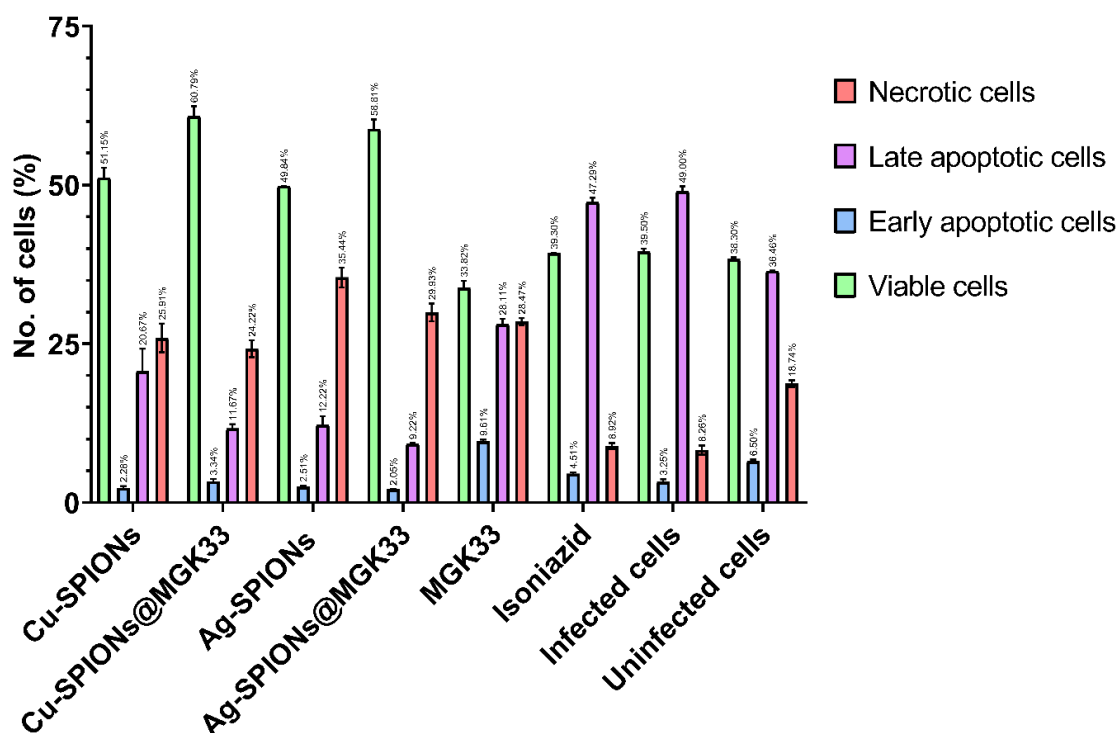


Figure 5.3. Percentage number of viable, early apoptotic, late apoptotic and necrotic cells after 24 hours of treatment with Cu-SPIONs, Cu-SPIONs@MGK33, Ag-SPIONs, Ag-SPIONs@MGK33 and MGK33. Isoniazid was used as a control for antimycobacterial activity. In the figure, $n = 2$.

In literature, clearance of early apoptotic cells is described to be associated with anti-inflammatory and tolerogenic responses, while the removal of late apoptotic and necrotic cells promotes inflammation and autoimmune responses [16]. Furthermore, early apoptotic cells *in vitro* are known to undergo late apoptosis due to the absence of clearance [18]. Seeing that the cell populations were mostly found to have entered late apoptosis and necrosis after 24 hours of treatment in this study, the MGK33 and Cu-SPIONs treatments which both had the highest

number of late apoptotic cells (28.11% and 20.67%, respectively) may be re-evaluated with flow cytometry analyzed at multiple time points, e.g., hourly, in order to quantify early apoptosis accurately.

5.3.3 Time-dependent survival of intracellular bacteria in RAW 264.7 macrophage cells

Results from CFU enumeration of *M. smegmatis* mc²155 plated out from infected RAW 264.7 macrophage cells treated with various agents in this study are shown in Table 5.1.

Table 5.1. Survival of intracellular *M. smegmatis* mc²155 determined by counting of colony forming units (CFUs) after plating out at 4 different time-points ($n = 3$, mean \pm standard deviation).

Treatment	Concentration	Colony forming units per mL (CFU/mL)			
		6 Hrs	12 Hrs	18 Hrs	24 Hrs
Cu-SPIONs	1.96 μ g/mL	> 650	16 \pm 7	11 \pm 9	35 \pm 14
Cu-SPIONs@MGK33	1.96 μ g/mL	> 650	48 \pm 18	82 \pm 33	43 \pm 17
Ag-SPIONs	1.96 μ g/mL	> 650	37 \pm 37	11 \pm 8	34 \pm 17
Ag-SPIONs@MGK33	1.96 μ g/mL	> 650	41 \pm 21	143 \pm 49	43 \pm 17
MGK33	1.96 μ g/mL	> 650	29 \pm 19	48 \pm 29	11 \pm 3
Isoniazid	1.96 μ g/mL	> 650	73 \pm 11	169 \pm 69	153 \pm 69
Infected cells (control)	-	> 650	597 \pm 47	604 \pm 32	139 \pm 47
Uninfected cells (control)	-	0	0	0	0

Treatment of infected RAW 264.7 macrophage cells with Cu-SPIONs and Ag-SPIONs resulted in lower intracellular bacterial burden after 24 hours of treatment, that is when compared with the outcomes from the isoniazid treatment and infected cells without any treatment. The outcomes at the 18-hour and 24-hour time points for Cu-SPIONs and Ag-SPIONs differed slightly, suggesting that the two bi-metallic nanoparticles had similar mechanisms of activity.

In a previous study (Chapter 4), the two bi-metallic nanoparticles were shown to possess antimycobacterial activity with minimum inhibitory concentrations (MICs) of 15.63 μ g/mL for Cu-SPIONs, and 7.81 μ g/mL for Ag-SPIONs. In this study, these MIC concentrations could not be used in the treatment of infected RAW 264.7 macrophage cells as they were found to be

cytotoxic, thus lower concentrations 1.96 µg/mL for both bi-metallic nanoparticles were opted for after cell viability assays.

Cu-SPIONs@MGK33 and Ag-SPIONs@MGK33 showed lower antimycobacterial activity compared with their naked counterparts, Cu-SPIONs and Ag-SPIONs, respectively. This was consistent with observations made in Chapter 4, where it was concluded that the coating of the surfaces of nanoparticles with the MGK33 extract is likely to result in the reduction of the surface area or sites available to participate in chemical reactions. After 24 hours of treatment, the fungal extract, MGK33, proved to be the most potent against intracellular bacteria recorded as 11 ± 3 CFU/mL, the lowest in this study.

5.4 Conclusions

In this study, the immunomodulation activities of Cu-SPIONs, Cu-SPIONs@MGK33, Ag-SPIONs, Ag-SPIONs@MGK33 and MGK33 were investigated on RAW 264.7 macrophage cells infected with *M. smegmatis* mc²155. The results showed that Cu-SPIONs were able to induce higher levels of late apoptosis in infected RAW 264.7 macrophage cells, compared to Cu-SPIONs@MGK33, Ag-SPIONs and Ag-SPIONs@MGK33. The fungal extract, MGK33, was able to induce the highest level of early apoptosis in this study which was observed to be 9.61%. In addition, MGK33 was found to be the most potent against intracellular bacteria after recording the lowest number of viable bacteria at 11 ± 3 CFU/mL after 24 hours of treatment. It was concluded that surface modification of nanoparticles using organic compounds results in a change in the bioactivity of the nanoparticles. In this study, Cu-SPIONs and Ag-SPIONs coated with the MGK33 fungal extract showed reduced cytotoxic activity and bactericidal effects against intracellular bacteria. Further studies should be done to isolate and purify compounds from the MGK33 crude extract to identify the compound(s) with immunomodulatory activities.

5.5 References

1. WHO *Global Tuberculosis Report 2021*; World Health Organization: Geneva, 2021.
2. Giacomini, E.; Sotolongo, A.; Iona, E.; Severa, M.; Remoli, M.E.; Gafa, V.; Lande, R.; Fattorini, L.; Smith, I.; Manganelli, R.; et al. Infection of Human Dendritic Cells with a *Mycobacterium tuberculosis* SigE Mutant Stimulates Production of High Levels of Interleukin-10 but Low Levels of CXCL10: Impact on the T-Cell Response. *Infect. Immun.* **2006**, *74*, 3296–3304, doi:10.1128/IAI.01687-05.
3. Dallenga, T.; Schaible, U.E. Neutrophils in Tuberculosis--First Line of Defence or Booster of Disease and Targets for Host-Directed Therapy? *Pathog. Dis.* **2016**, *74*, doi:10.1093/femspd/ftw012.
4. Khan, N.; Vidyarthi, A.; Javed, S.; Agrewala, J.N. Innate Immunity Holding the Flanks until Reinforced by Adaptive Immunity against *Mycobacterium tuberculosis* Infection. *Front. Microbiol.* **2016**, *7*, 1–9, doi:10.3389/fmicb.2016.00328.
5. Bussi, C.; Gutierrez, M.G. *Mycobacterium tuberculosis* Infection of Host Cells in Space and Time. *FEMS Microbiol. Rev.* **2019**, *43*, 341–361, doi:10.1093/femsre/fuz006.
6. Ryndak, M.B.; Laal, S. *Mycobacterium tuberculosis* Primary Infection and Dissemination: A Critical Role for Alveolar Epithelial Cells. *Front. Cell. Infect. Microbiol.* **2019**, *9*, doi:10.3389/fcimb.2019.00299.
7. Johnston, B.; Burns, A.R.; Suematsu, M.; Issekutz, T.B.; Woodman, R.C.; Kubes, P. Chronic Inflammation Upregulates Chemokine Receptors and Induces Neutrophil Migration to Monocyte Chemoattractant Protein-1. *J. Clin. Invest.* **1999**, *103*, 1269–1276.

8. Sia, J.K.; Georgieva, M.; Rengarajan, J. Innate Immune Defenses in Human Tuberculosis: An Overview of the Interactions between *Mycobacterium tuberculosis* and Innate Immune Cells. *J. Immunol. Res.* **2015**, *2015*, e747543, doi:10.1155/2015/747543.
9. Zhai, W.; Wu, F.; Zhang, Y.; Fu, Y.; Liu, Z. The Immune Escape Mechanisms of *Mycobacterium tuberculosis*. *Int. J. Mol. Sci.* **2019**, *20*, doi:10.3390/ijms20020340.
10. Cruz, A.; Fraga, A.G.; Fountain, J.J.; Rangel-Moreno, J.; Torrado, E.; Saraiva, M.; Pereira, D.R.; Randall, T.D.; Pedrosa, J.; Cooper, A.M.; et al. Pathological Role of Interleukin 17 in Mice Subjected to Repeated BCG Vaccination after Infection with *Mycobacterium tuberculosis*. *J. Exp. Med.* **2010**, *207*, 1609–1616, doi:10.1084/jem.20100265.
11. Danelishvili, L.; Yamazaki, Y.; Selker, J.; Bermudez, L.E. Secreted *Mycobacterium tuberculosis* Rv3654c and Rv3655c Proteins Participate in the Suppression of Macrophage Apoptosis. *PLoS One* **2010**, *5*, e10474, doi:10.1371/journal.pone.0010474.
12. Aguilo, J.; Marinova, D.; Martin, C.; Pardo, J. ESX-1-Induced Apoptosis during Mycobacterial Infection: To Be or Not to Be, That Is the Question. *Front. Cell. Infect. Microbiol.* **2013**, *3*.
13. Abdalla, A.E.; Ejaz, H.; Mahjoob, M.O.; Alameen, A.A.M.; Abosalif, K.O.A.; Elamir, M.Y.M.; Mousa, M.A. Intelligent Mechanisms of Macrophage Apoptosis Subversion by *Mycobacterium*. *Pathogens* **2020**, *9*, 218, doi:10.3390/pathogens9030218.
14. Westman, J.; Grinstein, S.; Marques, P.E. Phagocytosis of Necrotic Debris at Sites of Injury and Inflammation. *Front. Immunol.* **2020**, *10*.

15. Poon, I.K.H.; Hulett, M.D.; Parish, C.R. Molecular Mechanisms of Late Apoptotic/Necrotic Cell Clearance. *Cell Death Differ.* **2010**, *17*, 381–397, doi:10.1038/cdd.2009.195.
16. Poon, I.K.H.; Hulett, M.D.; Parish, C.R. Molecular Mechanisms of Late Apoptotic/Necrotic Cell Clearance. *Cell Death Differ.* **2010**, *17*, 381–397, doi:10.1038/cdd.2009.195.
17. Crowley, L.C.; Scott, A.P.; Marfell, B.J.; Boughaba, J.A.; Chojnowski, G.; Waterhouse, N.J. Measuring Cell Death by Propidium Iodide Uptake and Flow Cytometry. *Cold Spring Harb. Protoc.* **2016**, *2016*, doi:10.1101/pdb.prot087163.
18. Stepanek, O.; Brdicka, T.; Angelisova, P.; Horvath, O.; Spicka, J.; Stockbauer, P.; Man, P.; Horejsi, V. Interaction of Late Apoptotic and Necrotic Cells with Vitronectin. *PLOS ONE* **2011**, *6*, e19243, doi:10.1371/journal.pone.0019243.
19. Jnawali, H.N.; Ryoo, S. First– and Second–Line Drugs and Drug Resistance. In *Tuberculosis*; Mahboub, B.H., Vats, M.G., Eds.; IntechOpen: Rijeka, 2013.
20. Dookie, N.; Rambaran, S.; Padayatchi, N.; Mahomed, S.; Naidoo, K. Evolution of Drug Resistance in Mycobacterium Tuberculosis: A Review on the Molecular Determinants of Resistance and Implications for Personalized Care. *J. Antimicrob. Chemother.* **2018**, *73*, 1138–1151, doi:10.1093/jac/dkx506.
21. Gülbay, B.E.; Gürkan, O.U.; Yildiz, O.A.; Onen, Z.P.; Erkeköl, F.O.; Baççioğlu, A.; Acican, T. Side Effects Due to Primary Antituberculosis Drugs during the Initial Phase of Therapy in 1149 Hospitalized Patients for Tuberculosis. *Respir. Med.* **2006**, *100*, 1834–1842, doi:10.1016/j.rmed.2006.01.014.

22. El-Din, M.A.T.; Halim, H.A.A.-E.; El-Tantawy, A.M. Adverse Reactions among Patients Being Treated for Multi-Drug Resistant Tuberculosis in Egypt from July 2006 to January 2009. *Egypt. J. Chest Dis. Tuberc.* **2015**, *64*, 657–664, doi:10.1016/j.ejcdt.2015.05.011.
23. Zumla, A.; Rao, M.; Wallis, R.S.; Kaufmann, S.H.E.; Rustomjee, R.; Mwaba, P.; Vilaplana, C.; Yeboah-Manu, D.; Chakaya, J.; Ippolito, G.; et al. Host-Directed Therapies for Infectious Diseases: Current Status, Recent Progress, and Future Prospects. *Lancet Infect. Dis.* **2016**, *16*, e47–e63, doi:10.1016/S1473-3099(16)00078-5.
24. Cannella, V.; Altomare, R.; Chiaramonte, G.; Di Bella, S.; Mira, F.; Russotto, L.; Pisano, P.; Guercio, A. Cytotoxicity Evaluation of Endodontic Pins on L929 Cell Line. *BioMed Res. Int.* **2019**, *2019*, 3469525, doi:10.1155/2019/3469525.
25. Triboulet, S.; Aude-Garcia, C.; Carrière, M.; Diemer, H.; Proamer, F.; Habert, A.; Chevallet, M.; Collin-Faure, V.; Strub, J.-M.; Hanau, D.; et al. Molecular Responses of Mouse Macrophages to Copper and Copper Oxide Nanoparticles Inferred from Proteomic Analyses*. *Mol. Cell. Proteomics* **2013**, *12*, 3108–3122, doi:10.1074/mcp.M113.030742.
26. Wypij, M.; Jędrzejewski, T.; Ostrowski, M.; Trzcińska, J.; Rai, M.; Golińska, P. Biogenic Silver Nanoparticles: Assessment of Their Cytotoxicity, Genotoxicity and Study of Capping Proteins. *Molecules* **2020**, *25*, 3022, doi:10.3390/molecules25133022.
27. Alsaleh, N.B.; Minarchick, V.C.; Mendoza, R.P.; Sharma, B.; Podila, R.; Brown, J.M. Silver Nanoparticle Immunomodulatory Potential in Absence of Direct Cytotoxicity in RAW 264.7 Macrophages and MPRO 2.1 Neutrophils. *J. Immunotoxicol.* **2019**, *16*, 63–73, doi:10.1080/1547691X.2019.1588928.

28. Hsu, L.-Y.; Lai, L.-Y.; Hsieh, P.-F.; Lin, T.-L.; Lin, W.-H.; Tasi, H.-Y.; Lee, W.-T.; Jou, R.; Wang, J.-T. Two Novel KatG Mutations Conferring Isoniazid Resistance in *Mycobacterium tuberculosis*. *Front. Microbiol.* **2020**, *11*.
29. Cade, C.E.; Dlouhy, A.C.; Medzihradzky, K.F.; Salas-Castillo, S.P.; Ghiladi, R.A. Isoniazid-Resistance Conferring Mutations in *Mycobacterium tuberculosis* KatG: Catalase, Peroxidase, and INH-NADH Adduct Formation Activities. *Protein Sci.* **2010**, *19*, 458–474, doi:10.1002/pro.324.
30. Kim, S.-H.; Cho, S.-N.; Lim, Y.-J.; Choi, J.-A.; Lee, J.; Go, D.; Song, C.-H. Phagocytosis Influences the Intracellular Survival of *Mycobacterium smegmatis* via the Endoplasmic Reticulum Stress Response. *Cell Biosci.* **2018**, *8*, 52, doi:10.1186/s13578-018-0250-2.
31. Fribley, A.; Zhang, K.; Kaufman, R.J. Regulation of Apoptosis by the Unfolded Protein Response. *Methods Mol. Biol. Clifton NJ* **2009**, *559*, 191–204, doi:10.1007/978-1-60327-017-5_14.
32. Wang, J.; Ge, P.; Qiang, L.; Tian, F.; Zhao, D.; Chai, Q.; Zhu, M.; Zhou, R.; Meng, G.; Iwakura, Y.; et al. The Mycobacterial Phosphatase PtpA Regulates the Expression of Host Genes and Promotes Cell Proliferation. *Nat. Commun.* **2017**, *8*, 244, doi:10.1038/s41467-017-00279-z.
33. Esmaeili Govarchin Ghaleh, H.; Zarei, L.; Mansori Motlagh, B.; Jabbari, N. Using CuO Nanoparticles and Hyperthermia in Radiotherapy of MCF-7 Cell Line: Synergistic Effect in Cancer Therapy. *Artif. Cells Nanomedicine Biotechnol.* **2019**, *47*, 1396–1403, doi:10.1080/21691401.2019.1600529.

Chapter 6

General conclusions and future directions

6.1 Conclusions from this study

The purpose of this study was to investigate the antimycobacterial activity of extracts from marine fungi associated with ascidians. The successful isolation of filamentous fungi from the tissues of ascidians collected in this study corroborated findings by other researchers who performed similar studies. The identification of ascidian species invasive to the Western Cape coasts was found to be evidence of new species introduction by fouling boats from other regions of the world [1]. Even though invasive species can be harmful to the natural flora and fauna, the fungus, *Clonostachys rogersoniana* MGK33 which was found to possess antimycobacterial activity was isolated from an invasive, solitary ascidian, *Ascidiella aspersa*. This led to the conclusion that invasive marine and terrestrial multicellular organisms potentially associate with microorganisms which impart unique properties that assist the multicellular organism to survive. Compounds from the invasive species and their microbial associates may possess novel bioactivities.

This study also sought to synthesize superparamagnetic iron oxide nanoparticles (SPIONs), surface modify them with various metals which include nickel, zinc, gold, copper and silver, and then functionalize the bi-metallic SPIONs with a fungal extract possessing antimycobacterial activity. The magnetic properties of SPIONs were utilized in separating nanoparticles from mixtures (magnetic separation) and thus removing the by products from reactions, easily. In therapy, a magnetic field gradient can potentially be used to guide SPIONs to the target site and retain them for as long as required. Furthermore, this study showed that Cu-SPIONs and Ag-SPIONs were the most potent antimycobacterial agents investigated,

surpassing even the antimycobacterial activity SPIONs modified with the fungal extract, MGK33. Since only five metals (nickel, zinc, gold, copper and silver) were utilized in this study to modify the surface of SPIONs, the exploration of other transition metals such as cadmium, platinum and vanadium may likely result interesting and novel mechanisms of action.

Since the fungal extract, MGK33, induced the highest early apoptosis percentage in this study, with observably high late apoptosis and necrosis, it likely that the numerous compounds in the crude extract were responsible for the mixed observations as various cell-death pathways were likely activated by the action of these compounds. Bioactivity guided fractionation will allow for the identification of compounds responsible for the observed bioactivity and also for the determination of molecular mechanisms of action in inducing cell death. Among others, bionectin F was a compound in this study as it was identified from the MGK33 extract. Evaluating its mechanism of action against Mycobacteria will be a valuable contribution to the body of knowledge on this compound. Furthermore, bionectin F may further be explored in synergistic studies with other first-line TB drugs to reduce the treatment duration of TB patients.

6.2 Limitations of this study

A major limitation in this study was the small sample size of ascidians collected from False Bay and Saldanha Bay. Only eight samples were collected from each of the two locations and thus can be argued as a small sample size and a potential limitation to the diversity of cultivable fungi that could be obtained in this study. In another study involving the isolation of filamentous fungi bacteria from marine macroorganisms, nine samples which included two ascidians were collected from three locations [2]. The ascidians, *Didemnum* sp. and *Didemnum ligulum* yielded 18 and 32 bacterial isolates, respectively, while *Didemnum* sp. yielded 63

filamentous fungal isolates [2]. Since many of the microbial isolates were repeatedly isolated from the various marine macroorganisms, statistical calculations by the authors led them to conclude that the cultivable microbial isolates showed low diversity indices [2]. In this present study, the researchers opted for two locations that are 176 km away from each other which also have different climatic conditions.

In this study, extracts from fungal isolates were evaluated in their crude form, in other words, pure compound purification was not performed. Methanol, an organic solvent, was used to extract metabolites from the air-dried solid state fermentation cultures of fungal isolates and the extracts were concentrated using a rotary evaporator. This practice allows the concentrated crude extracts to be tested in order to determine the activity of the compounds in the extract. The major limitation is that it is challenging to attribute observed bioactivity to individual compounds in an extract, especially when the pure form of the compounds in the extract have not been previously profiled the activity under investigation. Due to insufficient time in this study to conduct bio-guided fractionation and pure compound identification, an *in silico* approach (molecular docking and simulation) in order to predict the compound(s) responsible for the antimycobacterial activity observed from the extract of *C. rogersoniana* MGK33. *In silico* molecular docking and simulation studies are effective where 3D crystallized structures of protein have been described, such as those from *Mycobacterium tuberculosis* H37Rv [3].

Utilizing a fungal crude extract to modify the surfaces of Cu-SPIONs and Ag-SPIONs resulted in modified nanoparticles with slightly reduced antimycobacterial activity. The use purified compounds from the bioactive fungal extract to modify the nanoparticles may achieve an increase in antimycobacterial activity, as opposed to observations in this study.

In this study, flow-cytometry was performed after 24 hours of treatment of *Mycobacterium smegmatis* mc²155-infected RAW 264.7 macrophage cells. As a result, cells in most of the

treatments had already progressed from early apoptosis to late apoptosis and thus resulting in earlier events being unaccounted. In order to account for early apoptotic events, flow-cytometry should be done at multiple time points in order to track the progress of cells from early apoptosis to late apoptosis.

6.3 Future directions

This study demonstrated that filamentous marine fungi are indeed a reservoir of bioactive compounds. Future related studies should seek to isolate fungi from extreme marine environments which include deep-sea hot hydrothermal vents, cold seeps, anoxic hypersaline lakes and even water droplets trapped in oil spills. Microbial populations in these environments are likely to present novel compounds with interesting bioactivities.

Co-culturing fungi with *M. tuberculosis* could potentially result in the activation of silent biosynthetic gene clusters coding for secondary metabolites that are potentially antimycobactericidal. These compounds can be conjugated to magnetic nanoparticles to produce nano-metabolite anti-TB drugs which are externally directed using a magnetic gradient to the site of infection, such as granulomas in the lungs with poor penetration to some of the conventional drugs.

The author also noted that natural product drug discovery studies employing a multi-disciplinary approach are likely to yield more success in identification of lead compounds with potentially low susceptibility to resistance by *M. tuberculosis* and high chances of success in clinical trials.

References

1. Clarke Murray, C.; Pakhomov, E.A.; Therriault, T.W. Recreational Boating: A Large Unregulated Vector Transporting Marine Invasive Species. *Divers. Distrib.* **2011**, *17*, 1161–1172, doi:10.1111/j.1472-4642.2011.00798.x.
2. Menezes, C.B.A.; Bonugli-Santos, R.C.; Miqueletto, P.B.; Passarini, M.R.Z.; Silva, C.H.D.; Justo, M.R.; Leal, R.R.; Fantinatti-Garboggini, F.; Oliveira, V.M.; Berlinck, R.G.S.; et al. Microbial Diversity Associated with Algae, Ascidians and Sponges from the North Coast of São Paulo State, Brazil. *Microbiol. Res.* **2010**, *165*, 466–482, doi:10.1016/j.micres.2009.09.005.
3. Shilpi, J.A.; Ali, M.T.; Saha, S.; Hasan, S.; Gray, A.I.; Seidel, V. Molecular Docking Studies on InhA, MabA and PanK Enzymes from *Mycobacterium tuberculosis* of Ellagic Acid Derivatives from *Ludwigia adscendens* and *Trewia nudiflora*. *Silico Pharmacol.* **2015**, *3*, 10, doi:10.1186/s40203-015-0014-1.

Appendix A

Marine (ascidian) samples from Saldanha Bay






A1 Background


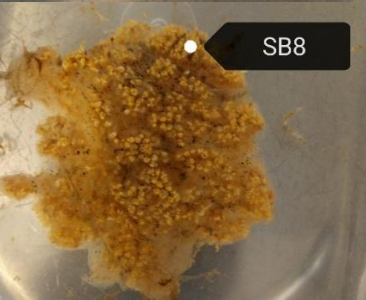




Different species of both native and invasive ascidians collected from Saldanha Bay (33° 1' 36.06" S, 17° 57' 39.55" E) and from False Bay (34° 11' 28.40" S, 18° 26' 2.96" E) on the 9th and 11th of September 2019 respectively. The ascidians were collected from perplex plates that had been submerged in water from the 2nd and 4th of April 2019 (23 weeks) at both sites, at a depth of 1.5 m. Both sites serve as marinas for local and international yachts and small boats. Due to the extensive overgrowth on the plates (Figure A1), the organisms were transported the laboratory attached to their plates in large containers filled with chilled sea water. Upon arriving at the laboratory, the samples were cooled to 4 °C and were processed within 24 hours.

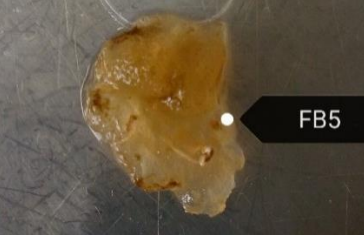





Figure A1. Ascidians collected from Saldanha Bay. The image on the left shows the excessive growth of ascidians on one of the plates, the image on the right shows another plate with some ascidians and the container in which they were transported to the laboratory.

Table A1. Saldanha Bay and False Bay Samples collected and their fungal isolates (SB is Saldanha Bay and FB is False Bay).

Sample code	Photograph	Morphological feature based identity	Fungal isolates (Total No.)
SB1		<ul style="list-style-type: none"> • Common name: White ringed ascidian • Scientific name: <i>Botryllus magnicoecus</i> • Colonial • Native 	MGK26 (1 isolate)
SB2		<ul style="list-style-type: none"> • Common name: White ringed ascidian • Scientific name: <i>Botryllus magnicoecus</i> • Colonial • Native 	MGK2, MGK3, MGK6, MGK8, MGK20, MGK31 (6 isolates)
SB3		<ul style="list-style-type: none"> • Common name: Sea vase • Scientific name: <i>Ciona robusta</i> • Solitary • Invasive 	MGK7, MGK9, MGK10, MGK34, MGK36, MGK51 (6 isolates)
SB4		<ul style="list-style-type: none"> • Common name: Waxy sea squirt • Scientific name: <i>Asterocarpa humilis</i> • Solitary • Invasive 	(0 isolates)
SB5		<ul style="list-style-type: none"> • Common name: White ringed ascidian • Scientific name: <i>Botryllus magnicoecus</i> • Colonial • Native 	MGK25, MGK39, MGK49 (3 isolates)
SB6		<ul style="list-style-type: none"> • Common name: Waxy sea squirt • Scientific name: <i>Asterocarpa humilis</i> • Solitary • Invasive 	(0 isolates)

<p>SB7</p>		<ul style="list-style-type: none"> • Common name: The light bulb ascidian • Scientific name: <i>Clavelina lepadiformis</i> • Solitary • Invasive 	<p>MGK42, MGK48 (2 isolates)</p>
<p>SB8</p>		<ul style="list-style-type: none"> • Common name: ? • Scientific name: <i>Botryllus gregalis</i> • Colonial • Native 	<p>MGK47, MGK53 (2 isolates)</p>
<p>FB1</p>		<ul style="list-style-type: none"> • Common name: Golden star ascidian • Scientific name: <i>Botryllus schlosseri</i> • Colonial • Invasive 	<p>MGK5, MGK21, MGK35 (3 isolates)</p>
<p>FB2</p>		<ul style="list-style-type: none"> • Common name: European sea squirt • Scientific name: <i>Ascidella aspersa</i> • Solitary • Invasive 	<p>MGK52, MGK55, MGK56, MGK57 (4 isolates)</p>
<p>FB3</p>		<ul style="list-style-type: none"> • Common name: The light bulb ascidian • Scientific name: <i>Clavelina lepadiformis</i> • Solitary • Invasive 	<p>MGK14, MGK15, MGK30 (3 isolates)</p>
<p>FB4</p>		<ul style="list-style-type: none"> • Common name: Orange-tipped sea squirt • Scientific name: <i>Corella eumyota</i> • Solitary • Invasive 	<p>MGK13, MGK16 (2 isolates)</p>

<p>FB5</p>		<ul style="list-style-type: none"> • Common name: European sea squirt • Scientific name: <i>Ascidella aspersa</i> • Solitary • Invasive 	<p>MGK17, MGK22, MGK33, MGK41 (4 isolates)</p>
<p>FB6</p>		<ul style="list-style-type: none"> • Common name: Red-rust bryozoan • Scientific name: <i>Watersporia subtorquata</i> • Colonial • Invasive <p>*FB6 – Already dead on the time of sampling</p>	<p>MGK28, MGK46 (2 isolates)</p>
<p>FB7</p>		<ul style="list-style-type: none"> • Common name: Meandering ascidian • Scientific name: <i>Botryllus meandrus</i> • Colonial • Native 	<p>MGK19, MGK24 (2 isolates)</p>
<p>FB8</p>		<ul style="list-style-type: none"> • Common name: White ringed ascidian • Scientific name: <i>Botryllus magnicoecus</i> • Colonial • Native 	<p>MGK23, MGK43, MGK44, MGK49, MK50, MGK54 (6 isolates)</p>

Total ascidian samples = 15

Total fungal isolates = 46

Appendix B1

Aligned mass spectra from metabolite extractions using nanoparticles

The tables present the aligned mass spectra from metabolite extractions using nanoparticles. Magnetic iron oxide nanoparticles were synthesized using the chemical co-precipitation method and then modified using gold, silver, copper, zinc and gold. The synthetic nanoparticles were then used to extract metabolites from a fungal extract (MGK33), and then the spent crude extracts from the Nano-extractions were analyzed using mass spectrometry to reveal the efficiency of extraction using nanoparticles.

The data is presented in a tabular form with 30 columns and 237 rows. The first and second column (A and B) are descriptors of peaks detected during the mass spectrometry analysis. The next set of four columns (C to F) respectively present peak m/z values, peak retention time (RT), peak height and peak area from the MGK33 spectral data. Subsequent sets of four columns present similar data from six samples of nanoparticles as follows: SPIONs@MGK33, Ni-SPIONs@MGK33, Zn-SPIONs@MGK33, Ag-SPIONs@MGK33, Au-SPIONs@MGK33, and Cu-SPIONs@MGK33.

The file is saved in MS Excel (*.xlsx) format and is 69 KB in size (<https://www.scidb.cn/s/ni6Jby>).

Appendix B2

Predicted molecular formula from the MGK33 extract

The table presents the 78 ion peaks were observed from the MGK33 extract between 12-13.5 minutes and the predicted molecular formula.

Retention time (min)	Title	Precursor m/z	Adduct	Height	Area	Predicted Formula
12.05	Unknown	281.2472	[M+H] ⁺	2130.272	6092.375	C18H32O2
12.05	Unknown	303.2297	[M+H] ⁺	14577.26	44345.51	C20H30O2
12.05	Unknown	871.5704	[M+H] ⁺	1061.762	5185.9	C55H74N4O5
12.06	Unknown	872.5741	[M+H] ⁺	1265.548	6434.049	C52H77N3O8
12.06	Unknown	887.5671	[M+H] ⁺	2535.347	24655.44	C55H74N4O6
12.43	Unknown	167.0339	[M+H] ⁺	1191.231	6134.777	C8H6O4
12.43	Unknown	279.1603	[M+H] ⁺	8563.908	64874.69	C16H22O4
12.43	Unknown	391.2838	[M+H] ⁺	13876.2	103955.3	C24H38O4
12.43	Unknown	392.2868	[M+H] ⁺	1189.237	6017.646	C23H37NO4
12.43	Unknown	414.27	[M+H] ⁺	1259.655	6602.023	C25H35NO4
12.43	Unknown	429.2389	[M+H] ⁺	1304.829	6256.262	C24H32N2O5
12.43	Unknown	430.2452	[M+H] ⁺	1467.793	7276.827	C22H31N5O4
12.43	Unknown	785.5801	[M+H] ⁺	1219.599	5842.11	C51H76O6
12.43	Unknown	798.5876	[M+H] ⁺	1154.463	6060.374	-
12.43	Unknown	799.5834	[M+H] ⁺	1761.702	8759.945	C45H83O9P
12.43	Unknown	803.5422	[M+H] ⁺	1848.052	9465.265	C46H70N6O6
12.43	Unknown	804.5447	[M+H] ⁺	1303.316	6237.102	C46H78NO8P
12.43	Unknown	805.548	[M+H] ⁺	1230.562	5422.025	C46H76O11
12.43	Unknown	820.5182	[M+H] ⁺	1840.296	8861.107	C45H73NO12
12.43	Unknown	819.5163	[M+H] ⁺	1016.479	4455.19	C46H75O10P
12.43	Unknown	783.5732	[M+H] ⁺	1634.171	9472.253	C48H78O8
12.43	Unknown	413.2662	[M+H] ⁺	1136.195	5998.769	C26H36O4
12.43	Unknown	393.2951	[M+H] ⁺	1607.066	7882.38	C24H40O4
12.43	Unknown	372.3179	[M+H] ⁺	1083.053	5280.529	C21H41NO4
12.43	Unknown	784.5768	[M+H] ⁺	1392.6	3115.679	C44H82NO8P
12.43	Unknown	371.3161	[M+H] ⁺	1624.971	7379.845	C22H42O4
12.61	Unknown	747.5314	[M+H] ⁺	1144.114	5313.502	C41H70N4O8
12.61	Unknown	339.3448	[M+H] ⁺	11574.03	101099.5	-
12.61	Unknown	338.3416	[M+H] ⁺	19764.45	126342.7	C22H43NO
12.66	Unknown	681.9944	[M+2H] ²⁺	1536.591	8432.784	-
12.68	Unknown	659.4799	[M+2H] ²⁺	1202.412	6239.548	-
12.68	Unknown	660.4849	[M+2H] ²⁺	2025.389	11406.09	-
12.74	Unknown	571.4274	[M+2H] ²⁺	1408.04	8034.604	-
12.65	Unknown	873.5798	[M+H] ⁺	2942.698	17694.88	C47H85O12P
12.65	Unknown	872.5753	[M+H] ⁺	1519.855	9053.555	C52H77N3O8

12.65	Unknown	871.5718	[M+H] ⁺	2295.889	15648.97	C55H74N4O5
12.71	Unknown	615.9572	[M+2H] ²⁺	2581.89	14570.04	-
12.71	Unknown	615.4537	[M+2H] ²⁺	1760.119	10260.8	-
12.62	Unknown	725.5199	[M+2H] ²⁺	3030.614	16371.87	-
12.73	Unknown	593.9434	[M+2H] ²⁺	2292.444	11730.21	-
12.73	Unknown	593.4417	[M+2H] ²⁺	1048.514	5333.615	-
12.69	Unknown	385.2461	[M+H] ⁺	20084.38	123813.9	C24H32O4
12.77	Unknown	549.9154	[M+2H] ²⁺	2199.239	11468.33	-
12.65	Unknown	703.5057	[M+2H] ²⁺	3195.411	16911.88	-
12.70	Unknown	639.9477	[M+H] ⁺	5479.836	33655.01	-
12.70	Unknown	647.9358	[M+H] ⁺	2120.115	15250.82	-
12.70	Unknown	637.466	[M+2H] ²⁺	3577.376	19352.33	-
12.69	Unknown	637.9681	[M+2H] ²⁺	2505.252	12532.26	-
12.71	Unknown	617.9339	[M+H] ⁺	5861.199	38215	-
12.71	Unknown	625.916	[M+H] ⁺	1565.764	9776.164	-
12.65	Unknown	681.4903	[M+2H] ²⁺	3263.471	17650.38	-
12.65	Unknown	704.0062	[M+2H] ²⁺	2317.384	11736.87	-
12.73	Unknown	595.9174	[M+H] ⁺	1138.908	5612.906	-
12.73	Unknown	603.9058	[M+H] ⁺	3239.831	14185.6	-
12.73	Unknown	606.3836	[M+H] ⁺	1927.04	7485.504	C31H51N5O7
12.77	Unknown	549.4138	[M+2H] ²⁺	2886.622	15157.97	-
12.62	Unknown	726.0208	[M+2H] ²⁺	1754.33	9388.838	-
12.75	Unknown	573.9063	[M+H] ⁺	34469.51	196974.3	-
12.68	Unknown	659.9796	[M+2H] ²⁺	1979.24	10094.13	-
12.75	Unknown	571.9257	[M+2H] ²⁺	1320.794	6436.446	-
12.79	Unknown	527.403	[M+H] ⁺	17627.26	96547.2	C34H54O4
12.79	Unknown	1036.771	[M+H] ⁺	4575.378	26538.5	-
12.80	Unknown	992.7476	[M+H] ⁺	13644.82	175043.1	C61H102NO7P
12.82	Unknown	948.7135	[M+H] ⁺	48694.66	891499.9	-
12.83	Unknown	904.6935	[M+H] ⁺	80494.36	1464026	C50H98NO10P
12.86	Unknown	860.6687	[M+H] ⁺	1385.541	7394.941	C48H94NO9P
12.88	Unknown	816.6396	[M+H] ⁺	5962.918	31533.29	C46H90NO8P
12.89	Unknown	772.6121	[M+H] ⁺	1177.375	6097.729	C44H86NO7P
12.91	Unknown	728.5897	[M+H] ⁺	1357.874	5868.855	C42H82NO6P
12.93	Unknown	684.5607	[M+H] ⁺	3525.39	17143.11	-
13.43	Unknown	873.5811	[M+H] ⁺	1170.129	5326.306	C47H85O12P
13.43	Unknown	872.5767	[M+H] ⁺	4288.603	27551.71	C52H77N3O8
13.43	Unknown	871.5735	[M+H] ⁺	8393.995	65531.32	C55H74N4O5
13.43	Unknown	610.1855	[M+H] ⁺	4442.993	22774.53	C28H35NO10S2
13.46	Unknown	248.1701	[M+H] ⁺	3710.482	19959.11	C15H21NO2
13.46	Unknown	247.1673	[M+H] ⁺	1927.122	9995.259	C16H22O2
13.47	Unknown	226.9531	[M+H] ⁺	7483.209	36816.71	-
13.47	Unknown	365.1057	[M+H] ⁺	1036.558	2889.237	C21H16O6

Appendix B3

Bionectin F extraction

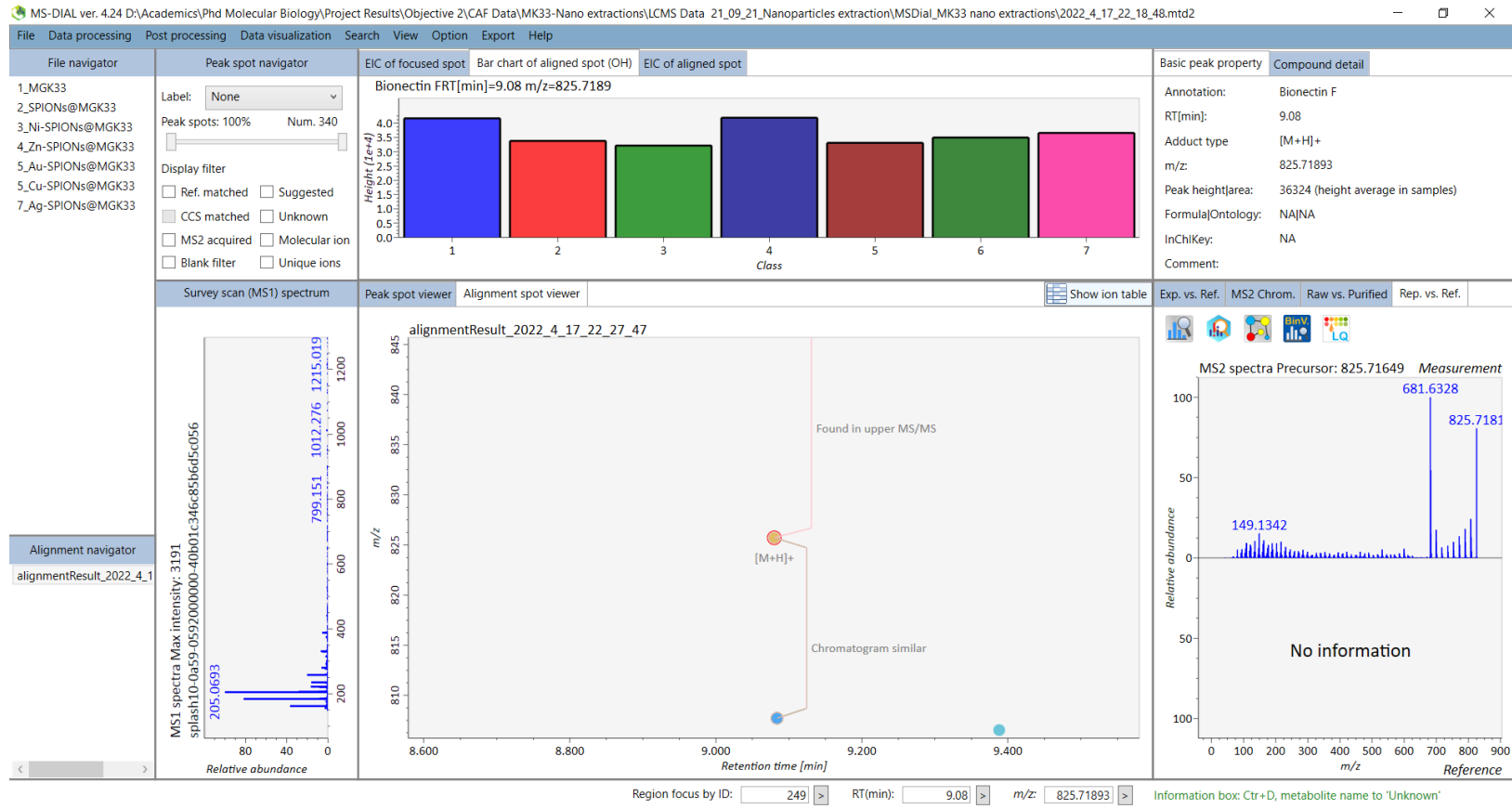


Figure B3-1. Bionectin F peak intensity compared among samples (SPIONs@MGK33, Ni-SPIONs@MGK33, Zn-SPIONs@MGK33, Au-SPIONs@MGK33, Cu-SPIONs@MGK33 and Ag-SPIONs@MGK33). Base peak intensity is represented as height in the bar graph.

Appendix B4

Antimycobacterial activity of SPIONs

The following images were captured during the optimization phase of the study and show broth culture flasks of *Mycobacterium smegmatis* mc²155 after 72 hours of treatment with mono- and bi-metallic SPIONs synthesized in this study.

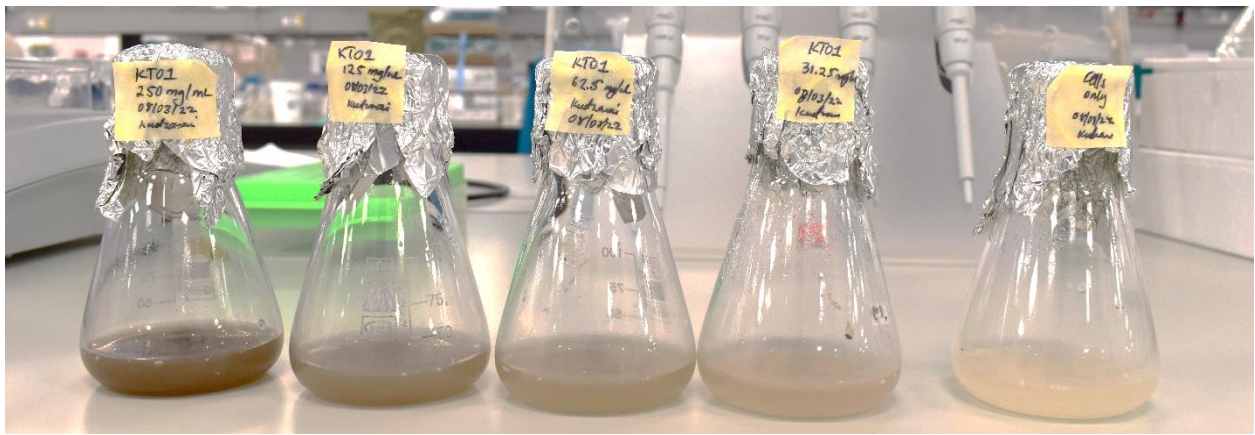


Figure B4-1. *M. smegmatis* mc²155 culture flasks after 72 hours of treatment with mono-metallic (naked) SPIONs, (designated KT01) in the figure. During optimization, treatments were performed at four concentrations as follows: 250, 125, 62.5 and 31.25 µg/mL. Untreated cells were used as a negative control. Visible growth was evident across all concentrations.

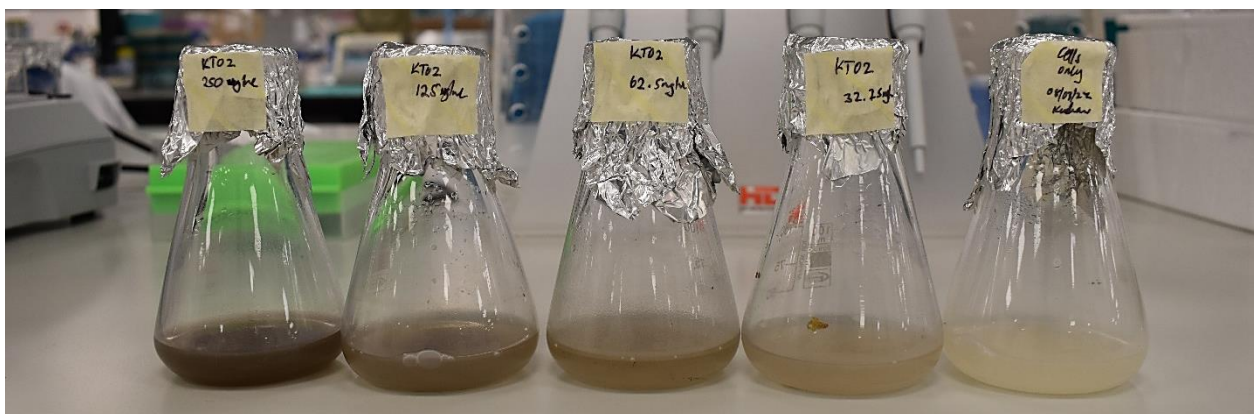


Figure B4-2. *M. smegmatis* mc²155 culture flasks after 72 hours of treatment with Ni-SPIONs, (designated KT02) in the figure. During optimization, treatments were performed at four concentrations as follows: 250, 125, 62.5 and 31.25 µg/mL. Untreated cells were used as a negative control. Visible growth was evident across all concentrations.

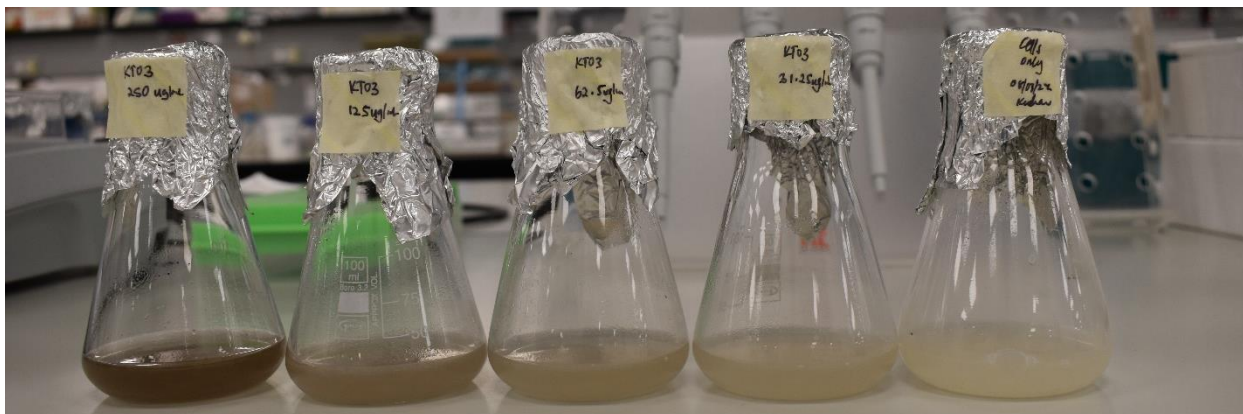


Figure B4-3. *M. smegmatis* mc²155 culture flasks after 72 hours of treatment with Zn-SPIONs, (designated KT03) in the figure. During optimization, treatments were performed at four concentrations as follows: 250, 125, 62.5 and 31.25 µg/mL. Untreated cells were used as a negative control. Visible growth was evident in the flasks treated with 125, 62.5 and 31.25 µg/mL of Zn-SPIONs. It was later confirmed that 250 µg/mL had a sterilizing effect (Figure S3-8).

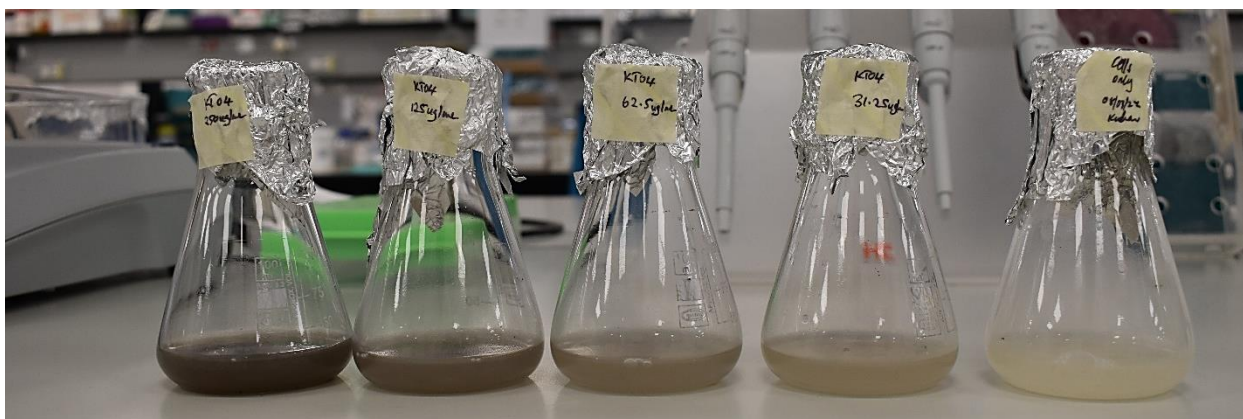


Figure B4-4. *M. smegmatis* mc²155 culture flasks after 72 hours of treatment with Au-SPIONs, (designated KT04) in the figure. During optimization, treatments were performed at four concentrations as follows: 250, 125, 62.5 and 31.25 µg/mL. Untreated cells were used as a negative control. Visible growth was evident across all concentrations.

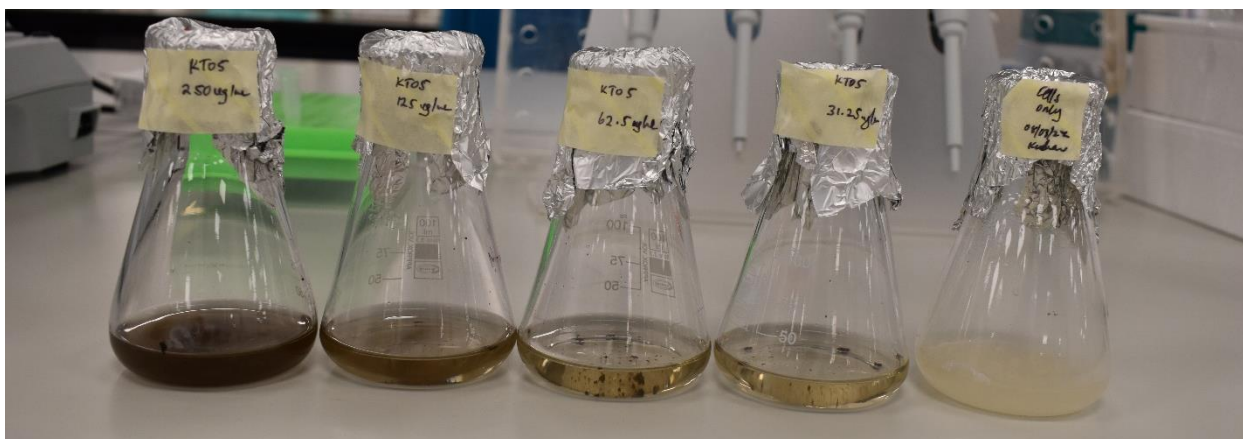


Figure B4-5. *M. smegmatis* mc²155 culture flasks after 72 hours of treatment with Cu-SPIONs, (designated KT05) in the figure. During optimization, treatments were performed at four concentrations as follows: 250, 125, 62.5 and 31.25 µg/mL. Untreated cells were used as a negative control. **No visible growth was evident across all concentrations.**

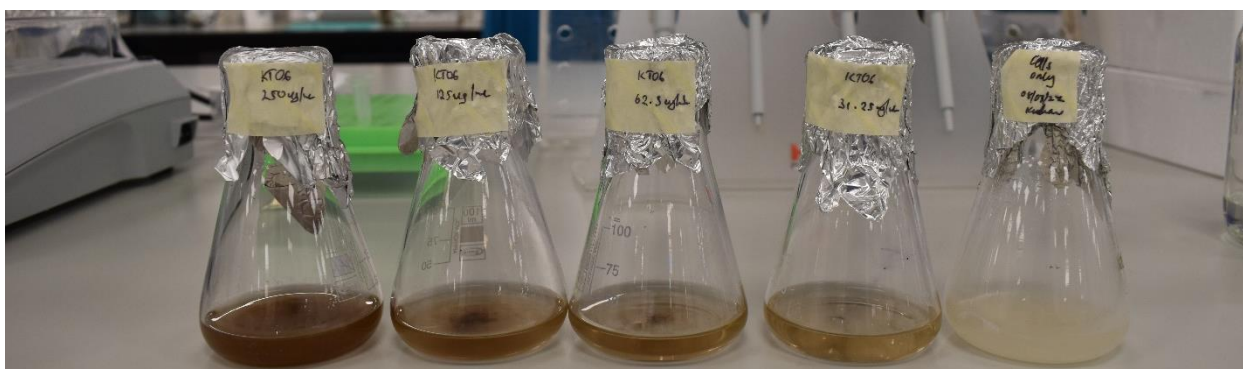


Figure B4-6. *M. smegmatis* mc²155 culture flasks after 72 hours of treatment with Ag-SPIONs, (designated KT06) in the figure. During optimization, treatments were performed at four concentrations as follows: 250, 125, 62.5 and 31.25 µg/mL. Untreated cells were used as a negative control. **No visible growth was evident across all concentrations.**

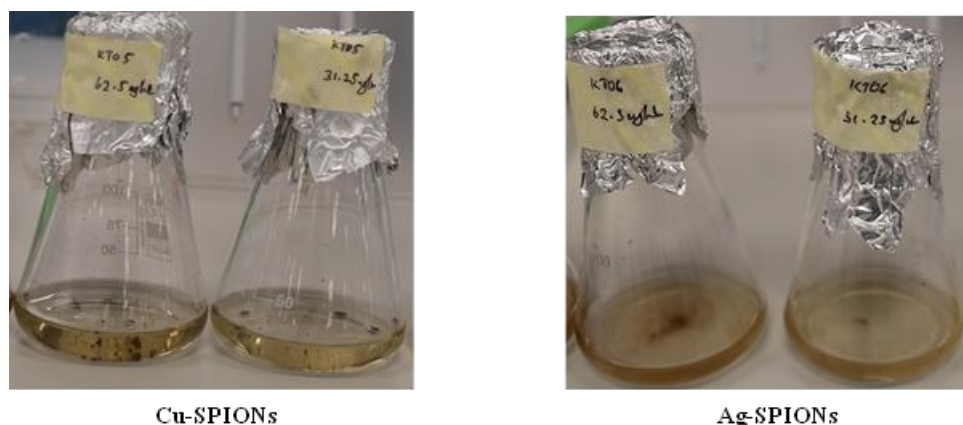


Figure B4-7. Close-up images of Cu-SPIONs (KT05) and Ag-SPIONs (KT06) culture flask-treatments at 62.5 and 31.25 $\mu\text{g/mL}$. The broth cultures are clear with no signs of bacterial growth. The brown colored substance were the nanoparticles suspended in solution.

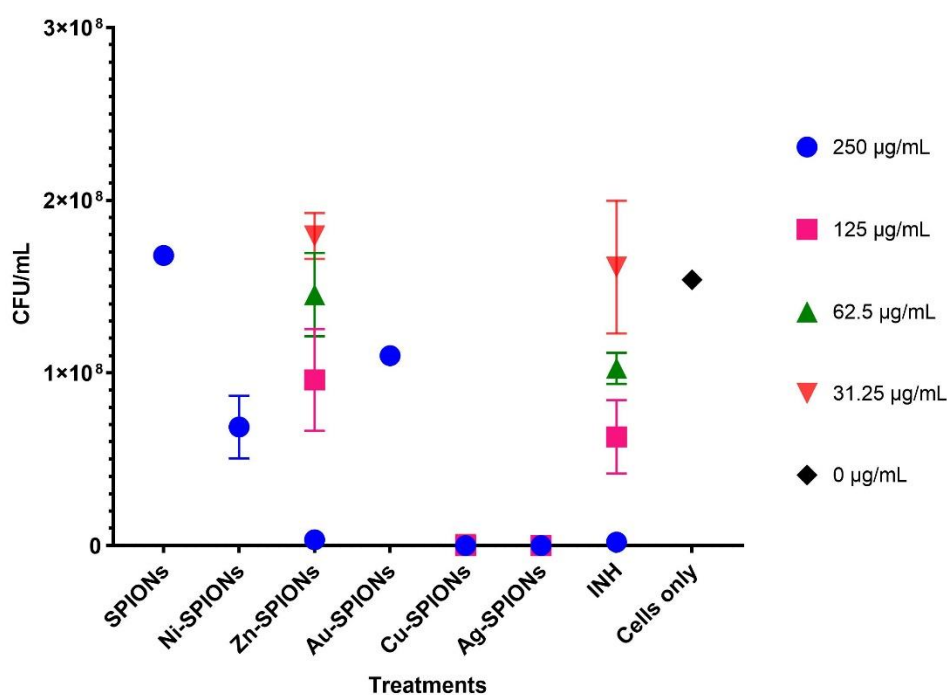


Figure B4-8. Colony forming units per milliliter (CFU/mL) of broth cultures after 72 hours of treatment with nanoparticles at various concentration (250, 125, 62.5 and 31.25 $\mu\text{g/mL}$) for selected samples. CFUs were determined by plating out of 50 μL a 10^{-4} dilution of each culture on Middlebrook 7H10 agar plates for 24 hours. The plot provides evidence that all Cu-SPIONs and Ag-SPIONs sterilized cultures at all concentrations tested. Zn-SPIONs and INH (isoniazid, a positive control), were only capable of sterilizing cultures at 250 $\mu\text{g/mL}$. CFUs for SPIONs and Ni-SPIONs and Au-SPIONs were only determined for the 250 $\mu\text{g/mL}$ treatments.

Appendix C

Annexin V-FITC and propidium iodide positive cells after 24 hours of treatment

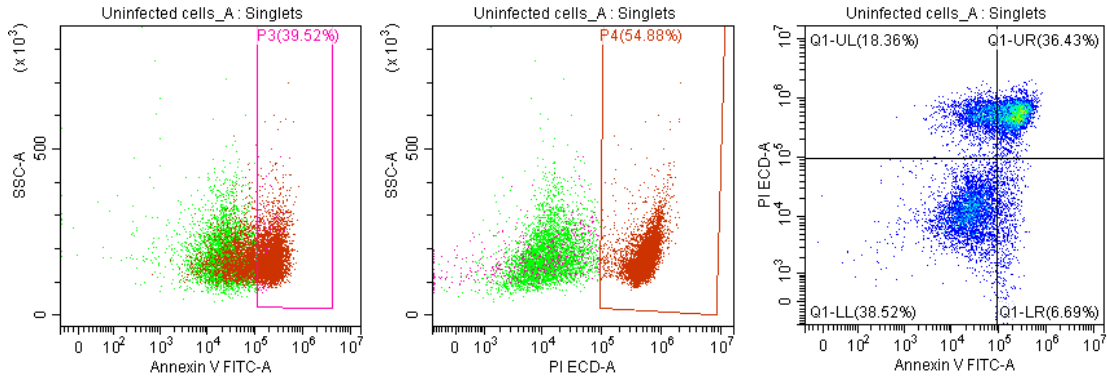


Figure C1. Uninfected cells (control) sample A.

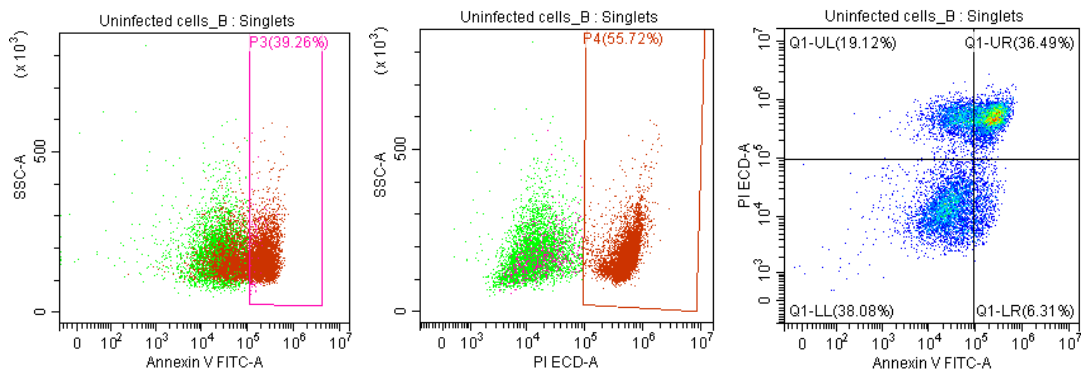


Figure C2. Uninfected cells (control) sample B.

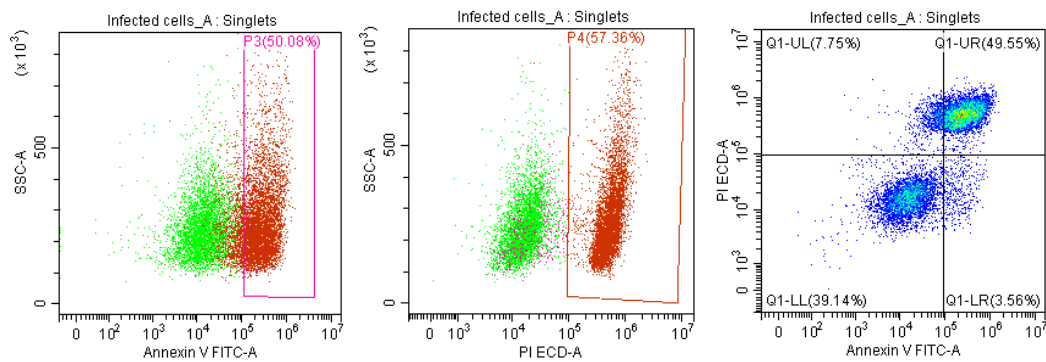


Figure C3. Infected cells (control) sample A.

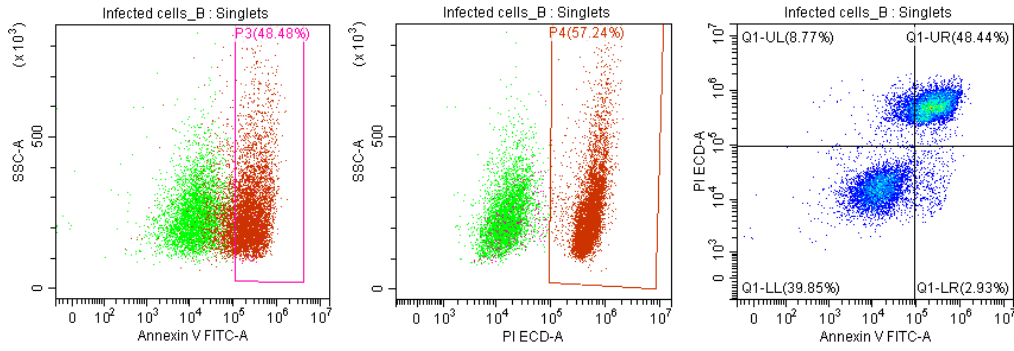


Figure C4. Infected cells (control) sample B.

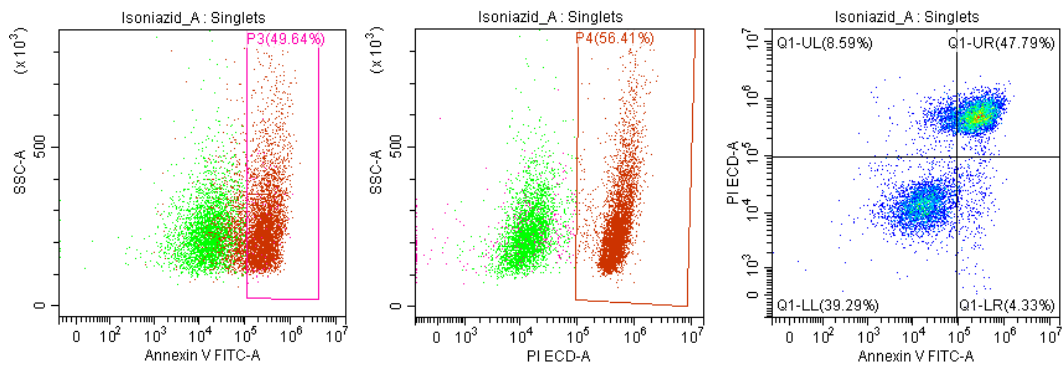


Figure C5. Isoniazid treatment (control) sample A.

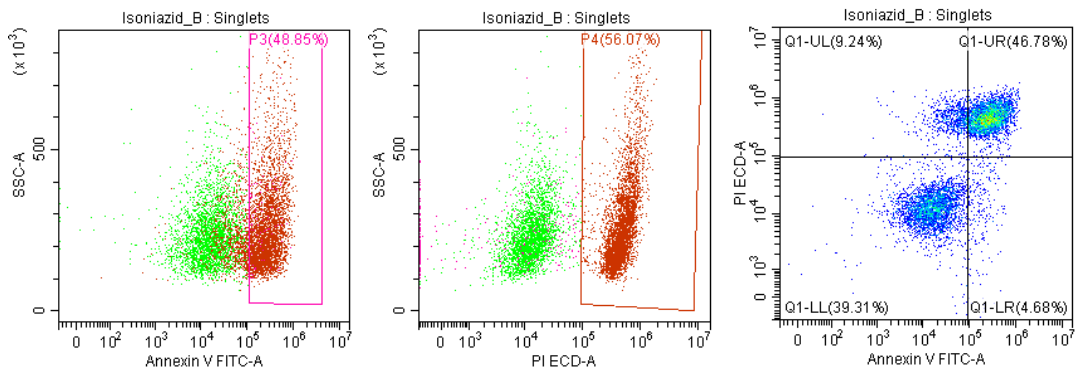


Figure C6. Isoniazid treatment (control) sample B.

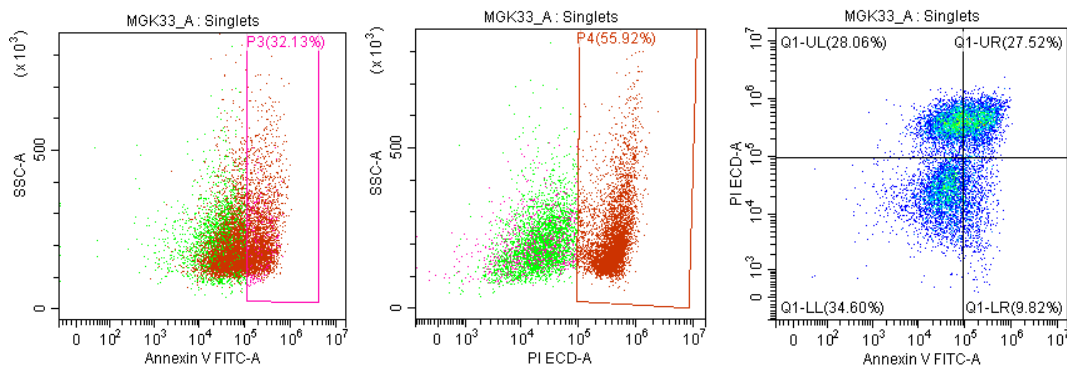


Figure C7. MGK33 treatment sample A.

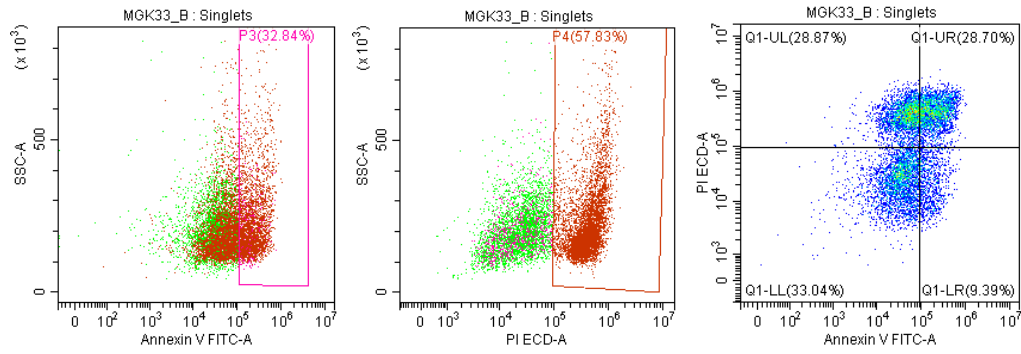


Figure C8. MGK33 treatment sample B.

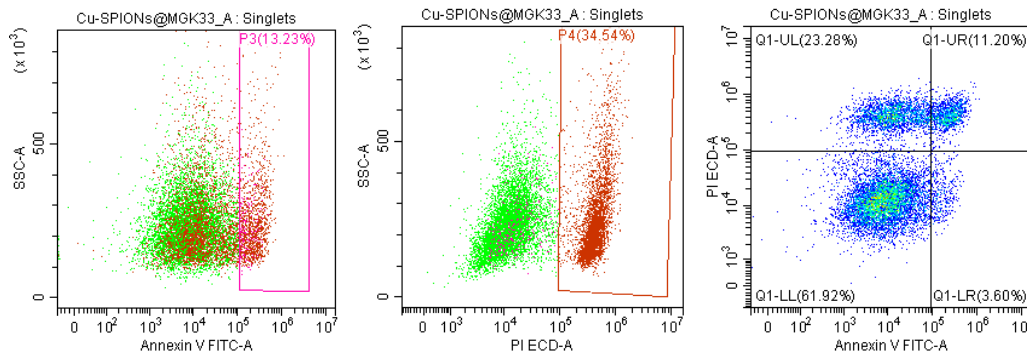


Figure C9. Cu-SPIONs@MGK33 treatment sample A.

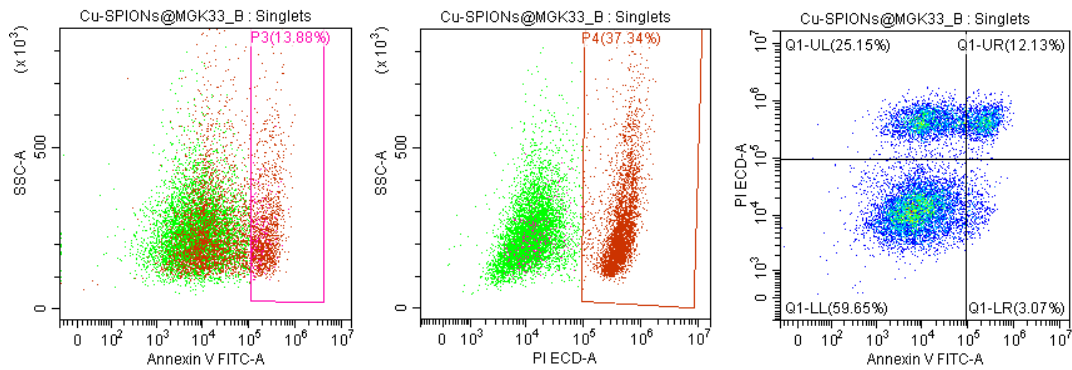


Figure C10. Cu-SPIONs@MGK33 treatment sample B.

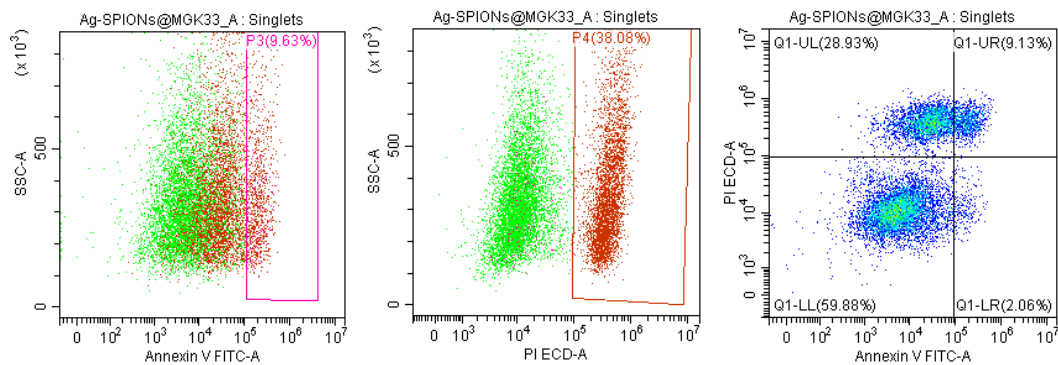


Figure C11. Ag-SPIONs@MGK33 treatment sample A.

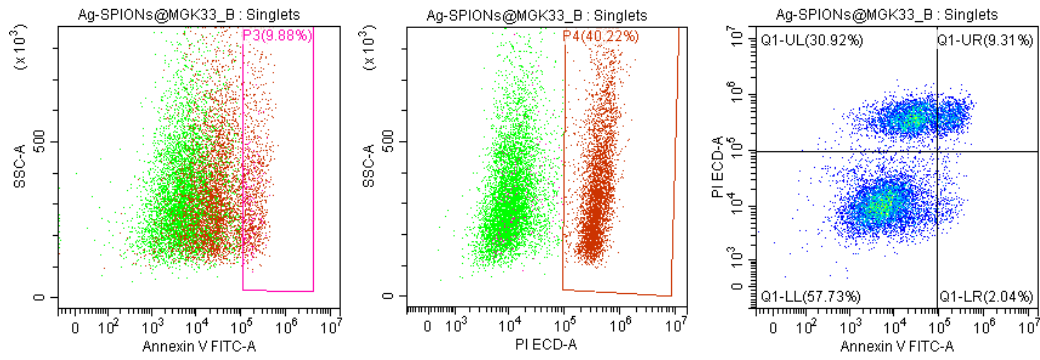


Figure C12. Ag-SPIONs@MGK33 treatment sample B.

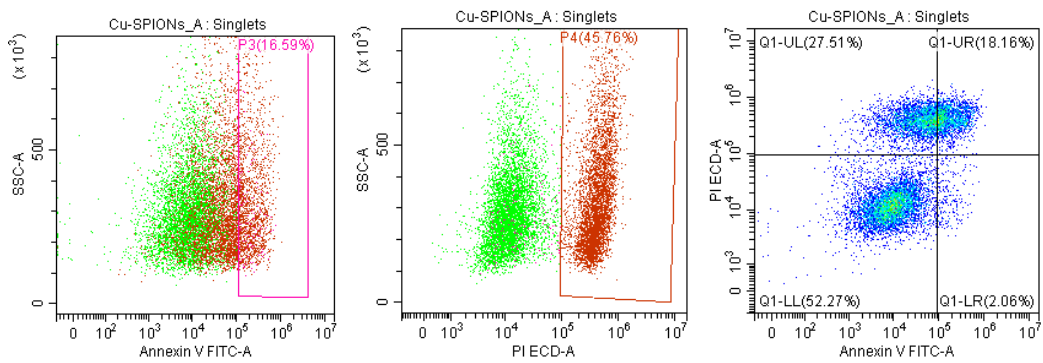


Figure C13. Cu-SPIONs treatment sample A.

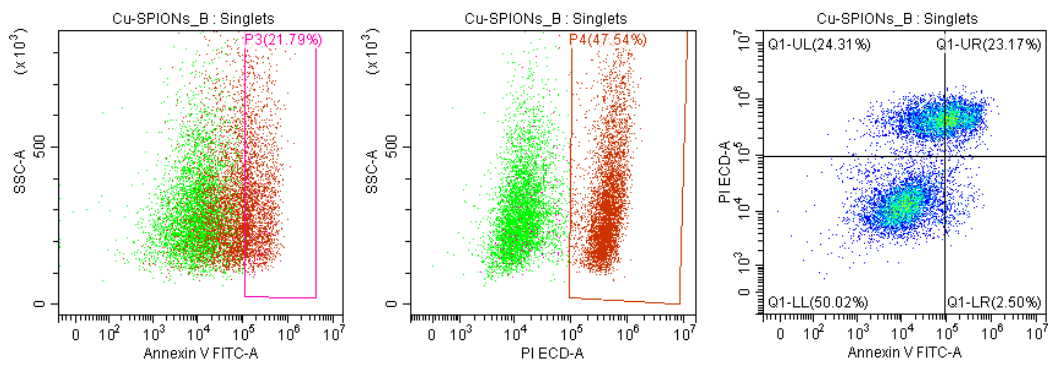


Figure C14. Cu-SPIONs treatment sample B.

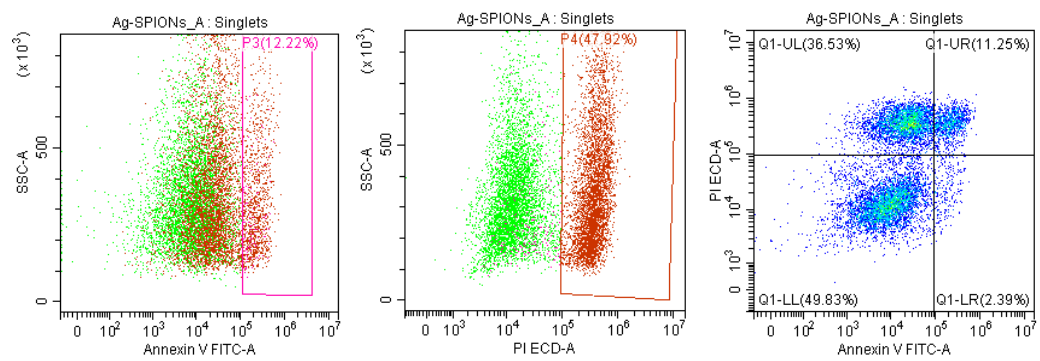


Figure C15. Ag-SPIONs treatment sample A.

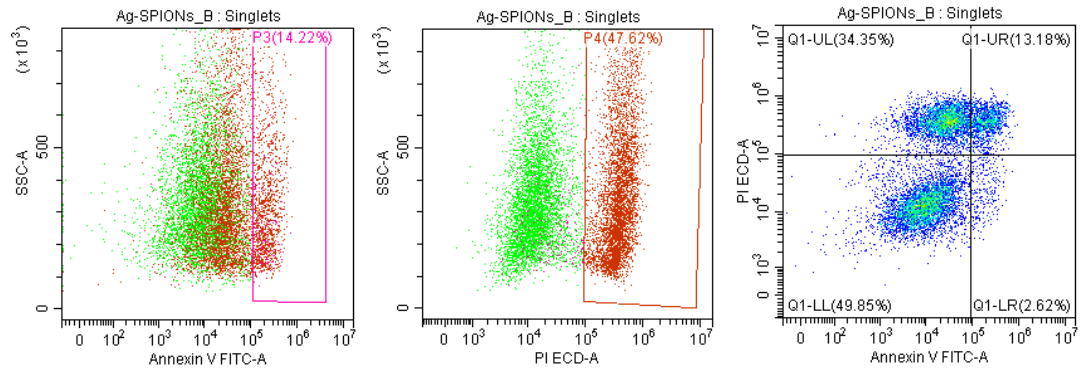


Figure C16. Ag-SPIONs treatment sample B.